

Effects of Propagation Techniques on Relative GPS Navigation

by

Nicholas C. Nuzzo, 2nd Lt, USMCR

B.S. Aerospace Engineering
United States Naval Academy, 1997

Submitted to the Department of Aeronautics and Astronautics in
partial fulfillment of the requirements for the degree of

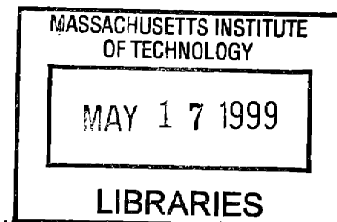
Master of Science in Aeronautics and Astronautics

at the

MASSACHUSETTS INSTITUTE OF TECHNOLOGY

February 1999

© 1999 Nicholas C. Nuzzo, All Rights Reserved.



Author Department of Aeronautics and Astronautics
January 1999

Approved by
Christopher M. D' Souza
Senior Member of the Technical Staff
The Charles Stark Draper Laboratory, Inc.
Technical Supervisor

Certified by
George T. Schmidt
Lecturer, Department of Aeronautics and Astronautics
Director of Education
The Charles Stark Draper Laboratory, Inc.
Thesis Supervisor

Accepted by
Jaime Peraire
Associate Professor of Aeronautics and Astronautics
Chairman, Department Graduate Committee

714

Effects of Propagation Techniques on Relative GPS Navigation

by

Nicholas C. Nuzzo

Submitted to the Department of Aeronautics and Astronautics on
January 8, 1999, in partial fulfillment of the requirements for the
degree of Master of Science in Aeronautics and Astronautics

Abstract

Various service vehicles are being developed to resupply the International Space Station (ISS). These service vehicles and the ISS will perform automated space rendezvous. The performance of a relative GPS navigation filter for this application is presented. Specifically, the effects of four different techniques for propagating the filter state are demonstrated and evaluated. These techniques include, (1) integration of the equations of motion accounting for J_2 , J_3 , J_4 and aerodynamic drag, (2) first-order equations of relative motion that account for the effects of J_2 and include a second-order conic approximation, (3) the Universal Keplerian state transition matrix, and (4) the use of the Clohessy-Wiltshire equations of relative motion. GPS measurements were simulated and included errors due to Selective Availability, clock bias, clock drift, and receiver noise. The relative navigation filter used pseudorange and delta-range measurements to estimate the filter state which included the relative position and relative velocity between the vehicles conducting the space rendezvous.

The results demonstrated that all four techniques surpassed the performance requirements on relative position and velocity errors. However, integrating the equations of motion, technique (1), resulted in the best performance. The filter state errors for this technique were the smallest and remained within the 3σ covariance bounds for all the cases studied. Effects due to eccentricity were observed in the remaining propagation techniques with the worst noted in technique (4). The most significant perturbation was shown to be J_2 , producing significant propagation and filter errors when the state was being propagated by methods (3) and (4), which did not account for it.

Thesis Supervisor: George T. Schmidt
Title: Lecturer, Department of Aeronautics and Astronautics
Director of Education
The Charles Stark Draper Laboratory, Inc.

Technical Supervisor: Christopher N. D' Souza
Title: Senior Member of the Technical Staff
The Charles Stark Draper Laboratory, Inc.

Acknowledgements

January 8, 1998

Life continues to teach me that I never succeed alone. Below is a conglomeration of those who helped me in this endeavor. No amount of words can express my gratitude towards them. Nonetheless, I thank them all.

The Marine and Navy officers on and off the Yard, Naval Academy professors, and Iceberg for helping me make the decision to pursue graduate studies at MIT.

Chris DSouza, my technical supervisor, for his patience, support, and encouragement. His door was always open for me. Paul Lawrence, for his devotion and time that went along with all his help with one of his first creations at Draper Lab - the GPS simulator. Stan Shepperd, for all his assistance with the Universal Keplerian state transition matrix and help in general. It amazes me how many times I had heard and read his name and he was always just next door. Arny Soltz, the coding genius and problem finder, for all his time and answers to my problems. Doug Fuhry, man of resources, for his amazing office library and his support. Chris Stoll and Tony Bogner, the computer gurus, for their continuous support in the fight against the computer gremlins. Mark Efstratiou and Greg Barton, for their support. George Schmidt, my thesis advisor, for taking me on as possibly his last masters student, for his help, extreme patience, and support.

Jean Kechichian, for his tremendous help in getting his algorithm to work. We used every form of communication: phone, fax, e-mail, and even regular mail and he always happily sacrificed his time for me. I hope I am able to thank him in person someday.

Former Draper Fellows: Matt, Tony, Christina, Atif and Rudy, for passing down all their advice and knowledge before they left. The torch will, once again, be passed. Fellow Draper Fellows: Chisholm and Pat, the smartest guys (my age) I know, for getting me through MIT classes. As far as I'm concerned, they were my professors here. Geoff, my former office-mate who deserted me for a better office, and Mike "Spam-Man-Kaboom," who changed my impression, a little, on zoombies, and all their help with classes. Bob and Nate, classmates from the Boat School, who kept my spirits up with their "war stories" - Robur Per Sacrificium.

Carla Haroz, for her friendship, unconditional love, moral and emotional support, and encouragement I did not always deserve. Thank you for helping me through classes and even typing my references. *Mrah!*

My Mom and Dad, for their constant love and support. My brother, Costa, for knowing how to make me laugh. I love you all.

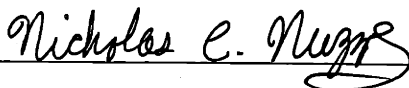
Most especially, I want to thank God. He has never forsaken me despite my unworthiness. As I continue to learn what His plan is for me, I will strive to trust Him even more. Thank You for everything! The Lord replied,

"The time when you have seen only one set of footprints is when I carried you" -Footprints

This thesis was prepared at The Charles Stark Draper Laboratory, Inc., under Independent Research and Development #18646

Publication of this thesis does not constitute approval by the Draper Laboratory or the sponsoring agency of the findings or conclusions contained herein. It is published for the exchange and stimulation of ideas.

Permission is hereby granted by the author to the Massachusetts Institute of Technology to reproduce any or all of this thesis.

A handwritten signature in cursive script, reading "Nicholas C. Nuzzo", is written over a horizontal line.

Nicholas C. Nuzzo

Table of Contents

1 Introduction.....	19
1.1 Problem Background and Motivation.....	19
1.2 Prior Research.....	22
1.3 Thesis Overview	25
1.4 Chapter Summary	26
2 Background	29
2.1 Global Positioning System.....	29
2.2 Relative GPS.....	36
2.3 Kalman Filtering	37
2.4 Chapter Summary	43
3 Orbit and GPS Models	45
3.1 Reference Frames.....	45
3.2 Orbit Model.....	47
3.3 GPS Simulation.....	54
3.4 Summary of Models.....	64
3.5 GDOP Considerations.....	66
3.6 Chapter Summary	68
4 Filter Design	69
4.1 Filter State.....	69
4.2 State Dynamics	70
4.3 Measurement Matrix.....	83
4.4 Covariance Matrix	86
4.5 Chapter Summary	92
5 Results	93
5.1 Description of Cases	93
5.2 Effects of Propagation Techniques	98
5.3 Effects of Eccentricity on Propagation with the Clohessy-Wiltshire State Transition Matrix.....	118
5.4 Effects of GDOP and Number of Common Satellites	133
5.5 Computation Costs.....	135
5.6 Summary of Propagation Methods	136
5.7 Chapter Summary	137
6 Conclusions and Recommendations.....	139
6.1 Conclusions.....	139
6.2 Recommendations for Future Work.....	142
6.3 Chapter Summary	143

Appendix A Converting between the Hill Frame and the Inertial Frame	145
A.1 Converting from the Inertial Frame to the Hill Frame.....	145
A.2 Converting from the Hill Frame to the Inertial Frame.....	151
Appendix B Equations for Constants in Kechichian's Algorithm.....	155
B.1 Initial Conditions	155
B.2 Coefficients	157
B.3 Conversion to Inertial Frame	167
Appendix C Errata in References	171
C.1 Errors in Reference [2].....	171
C.2 Errors in Reference [14].....	171
References.....	173

List of Figures

Figure 1.1: Total ETS-VII Rendezvous and Docking Experiment System ^[15]	24
Figure 2.1: The Space, Control, and User Segments of GPS ^[28, p. 30]	30
Figure 2.2: GPS satellite constellation with 6 orbital planes ^[25, p. 1-3, 28, p. 39]	31
Figure 2.3: Illustration of Good and Poor GDOP ^[26]	35
Figure 2.4: Relative Navigation with GPS ^[1]	36
Figure 2.5: The Discrete Kalman Filter	39
Figure 3.1: Summary of Reference Frames	46
Figure 3.2: Orbit Geometry.....	48
Figure 3.3: Outline of GPS Simulation.....	55
Figure 3.4: Sample Plot of SA Error Contribution to the Pseudorange Measurements	61
Figure 3.5: GPS Clock Drift, Random Walk	62
Figure 3.6: GPS Clock Bias, the Integral of Random Walk	63
Figure 3.7: GPS Pseudorange Measurement Error Less GPS Clock Bias.....	64
Figure 3.8: Sample Plot of GDOP	67
Figure 4.1: Target Local Frame	84
Figure 5.1: Orbit Design of Cases Studied	94
Figure 5.2: Relative Position Truth (Case 1)	96
Figure 5.3: Relative Velocity Truth (Case 1).....	97
Figure 5.4: GPS Clock Error Differences Truth (Case 1).....	97
Figure 5.5: Relative Position Propagation Errors	99
Figure 5.6: Relative Velocity Propagation Errors.....	100
Figure 5.7: Relative Position Propagation Errors (magnified)	101

Figure 5.8: Relative Velocity Propagation Errors (magnified).....	102
Figure 5.9: Position Filter Errors when Propagating with the Clohessy-Wiltshire State Transition Matrix (Case 1)	106
Figure 5.10: Velocity Filter Errors when Propagating with the Clohessy-Wiltshire State Transition Matrix (Case 1)	107
Figure 5.11: Clock Filter Errors when Propagating with the Clohessy-Wiltshire State Transition Matrix (Case 1)	108
Figure 5.12: Position Filter Errors when Propagating with the Keplerian State Transition Matrix (Case 1)	109
Figure 5.13: Velocity Filter Errors when Propagating with the Keplerian State Transition Matrix (Case 1)	110
Figure 5.14: Clock Filter Errors when Propagating with the Keplerian State Transition Matrix (Case 1)	111
Figure 5.15: Position Filter Errors when Propagating with Kechichian's Analytic Method (Case 1)	112
Figure 5.16: Velocity Filter Errors when Propagating with Kechichian's Analytic Method (Case 1)	113
Figure 5.17: Clock Filter Errors when Propagating with Kechichian's Analytic Method (Case 1)	114
Figure 5.18: Position Filter Errors when Propagating by Integrating the Equations of Motion (Case 1)	115
Figure 5.19: Velocity Filter Errors when Propagating by Integrating the Equations of Motion (Case 1)	116
Figure 5.20: Clock Filter Errors when Propagating by Integrating the Equations of Motion (Case 1)	117
Figure 5.21: Position Filter Errors when Propagating with the Clohessy-Wiltshire State Transition Matrix (Case 2)	119
Figure 5.22: Velocity Filter Errors when Propagating with the Clohessy-Wiltshire State Transition Matrix (Case 2)	120
Figure 5.23: Clock Filter Errors when Propagating with the Clohessy-Wiltshire State Transition Matrix (Case 2)	121

Figure 5.24: Position Filter Errors when Propagating by Integrating the Equations of Motion (Case 2)	122
Figure 5.25: Velocity Filter Errors when Propagating by Integrating the Equations of Motion (Case 2)	123
Figure 5.26: Clock Filter Errors when Propagating by Integrating the Equations of Motion (Case 2)	124
Figure 5.27: Position Filter Errors when Propagating with the Clohessy-Wiltshire State Transition Matrix (Case 3)	125
Figure 5.28: Velocity Filter Errors when Propagating with the Clohessy-Wiltshire State Transition Matrix (Case 3)	126
Figure 5.29: Clock Filter Errors when Propagating with the Clohessy-Wiltshire State Transition Matrix (Case 3)	127
Figure 5.30: Position Filter Errors when Propagating by Integrating the Equations of Motion (Case 3)	128
Figure 5.31: Velocity Filter Errors when Propagating by Integrating the Equations of Motion (Case 3)	129
Figure 5.32: Clock Filter Errors when Propagating by Integrating the Equations of Motion (Case 3)	130
Figure 5.33: Relationship between Filter State Error and Eccentricity when Propagating with the Clohessy-Wiltshire State Transition Matrix	131
Figure 5.34: Relationship between Filter State Error and Separation when Propagating with the Clohessy-Wiltshire State Transition Matrix	132
Figure 5.35: Number of Common GPS Satellites between the Chaser Vehicle and the Target Vehicle (Case 3)	133
Figure 5.36: GDOP Values with respect to the Target (Case 3)	134
Figure A.1: The Hill Frame Redefined as the FRD Frame	146

List of Tables

Table 3.1: Terminology and Symbols of Orbital Elements	47
Table 3.2: GPS Ephemeris Data Definitions ^[13, 35]	56
Table 3.3: Computation of a Satellite's ECEF Position Vector ^[13]	57
Table 3.4: Coefficients for AR Model	60
Table 3.5: Pseudorange and Delta-range White Noise Variances	63
Table 3.6: Summary of Models	65
Table 5.1: Orbital Parameters of Target Vehicle	93
Table 5.2: Remaining Orbital Parameters	95
Table 5.3: Notation for Propagation Techniques	98
Table 5.4: Spectral Values of the Process Noise	104
Table 5.5: Computations Required for Each Propagation Technique	135

List of Symbols, Acronyms, Abbreviations, Notation, and Constants

List of Symbols

a	semimajor axis
a	acceleration
a_i	i^{th} component of line of sight vector
$a(k)$	SA k^{th} filter coefficient
b	clock bias, or semi-minor axis
c	speed of light
c_d	coefficient of drag
d	clock drift
d	drag (subscript)
e	eccentricity
e	estimate error
f	true anomaly
i	inclination
h	angular momentum
m	mass
n	mean motion
p	SA model order
q	spectral strength
r	magnitude of true range, or magnitude of position
r_E	radius of the Earth
s	number of selected satellites
t	time
t_{0e}	reference time of ephemeris
u, v, w	velocity components
v	measurement error noise, or velocity (vector)
w	propagation error noise
x	state vector
x, y, z	position components
$y(t)$	SA model output
z	measurement vector
A	system matrix
$Af0$	zero th order clock correction
$Af1$	first order clock correction

Eeccentric anomaly
$G(\tau)$noise input matrix
Hmeasurement matrix, or Hill frame (subscript)
J_2, J_3, J_4second, third, and fourth zonal harmonics
Iinertial frame (subscript)
KKalman gain, or Kechichian frame (subscript)
Lgeocentric latitude, or Local frame
Mmean anomaly
Nmatrix of line of sight vectors
Perror covariance matrix
P_nLegendre polynomial
Qcovariance matrix of system modeling errors
$Q(\tau)$spectral density matrix
Rcovariance matrix of measurement noise
Scross-sectional area perpendicular to direction of motion
X, Y, Zx-, y-, and z-axes of a reference frame
αwhite Gaussian noise
θargument of latitude
μEarth's gravitational parameter,
ρpseudorange
$\dot{\rho}$delta-range
ρ_datmospheric density
σstandard deviation
ϕVinti potential function
ωargument of perigee
$\vec{\omega}_E$Earth angular velocity
Δrrange error due to clock bias
Δttime increment
Δt_{user}user's clock error
Δt_{SV}SV clock error
Φstate transition matrix
Ωlongitude of ascending node
$\dot{\Omega}$rate of change of Ω

$\dot{\Omega}_E$ Earth rotation rate

List of Acronyms

AR AutoRegressive
ARP ATV Rendezvous Pre-development
ATV Automated Transfer Vehicle
C-W Clohessy-Wiltshire
DGPS Differential GPS
DoD Department of Defense
DOLT Dynamic Open Loop Test
DoT Department of Transportation
ECEF Earth-Centered Earth-Fixed
ESA European Space Agency
ETS Engineering Test Satellite
FLOPS FLoating OPerationS count
FRD Forward-Right-Down
GDOP Geometric Dilution Of Precision
GPS Global Positioning System
HTV H-II Transfer Vehicle
ID (SV) IDentification number
ISS International Space Station
KSTM Keplerian STM
LEO Low Earth Orbit
NASA National Aeronautic and Space Administration
NASDA NAional Space Development Agency
RGPS Relative GPS
RVD Rendezvous and Docking
SA Selective Availability
SV (GPS) Satellite Vehicle

List of Abbreviations

atm atmosphere (subscript)
c chaser (subscript)
rel relative (subscript)
t target (subscript)

List of Notation

\hat{z} a vector
 \hat{z} unit vector of \hat{z}
z magnitude of vector \hat{z} , or a scalar
 z_x, z_y, z_z components of vector \hat{z}
 z_i value of z at time increment i

- z_N z in the N-frame
- z_0 z at epoch (initial time, $t = 0$)
- \dot{z} first time derivative of z
- \ddot{z} second time derivative of z
- Z a matrix, some scalars (annotated)
- \bar{z} a priori estimate of z
- \hat{z} updated estimate of z
- $y|z$ y conditioned on z
- $E[]$ expected value of expression in []
- s_z $\sin z$
- c_z $\cos z$
- $O_{m \times n}$ ($m \times n$) zero matrix

Note: Exceptions are annotated in the text.

List of Constants

$$c = 2.99792458 \times 10^8 \frac{m}{s}$$

$$r_E = 6.378136 \times 10^6 m$$

$$J_2 = 1.082628 \times 10^{-3}$$

$$J_3 = -2.538 \times 10^{-6}$$

$$J_4 = -1.593 \times 10^{-6}$$

$$\mu = 3.986005 \times 10^{14} \frac{m^3}{s^2}$$

$$\dot{\Omega}_E = 7.2921151 \times 10^{-5} \frac{rad}{s}$$

Chapter 1

Introduction

The purpose of this thesis is to analyze a navigation scheme for space rendezvous using Relative GPS (RGPS). Specifically, the effects of filter state propagation techniques will be explored. This chapter provides the background and motivation for the problem followed by the prior research done on the topic. An overview of the thesis contents concludes the chapter.

1.1 Problem Background and Motivation

The Global Positioning System (GPS) has proven to be an accurate navigation system for many applications including the navigation of aircraft, ships, and automobiles. However, more demanding applications have called for even higher accuracy in GPS-based navigation systems. GPS range errors due to satellite clock bias, satellite ephemeris errors, Selective Availability (SA), and atmospheric delays are unacceptable in applications such as the navigation of robotic vehicles in a caravan. This has led to the use and development of RGPS. RGPS increases the accuracy of GPS in applications requiring only relative position and velocity knowledge, otherwise known as relative navigation.

RGPS is applicable when two separate GPS receivers, each on its own vehicle, track the same GPS satellites at the same time. When this occurs, the common errors to both receivers, such as SA, satellite ephemeris errors, satellite clock errors, and atmospheric

delays due to the ionosphere, will cancel. This cancellation increases the accuracy of the relative navigation solution. RGPS will be discussed in further detail in **Chapter 2**.

With the current construction of the International Space Station (ISS) and the need for vehicles to service and maintain it, a new application for relative GPS has been proposed: navigation for space rendezvous. The Japanese H-II Transfer Vehicle (HTV) and the European Automated Transfer Vehicles (ATV) will rendezvous with the ISS in order to provide logistic support, such as re-supply and required servicing. These vehicles will use RGPS for navigation during the long-range operations (20 km to 500 m) of the rendezvous. For the last 500 meters the navigation scheme will switch to a laser radar to obtain the even higher level of accuracy required for docking and/or berthing.

Until now, space rendezvous performed by the National Aeronautics and Space Administration (NASA) has used human control throughout the operation including both operators in space vehicles and ground control. This method is both costly and inefficient. Through the use of RGPS and the laser radar, the whole operation can be automated which would reduce the cost and allow astronauts and ground personnel to focus on other important tasks.

The objective of this thesis is to analyze a RGPS system that can be used for relative navigation and rendezvous. The main component of this RGPS system is a Kalman filter, or a GPS Relative Navigation Filter. This navigation filter uses GPS pseudoranges and delta-ranges to estimate the relative position and relative velocity between the two GPS receivers located on the two vehicles performing rendezvous and docking (RVD). Throughout this thesis these vehicles will be referred to as the chaser and target vehicles.

The main effort of this thesis is focused on determining the best method of propagating the filter state in order to obtain the best estimates.

The first step is the development of a model for the needed GPS data. The orbits of the vehicles performing rendezvous are used as input for a GPS software simulation which produces pseudoranges, delta-ranges, and other satellite information. Several important issues must be considered. One is that the receivers of both the chaser and target vehicles must track the same satellites at the same time. Consequently, the visibility of the GPS satellites is a concern. Another concern is selecting the optimal geometry when more than four satellites are in view. The GPS software simulator accounts for all these issues.

The next step, and primary focus of this thesis, is the analysis of the relative navigation filter that will use the GPS observables (pseudoranges and delta-ranges) to estimate the states. The main objective is to safely navigate the chaser vehicle to its target by meeting or surpassing the following performance requirements^[9]:

position error	< 10 m	(3 σ)
velocity error	< 0.05 m/s	(3 σ)

One method of improving the accuracy will be to use higher order analytic solutions in the propagation of the state and covariance. Nonetheless, the greatest effort is focused on improving the method of state propagation in order to improve the overall performance of the navigation filter.

The results of this thesis will be a relative navigation scheme that improves upon current ones and, with minor adjustments, one that can be used for any RGPS application in

space. RPGS has tremendous potential for automated rendezvous. As long as the main concern is the relative position and relative velocity between two vehicles, and not their absolute positions and velocities, the applications of relative GPS in space navigation are limitless.

1.2 Prior Research

RGPS has not been used for space navigation thus far. However, a significant amount of research was conducted in the 1990s. This research can be divided into three general areas: experiments and research done by and for NASA, the European Space Agency (ESA), and the NATIONAL Space Development Agency (NASDA) of Japan. Much of the research resulted from cooperative efforts between these agencies.

NASA has shown interest in using RGPS for space rendezvous for the shuttle. Several shuttle missions, including STS-69, 77, 80, 87, and 91 each had experiments to test various aspects of the concept. Some of the conclusions are: RGPS provides sufficiently accurate relative navigation to allow control of the orbiter's trajectory until very close to the space station. However, it is not sufficient for docking and/or berthing.^[7] Having the chaser and target view the same satellites is not easily achieved.^[27] In one study focusing on chaser-to-target separations of 2 km and less, a relative navigation filter eliminated the effects of SA and the ionosphere with relative position and velocity accuracies of 2 m and 8 cm/sec (1- σ), respectively. This study also showed that no degradation in the estimates were observed when the number of common GPS satellites is intentionally reduced provided that measurements from four common GPS satellites are available.^[10] Another

study, on the other hand, expected improvements in performance when using a 6 channel or even an all-in-view receiver as opposed to a 4 channel receiver.^[36]

ESA is conducting its own research and development of a relative navigation filter to use on the ATV that will rendezvous with the ESA module of the ISS. Rendezvous techniques studies are being conducted under ESA's ATV Rendezvous Pre-development (ARP) contract. These studies have focused on minimizing the needed software and have obtained satisfactory performance. Position errors of 2.5 m and velocity errors of 5 mm/sec ($3\text{-}\sigma$) were obtained using a high-fidelity functional (i.e. software) simulator while keeping the state vector at a reasonable size (8 states).^[9] Another study focused on the issues of GPS visibility for a Shuttle rendezvous with MIR. At certain shuttle attitudes, this study showed that there were times when less than four GPS satellites were visible.^[19] Yet another study illustrated the need for the largest possible commonality of GPS antenna coverage between both spacecraft.^[21] Lastly, one lesson learned was that developing complex and high accuracy RGPS software packages required special attention in adapting the algorithm to the specific receiver design.^[18]

Finally, NASDA has also conducted research in the area of RGPS. Traditionally, NASDA has tested their concepts in space with the Engineering Test Satellites (ETS) before implementing them on actual space vehicles. The 7th satellite in the series is devoted to relative GPS navigation. ETS-VII is the first automated test of relative GPS in space with experiments being conducted at the time this thesis was being written. The test satellite consists of two satellites, a "Chaser" and a "Target," as illustrated in **Figure 1.1**. The Chaser releases the Target and performs a Rendezvous and Docking (RVD) experiment. Prior to launch, the ETS-VII relative navigation system was tested and verified in

four steps: software-level test, component-level test, RVD subsystem test, and satellite system integration test. Within the RVD subsystem test the subsystem was evaluated with the Dynamic Open Loop Test (DOLT) methodology. NASDA executed DOLT in a ground test with a GPS simulator with results in accuracy of the relative position to as low as ten meters.^[16]

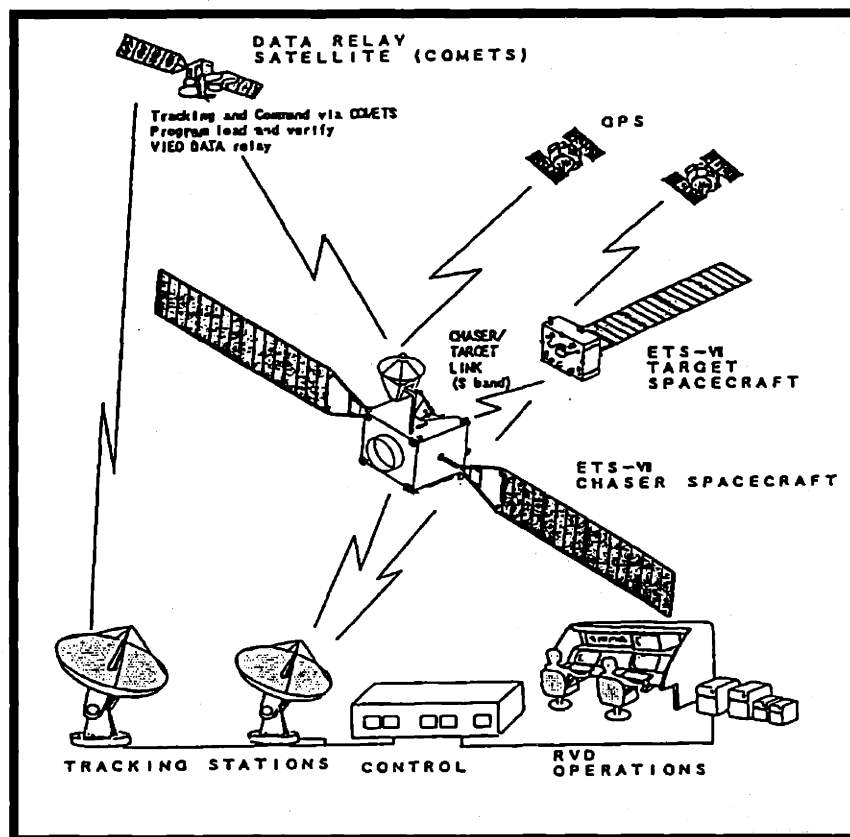


Figure 1.1: Total ETS-VII Rendezvous and Docking Experiment System^[15]

Recently, the ETS-VII conducted a series of RGPS performance tests and successfully conducted a rendezvous and docking experiment. Using RGPS for rendezvous with the ISS and other space vehicles is promising.

1.3 Thesis Overview

Chapter 2 provides the general background on the theory and applications associated with this thesis. Specifically, it outlines the Global Positioning System and its use in navigation, with emphasis on the application of Relative GPS. The chapter concludes with a brief overview of Kalman filtering.

Chapter 3 describes how the orbits for the chaser and target vehicles are created and what perturbation effects are modeled. It also describes the models used to obtain the GPS measurements required by the Kalman filter: the pseudorange and delta-range. The modeled GPS errors include SA, clock bias, clock drift, and receiver white noise. **Chapter 3** also provides a description of all the coordinate frames used throughout this thesis, as well as the method by which GDOP is computed.

The design of the Kalman filter is given in **Chapter 4**. A description of the state, the dynamics of the filter, and the techniques used to propagate the state are presented. These techniques propagate the state with: (1) integration of the equations of motion accounting for J_2 , J_3 , J_4 , and aerodynamic drag, (2) first-order equations of relative motion that account for the effects of J_2 and include a second-order conic approximation, (3) the Universal Keplerian state transition matrix, and (4) a state transition matrix derived from the Clohessy-Wiltshire equations of relative motion. This chapter also describes how the measurement matrix and the initial covariance matrix are obtained, as well as how the covariance matrix is propagated.

Chapter 5 includes all the results of the analysis. First, it presents the parameters associated with the cases tested. This is followed by a comparison of the propagation techniques with the state just being propagated and then being estimated by the filter. The effects of eccentricity, GDOP, and number of satellites on the performance of the filter are evaluated. Finally, a summary of the associated computation costs of each propagation technique as well as a general summary on each technique is provided.

Chapter 6 closes the thesis with conclusions and recommendations for future work. Note that each chapter ends with a summary of what was presented, as well as a lead into the following chapter.

Several appendices are also attached to supplement the thesis. **Appendix A** describes the conversion between two coordinate frames used throughout the study. **Appendix B** provides equations which supplement one of the propagation techniques used. Finally, **Appendix C** presents errata found in two of the references.

1.4 Chapter Summary

This chapter presented a brief background of the use of RGPS navigation for automated space rendezvous. It motivated the reason for using RGPS and for evaluating the techniques used to propagate the filter state. That is, to obtain the best estimates of the relative position and velocity of the vehicles conducting the rendezvous. This was followed by a summary of the prior research conducted on the topic by space agencies around the world. Finally, a general overview of the thesis contents was presented. The following

chapter presents the theoretical background required for this study which includes GPS, RGPS, and Kalman filtering.

Chapter 2

Background

The intent of this chapter is to provide a brief overview of the theory and applications associated with this thesis. Specifically, general background of the Global Positioning System and its use in navigation will be provided. This is followed by a description of the specific application of GPS known as RGPS. Finally, an overview of Kalman filtering is presented.

2.1 Global Positioning System

In the early 1960s, the U.S. military, NASA, and the Department of Transportation (DoT) showed interest in developing satellite systems for position determination.^[13] This led to the development of several systems, each improving upon the one before and finally to today's NAVSTAR Global Positioning Satellite System, most frequently referred to as GPS. This section provides a brief system summary, an overview of the GPS measurements, and concludes with a discussion of the errors found in these measurements.

2.1.1 System Summary

Three segments comprise the Global Positioning System. They are the Control Segment, the Space Segment, and the User Segment and are illustrated in **Figure 2.1**

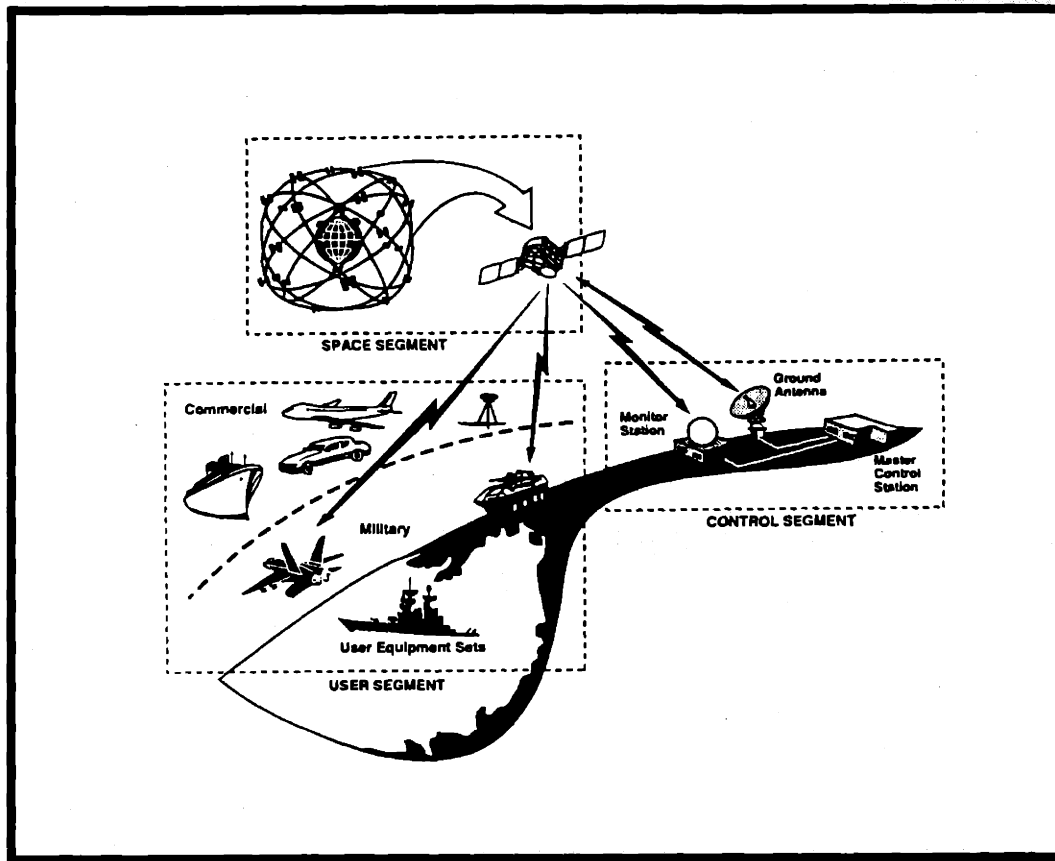


Figure 2.1: The Space, Control, and User Segments of GPS [28, p. 30]

The Control Segment is responsible for keeping track of all the GPS Satellite Vehicles (SV's) and updating the information required in the navigation message that the SV's transmit, such as satellite ephemeris and satellite clock corrections. The Space Segment consists of 24 SV's divided up equally into 6 orbits, with each orbital plane inclined 55 degrees to the equator as shown in **Figure 2.2**. Each SV continuously transmits a signal containing the navigation message. The User Segment includes anyone who is capable of receiving this signal. A combination of signals from selected satellites are used to compute a three-dimensional position and local time. [28, pp. 32-33]

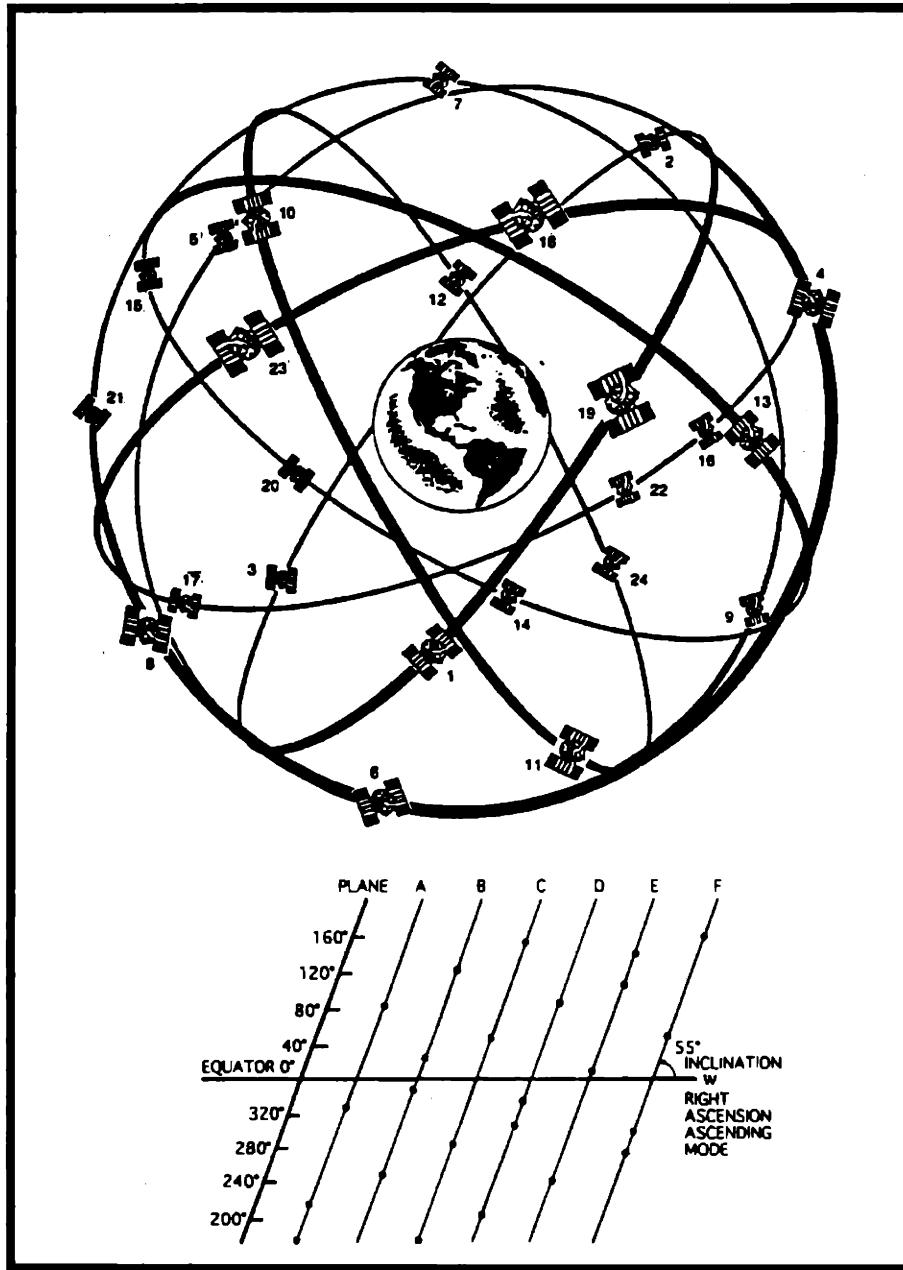


Figure 2.2: GPS satellite constellation with 6 orbital planes [25, p. 1-3, 28, p. 39]

2.1.2 Measurements

The navigation message that each satellite broadcasts consists of the satellite's orbital ephemeris, an almanac of all the other GPS satellites, system status indicators, and the

time of transmission along with a model of its accuracy degradation to account for the satellite's clock drift.^[1] GPS receivers take in this information and generate two measurements: pseudoranges and delta-ranges.

Since receiver clocks are not as accurate as the atomic clocks on GPS satellites, the received measurement will be offset by the time difference between the receiver clock and GPS time. Though very accurate, the SV clocks will also have errors. However, models of the SV clock errors are included in the navigation message so that the receiver can compensate. Due to the differences between the two clocks, the measured range will be different from the true range. This measurement is called the pseudorange and mathematically is expressed as:

$$\rho = c(\Delta t + \Delta t_{user} - \Delta t_{SV}) \quad (2.1)$$

where

ρ = pseudorange

c = speed of light = $2.99792458 \times 10^8 \frac{m}{s}$

Δt = signal transit time

Δt_{user} = user's clock error

Δt_{SV} = SV clock error

Since the error in the user's clock, or the receiver clock, is unknown, pseudoranges from four SV's are used to solve for the three components of the user's position and the error in its clock, or clock bias.^[1]

Pseudorange can also be thought of as the sum of the true range, r , with a small extra distance, Δr , due to the clock errors, or bias, b . This can be written as

$$\rho = r + \Delta r = r + cb \quad (2.2)$$

The delta-range measurement, $\dot{\rho}$, is obtained by differencing two subsequent pseudorange measurements.^[11] This results in the range error term, Δr , canceling out. Even though the range error term cancels out, a term related to the clock errors, specifically, the rate of change in clock bias, remains. This term is referred to as clock drift and is annotated as d . Delta-range can be thought of as the change in range to the SV over the measurement interval. Just as pseudoranges can be used to determine position and clock bias, delta-ranges can be used to determine the three components of the user's velocity and the clock drift, since it represents the average velocity over the interval.

2.1.3 Measurement Errors

Aside from the errors due to the clocks in both the GPS satellites and the receivers discussed in the previous section, there are many other significant errors associated with GPS. These errors can be categorized according to the segment in which they are formed or found.

The main errors in the Control Segment are associated with differences between the satellite ephemeris that is uploaded to the SV's and the truth. An incorrect representation of the SV ephemeris in the navigation message causes a slowly varying error, or bias, in the user's solution. Another source of error is introduced by a program called Selective Availability (SA) under the auspices of the Department of Defense (DoD). SA is accom-

plished by intentionally “dithering” the satellite clock frequency which introduces a time varying bias in the navigation signal.^[11] The purpose of SA is to limit GPS accuracy from unauthorized users.

The Space Segment errors include the instability of the SV clocks resulting in clock errors that may not be corrected by the Control Segment and errors in the SV navigation system. Unpredictable SV perturbations may be also be a source of error in this segment.^[25, p. 3-3]

The User Segment introduces a noise error associated with the receiver that results from noise produced in the code and carrier tracking loops, and mechanization errors.^[22] Depending on the user’s location, errors due to the atmosphere may be introduced. The GPS signal is delayed as it passes through the ionosphere (50 to 500 km) and the troposphere (ground to 13 km). In the application of this thesis these errors will be negligible since for Low Earth Orbit (LEO) users, atmospheric delays of measurements that are taken from overhead satellites will be fairly small. However, if measurements are taken to SV’s near or below the local horizontal, ionospheric delays may be significant.^[23] Another source of error in this segment is termed multipath. Multipath errors result from signals arriving to the receiver in other than direct paths from the SV, such as a reflection from the spacecraft’s surface. Multipath errors are obviously more significant for ground users since there are more objects near the receiver that may cause a signal reflection. Nonetheless, satellites may also be subject to significant multipath error due to solar panels. These errors, however, can be minimized by proper antenna design and placement.^[1]

It should also be noted in this section that the geometry of the selected four or more SV's plays a significant role in the accuracy of the navigation solution. The Geometric Dilution of Precision, or GDOP, is a parameter that represents this geometry. The values of GDOP is inversely proportional to the volume of a body formed by the top of unit vectors between the user and the SV's.^[11] Generally, SV's that are clustered overhead or to one side of the user represent a poor geometry, or a relatively high GDOP; whereas, one SV directly overhead with three SV's 120 degrees apart on the horizon is an ideal geometry, or low GDOP. This concept is illustrated in **Figure 2.3**.

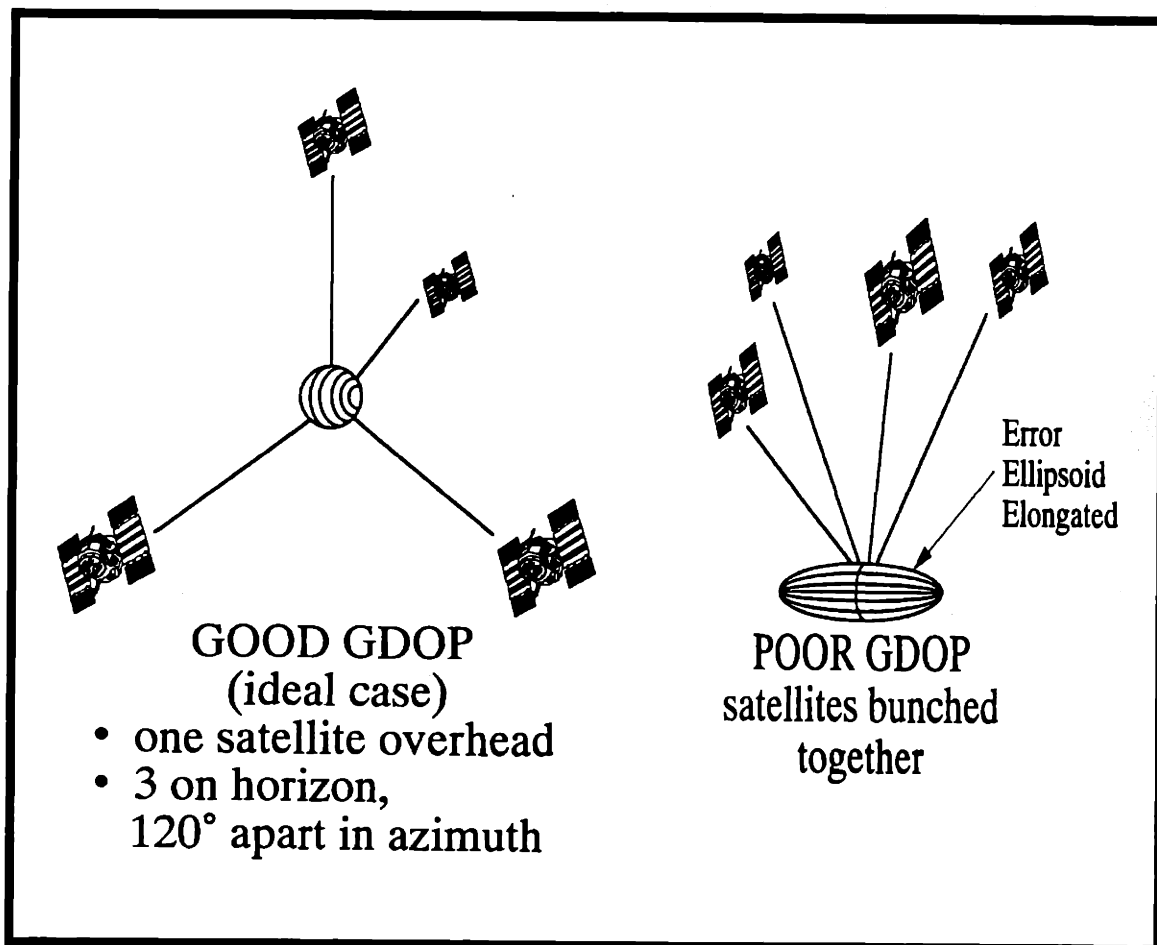


Figure 2.3: Illustration of Good and Poor GDOP^[26]

For this study, a GPS software simulation was used to obtain the required measurements of pseudoranges and delta-ranges needed to perform RGPS navigation. The simulator modeled the errors discussed above which are the most prevalent in orbital rendezvous to include clock bias, clock drift, receiver noise, and SA. A more detailed explanation of this simulation is presented in **Chapter 3**.

2.2 Relative GPS

In RGPS, as in Differential GPS (DGPS), two separate GPS receivers are used. The distinction between RGPS and DGPS is that in the latter the location of one of the receivers is precisely known, whereas in RGPS this is not the case. RGPS is ideal in applications where the main concern is the relative position of two vehicles and not necessarily their absolute positions. The key to both applications is that both receivers must be tracking the same GPS satellites at the same time as illustrated in **Figure 2.4**.

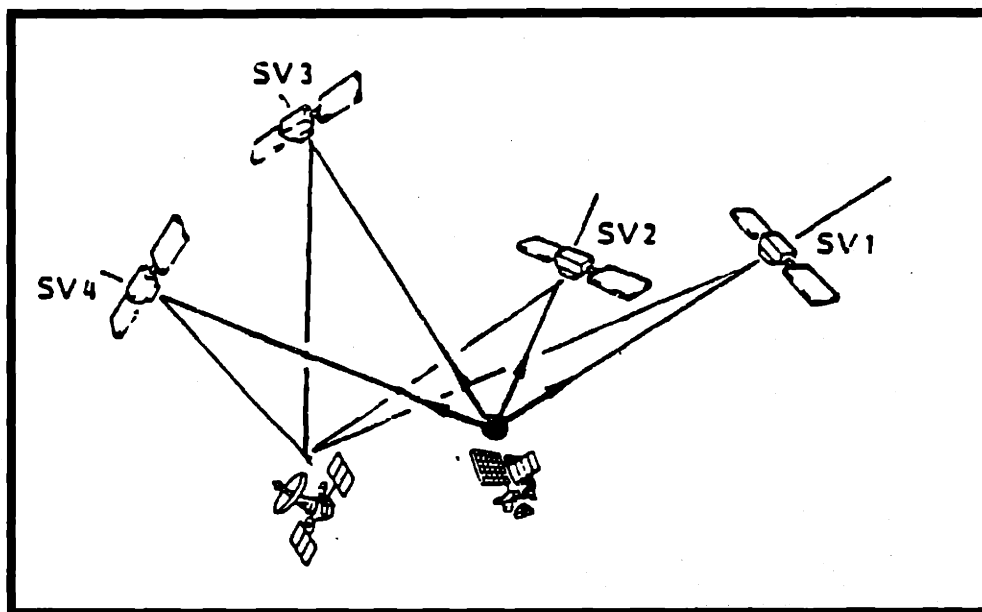


Figure 2.4: Relative Navigation with GPS^[1]

If they are, the common errors associated with the common SV's, such as Selective Availability (SA), satellite ephemeris errors, satellite clock errors, and atmospheric delays due to the ionosphere, will cancel when obtaining the navigation solution. These GPS "bias-like" range errors tend to be the significant ones while the remaining GPS "noise-like" range errors, such as multipath and receiver noise, are usually much smaller in magnitude.^[29] Multipath can be a source of large error. However, based on the discussion of the previous section, multipath errors will be relatively insignificant in space, assuming the antenna is properly designed and placed. Since both receivers must be tracking the same GPS satellites, these applications are limited by the distance between the receivers. If the receivers are too far, there will not be enough common SV's to obtain an accurate relative navigation solution. In some instances, if they are relatively close, the line of sight of one vehicle to a SV may be blocked by the other vehicle. Nonetheless, in applications where RGPS is feasible, significant improvements in accuracy of navigation is possible.

2.3 Kalman Filtering

One method of estimating a desired signal, or state, from noisy measurements, such as pseudoranges and delta-ranges, is to use a filtering technique. In 1960, R. E. Kalman introduced the Kalman filter, an algorithm which took advantage of a new tool - the digital computer. Though over 30 years old, this technique remains widely used by engineers who have adapted the filter for use in many applications. These applications include navigation, surveying, vehicle tracking, geology, oceanography, fluid dynamics, steel/paper/power industries, and demographic estimation.^[20]

Immediately following is a summary of the equations for a discrete Kalman filter taken from Brown.^[6] **Figure 2.5** also illustrates the Kalman filter for quick reference.

The basic assumption for the Kalman filter is that the random process to be estimated is modeled as both linear and first order and is expressed as

$$x_{i+1} = \Phi_i x_i + w_i \quad (2.3)$$

The measurements are assumed to be taken at discrete points of time according to the linear relationship

$$z_i = H_i x_i + v_i \quad (2.4)$$

where

$x_i = (n \times 1)$ state vector at time t_i

$\Phi_i = (n \times n)$ matrix relating x_i to x_{i+1} in the absence of a forcing function (if x_i is a sample of a continuous process, Φ_i is the State Transition Matrix (STM))

$w_i = (n \times 1)$ vector - assumed to be a white sequence with known covariance structure

$z_i = (m \times 1)$ vector measurement at time t_i

$H_i = (m \times n)$ matrix giving the ideal (noiseless) relationship between the measurement and the state vector at t_i

$v_i = (m \times 1)$ measurement error - assumed to be a white sequence with known covariance structure and having zero correlation with the w_i sequence

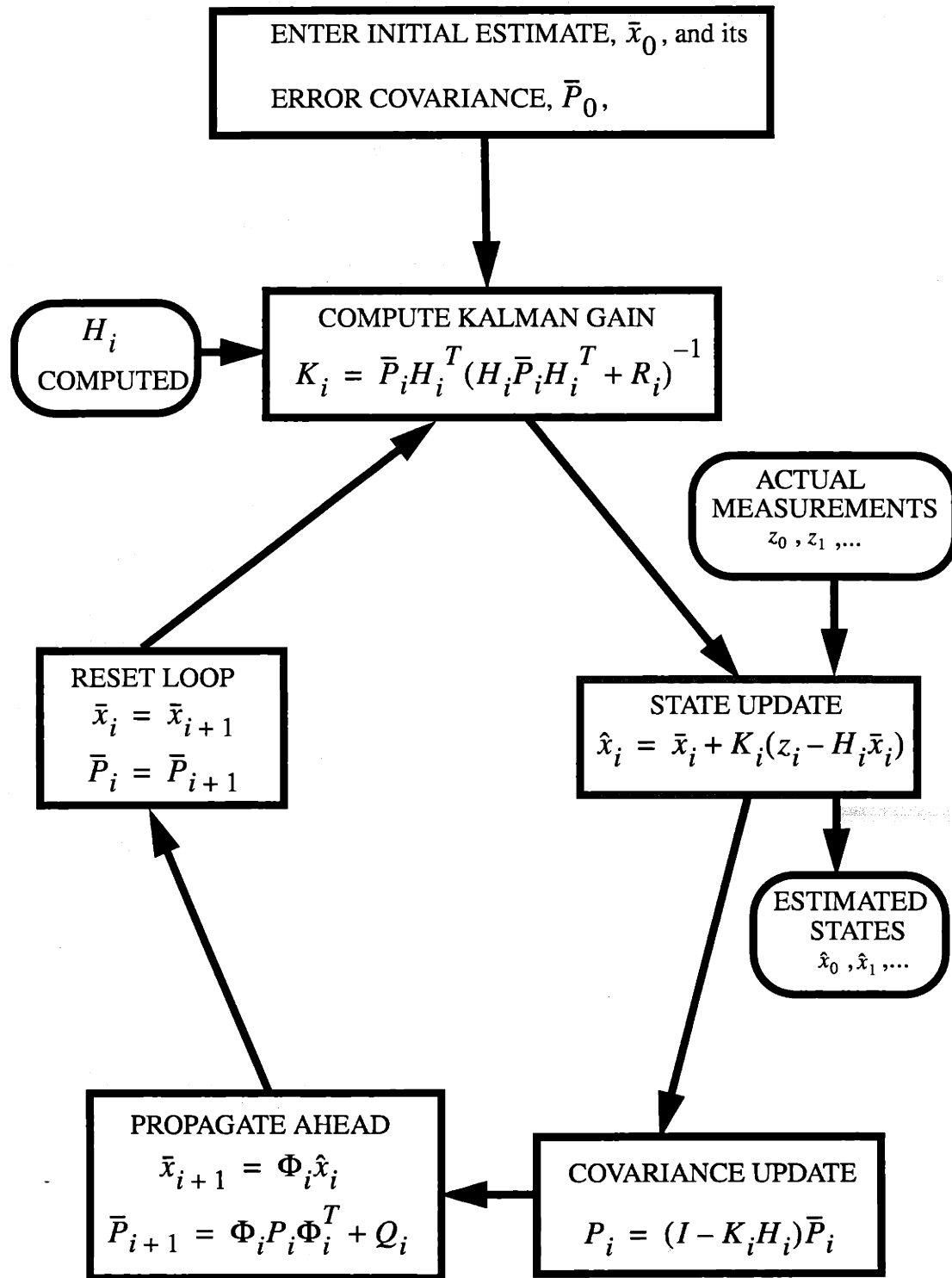


Figure 2.5: The Discrete Kalman Filter

The covariance matrices for the w_i and v_i vectors are given by

$$E[w_i w_k^T] = \begin{cases} Q_i, & k = i \\ 0, & k \neq i \end{cases} \quad (2.5)$$

$$E[v_i v_k^T] = \begin{cases} R_i, & k = i \\ 0, & k \neq i \end{cases} \quad (2.6)$$

$$E[w_i v_k^T] = 0 \quad (2.7)$$

where $E[\]$ is the expected value function.

An initial estimate of the process at time t_i based on all knowledge about the process prior to t_i is known. This prior, or *a priori*, estimate will be denoted as \bar{x}_i . Mathematically, \bar{x}_i is defined as

$$\bar{x}_i = E[x_i | y_{i-1}] \quad (2.8)$$

where x_i = the unknown, true state

y_{i-1} = a sequence of measurement data with the last measurement taken at t_{i-1}

$x_i | y_{i-1}$ = x_i conditioned on y_{i-1}

The difference between the *a priori* estimate and the true state is defined as the *a priori* estimate error, \bar{e}_i :

$$\bar{e}_i = \bar{x}_i - x_i \quad (2.9)$$

The estimate error is assumed to be unbiased, that is, the expected value is zero. The error covariance matrix associated with \bar{x}_i , \bar{P}_i , is defined by

$$\bar{P}_i = E[\bar{e}_i \bar{e}_i^T | y_{i-1}] \quad (2.10)$$

The Kalman filter updates the state by optimally “blending” the prior estimate with the noisy measurements according to

$$\hat{x}_i = \bar{x}_i + K_i(z_i - H_i \bar{x}_i) \quad (2.11)$$

where

\hat{x}_i = updated and best estimate of the true state, x_i

K_i = blending factor^[6], or Kalman gain

Similarly, the updated estimate, \hat{x}_i , is defined as

$$\hat{x}_i = E[x_i | y_i] \quad (2.12)$$

In this case the measurement sequence ends at t_i due to the knowledge of the “current” measurement.

The difference between the updated estimate and the true state is defined as the updated estimate error^[33], e_i :

$$e_i = \hat{x}_i - x_i \quad (2.13)$$

As before, the estimate error is assumed to be unbiased,. The error covariance matrix associated with \hat{x}_i , P_i , is defined by^[33]

$$P_i = E[e_i e_i^T | y_i] \quad (2.14)$$

with the sequence, once again, ending at t_i because of the current measurement. This matrix is computed from

$$P_i = (I - K_i H_i) \bar{P}_i \quad (2.15)$$

The Kalman gain, or the optimal blending factor, K_i , required in **Equation (2.11)** is found by minimizing the mean-square estimate error which leads to

$$K_i = \bar{P}_i H_i^T (H_i \bar{P}_i H_i^T + R_i)^{-1} \quad (2.16)$$

In order to continue the loop, an *a priori* estimate of the state and an associated covariance will be needed. This is done by projecting or propagating the state and covariance forward with

$$\bar{x}_{i+1} = \Phi_i \hat{x}_i \quad (2.17)$$

and

$$\bar{P}_{i+1} = \Phi_i P_i \Phi_i^T + Q_i \quad (2.18)$$

Equation (2.17) ignores the additional contribution of w_k given in **Equation (2.3)** since w_k has zero mean and is not correlated with any of the previous w 's. This propagation step is the focus of this thesis. Note that the state need not be propagated with a state transition matrix. Certain dynamics may be assumed and used to propagate forward in time by various methods such as integration. The propagation techniques used in this study are presented in **Chapter 4**.

The loop for the Kalman filter is now complete and can be repeated as many times as there are measurements for updating the state. In summary, the recursive equations associated with the Kalman filter constitute an algorithm that processes discrete measurements, z_i , into optimal estimates, \hat{x}_i .^[6]

2.4 Chapter Summary

This chapter provided the background in the theory and applications used in this study. Specifically, a system summary of GPS, the measurements it provides, and the associated measurement errors were presented. This was followed by a description of RGPS and Kalman filtering. The following chapter describes how the orbit and the GPS measurements presented in this chapter are modeled.

Chapter 3

Orbit and GPS Models

This chapter describes the models used to determine the orbits of the chaser and target vehicles and the pseudorange and delta-range measurements they obtain from the GPS satellites. Specifically, the models for generating SA, clock bias, clock drift, and white noise are presented. Prior to the model descriptions, the coordinate frames used throughout this thesis are presented. A summary of the models and a description of how GDOP is calculated conclude the chapter.

3.1 Reference Frames

Several frames are used for this study and conversions from one to another are done frequently. **Figure 3.1** depicts a summary of the frames used. The inertial frame, denoted with the letter I, is centered at the Earth's center and is non-rotating. The I frame's x-axis is aligned with the vernal equinox direction, the z-axis is aligned with the north pole, and the y-axis is perpendicular to the other two axes. The Earth-Centered, Earth-Fixed (ECEF) coordinate frame is also centered at the Earth's center. This frame, however, rotates with the Earth and its x-axis is in the equatorial plane always pointing towards the Greenwich Meridian. [28, pp. 31-32] Since the intent of this filter is to predict relative position and velocity a third frame is used called the Hill frame, denoted in **Figure 3.1** with the letter H. The origin of this frame is centered at the target vehicle, with the x-axis along the direction of motion, the z-axis directed radially inward along the local vertical, and the y-axis normal to the target orbit plane to complete the right-hand system. Note that the Hill frame is a

rotating, curvilinear frame; rotating because the origin is fixed on the target and curvilinear because the distance measured along the x-axis is the distance along and on the trajectory of the target vehicle.

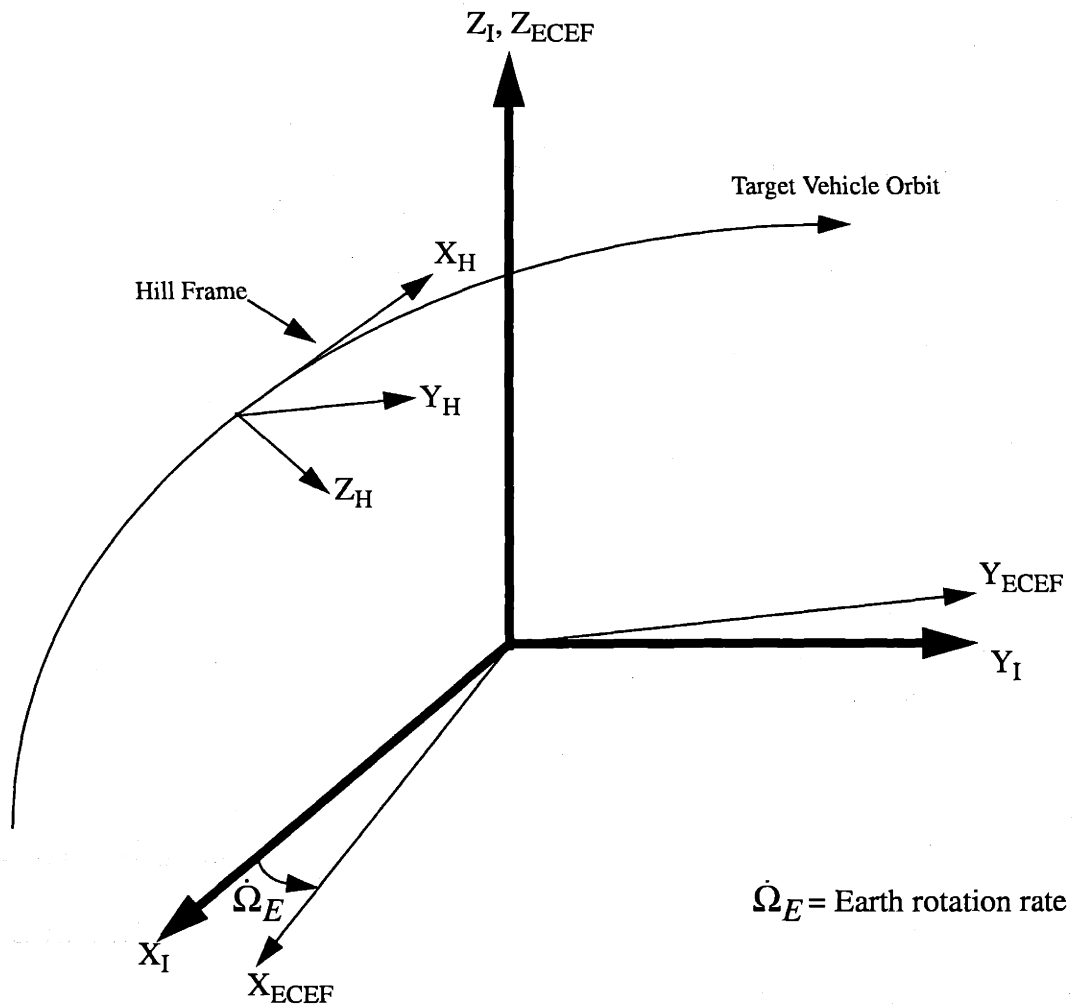


Figure 3.1: Summary of Reference Frames

3.2 Orbit Model

The first step in this study is to determine the trajectories of both the chaser and target vehicles which are simulated as non-maneuvering and in LEO. This begins with the determination of the initial position and velocity of each vehicle.

3.2.1 Determination of Initial Position and Velocity Values

The initial position and velocity of each orbit are determined by choosing the classical orbital elements at epoch of each orbit. These elements are given in **Table 3.1** and shown graphically in **Figure 3.2**.

Term	Symbol
Semimajor Axis	a
Eccentricity	e
Angle of Inclination	i
Longitude of Ascending Node	Ω
Argument of Periapse	ω
True Anomaly	f

Table 3.1: Terminology and Symbols of Orbital Elements

The frame used in **Figure 3.2** is the inertial frame defined in the previous section. The longitude of the ascending node is the angle along the equatorial plane between the x-axis of the inertial frame and the intersecting line between the orbital plane and the equatorial plane. The argument of periapse is along the orbital plane from this intersecting line to the line of periapse. The angle from the line of periapse to the position vector of the vehicle is

the true anomaly. The angular momentum vector, \vec{h} , is perpendicular to the orbital plane and the angle between this vector and the z-axis is the angle of inclination. The semimajor axis and eccentricity are shown in the top view of the orbit at the bottom of the figure.

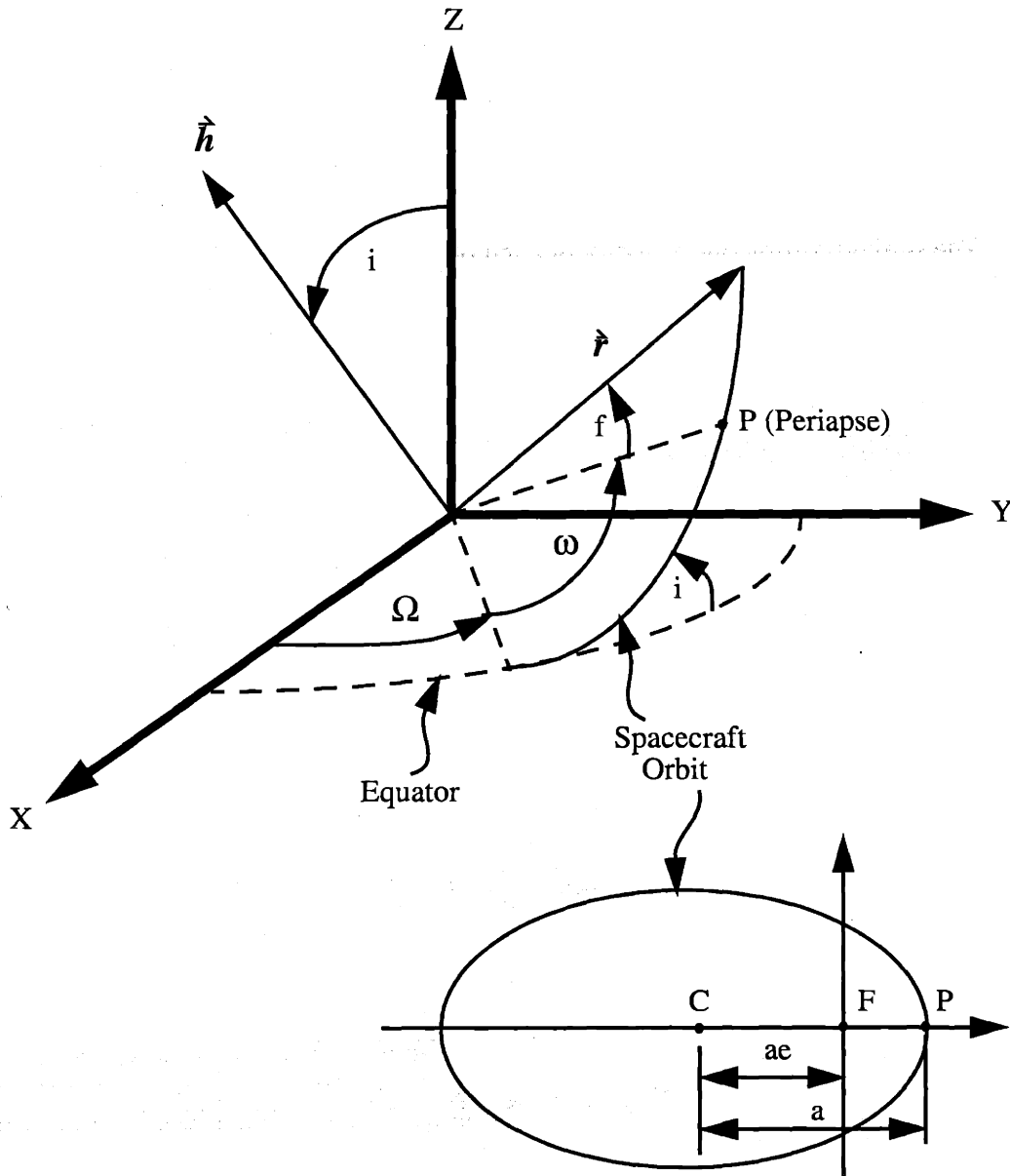


Figure 3.2: Orbit Geometry

Once the initial orbital elements and true anomaly are chosen, the corresponding initial position and velocity are obtained from [4]

$$\begin{aligned}\vec{r} = & r(\cos\Omega\cos\theta - \sin\Omega\sin\theta\cos i)\vec{i}_x \\ & + r(\sin\Omega\cos\theta + \cos\Omega\sin\theta\cos i)\vec{i}_y \\ & + r\sin\theta\sin i\vec{i}_z\end{aligned}\quad (3.1)$$

$$\begin{aligned}\vec{v} = & -\frac{\mu}{h}[\cos\Omega(\sin\theta + e\sin\omega) + \sin\Omega(\cos\theta + e\cos\omega)\cos i]\vec{i}_x \\ & -\frac{\mu}{h}[\sin\Omega(\sin\theta + e\sin\omega) - \cos\Omega(\cos\theta + e\cos\omega)\cos i]\vec{i}_y \\ & +\frac{\mu}{h}(\cos\theta + e\cos\omega)\sin i\vec{i}_z\end{aligned}\quad (3.2)$$

where

$\theta = \omega + f =$ the argument of latitude

$\vec{h} = \vec{r} \times \vec{v} = \sqrt{\mu a(1 - e^2)}\vec{i}_h =$ angular momentum vector

$\mu =$ Earth gravitational parameter $= 3.986005 \times 10^{14} \frac{m^3}{s^2}$

3.2.2 Orbit Propagation

The chaser and target vehicle orbits are modeled as nominally elliptical with perturbations due to the Earth's oblateness. The initial values of the position and velocity of each vehicle define the vehicle's orbit. These values are propagated forward by integrating the equations of motion described in the following paragraphs.

Assuming a two-body problem and a perfectly spherical earth with constant density, the trajectory of an orbiting vehicle can be determined using Newton's equations of motion:

$$\ddot{\vec{r}} + \frac{\mu}{r^3} \vec{r} = 0 \quad (3.3)$$

However, since the earth is actually oblate and asymmetric, perturbations exist which would result in significant errors in the solution to **Equation (3.3)**. These perturbations are accounted for through the use of a potential function, ϕ . If a potential function can adequately describe the perturbations, the resulting acceleration can be determined from

$$\dot{\vec{a}} = \nabla\phi = \frac{\partial\phi}{\partial x}\hat{i}_x + \frac{\partial\phi}{\partial y}\hat{i}_y + \frac{\partial\phi}{\partial z}\hat{i}_z \quad (3.4)$$

and one such potential function, according to Vinti is^[2]

$$\phi = \frac{\mu}{r} \left[1 - \sum_{n=2}^{\infty} J_n \left(\frac{r_E}{r} \right) P_n \sin L \right] \quad (3.5)$$

where

J_n = coefficients determined from experimental observation

r_E = equatorial radius of the earth = $6.378136 \times 10^6 m$

P_n = Legendre polynomials

$L = a \sin \frac{z}{r} =$ geocentric latitude.

The first four terms of **Equation (3.5)** are

$$\phi = \frac{\mu}{r} \left[1 - \frac{J_2}{2} \left(\frac{r_E}{r} \right)^2 (3 \sin^2 L - 1) - \frac{J_3}{2} \left(\frac{r_E}{r} \right)^3 (5 \sin^3 L - 3 \sin L) - \frac{J_4}{8} \left(\frac{r_E}{r} \right)^4 (35 \sin^4 L - 30 \sin^2 L + 3) \right] \quad (3.6)$$

where for the Earth

$$J_2 = \text{second zonal harmonic} = 1.082628 \times 10^{-3}$$

$$J_3 = \text{third zonal harmonic} = -2.538 \times 10^{-6}$$

$$J_4 = \text{fourth zonal harmonic} = -1.593 \times 10^{-6}$$

To obtain the acceleration, the partial derivative of ϕ is taken which yields

$$\ddot{x} = -\frac{\mu x}{r^3} \left[1 - J_2 \frac{3}{2} \left(\frac{r_E}{r} \right)^2 \left(5 \frac{z^2}{r^2} - 1 \right) + J_3 \frac{5}{2} \left(\frac{r_E}{r} \right)^3 \left(3 \frac{z}{r} - 7 \frac{z^3}{r^3} \right) - J_4 \frac{5}{8} \left(\frac{r_E}{r} \right)^4 \left(3 - 42 \frac{z^2}{r^2} + 63 \frac{z^4}{r^4} \right) \right] \quad (3.7)$$

$$\ddot{y} = -\frac{\mu y}{r^3} \left[1 - J_2 \frac{3}{2} \left(\frac{r_E}{r} \right)^2 \left(5 \frac{z^2}{r^2} - 1 \right) + J_3 \frac{5}{2} \left(\frac{r_E}{r} \right)^3 \left(3 \frac{z}{r} - 7 \frac{z^3}{r^3} \right) - J_4 \frac{5}{8} \left(\frac{r_E}{r} \right)^4 \left(3 - 42 \frac{z^2}{r^2} + 63 \frac{z^4}{r^4} \right) \right] \quad (3.8)$$

$$\ddot{z} = -\frac{\mu z}{r^3} \left[1 + J_2 \frac{3}{2} \left(\frac{r_E}{r} \right)^2 \left(3 - 5 \frac{z^2}{r^2} \right) + J_3 \frac{3}{2} \left(\frac{r_E}{r} \right)^3 \left(10 \frac{z}{r} - \frac{35 z^3}{3 r^3} - \frac{r}{z} \right) - J_4 \frac{5}{8} \left(\frac{r_E}{r} \right)^4 \left(15 - 70 \frac{z^2}{r^2} + 63 \frac{z^4}{r^4} \right) \right] \quad (3.9)$$

Note that $\sin L$ was replaced by $\frac{z}{r}$. Also note that if J_2 , J_3 , and J_4 are set to zero, or if only the first terms in **Equations (3.7)**, **(3.8)**, and **(3.9)** are considered, the resulting equations are the same as Newton's two-body equation, **Equation (3.3)**, in component form, as

expected.

Finally, since both vehicles are in LEO, acceleration due to drag is also modeled. Since drag is opposite to the velocity of the vehicle relative to the atmosphere,^[2] the first step is to determine the velocity of the atmosphere. This is taken to be

$$\dot{\mathbf{v}}_{atm} = \dot{\boldsymbol{\omega}}_E \times \mathbf{r} \quad (3.10)$$

where

$$\dot{\boldsymbol{\omega}}_E = \begin{bmatrix} 0 \\ 0 \\ \dot{\Omega}_E \end{bmatrix} = \text{Earth angular velocity}$$

The relative velocity of the vehicle with respect to the atmosphere can then be calculated from

$$\dot{\mathbf{v}}_{rel} = \dot{\mathbf{v}} - \dot{\mathbf{v}}_{atm} \quad (3.11)$$

where $\dot{\mathbf{v}}$ = vehicle velocity

The acceleration due to drag is determined by

$$\dot{\mathbf{a}}_d = -a_d \hat{\mathbf{v}}_{rel} \quad (3.12)$$

where

$$a_d = \frac{1}{2} \frac{\rho_d}{m} v_{rel}^2 S c_d \cong 5 \times 10^{-8} \frac{m}{s} \quad 1$$

1. D'Souza, C.N., *personal communication*, The Charles Stark Draper Laboratory, Inc., December 1997.

ρ_d = atmospheric density at vehicle's altitude

m = mass of vehicle

S = cross-sectional area of vehicle perpendicular to $\hat{\mathbf{v}}_{rel}$

c_d = coefficient of drag

$\hat{\mathbf{v}}_{rel} = \frac{\mathbf{v}_{rel}}{v_{rel}}$ = unit vector of relative velocity

Each component of the acceleration due to drag, a_{d_x} , a_{d_y} , and a_{d_z} are added to **Equations (3.7), (3.8), and (3.9)**, respectively. This yields the total perturbations which are accounted for in the modeling of the orbits. For completeness, these equations are:

$$\ddot{x} = -\frac{\mu x}{r^3} \left[1 - J_2 \frac{3}{2} \left(\frac{r_E}{r} \right)^2 \left(5 \frac{z^2}{r^2} - 1 \right) + J_3 \frac{5}{2} \left(\frac{r_E}{r} \right)^3 \left(3 \frac{z}{r} - 7 \frac{z^3}{r^3} \right) - J_4 \frac{5}{8} \left(\frac{r_E}{r} \right)^4 \left(3 - 42 \frac{z^2}{r^2} + 63 \frac{z^4}{r^4} \right) \right] + a_{d_x} \quad (3.13)$$

$$\ddot{y} = -\frac{\mu y}{r^3} \left[1 - J_2 \frac{3}{2} \left(\frac{r_E}{r} \right)^2 \left(5 \frac{z^2}{r^2} - 1 \right) + J_3 \frac{5}{2} \left(\frac{r_E}{r} \right)^3 \left(3 \frac{z}{r} - 7 \frac{z^3}{r^3} \right) - J_4 \frac{5}{8} \left(\frac{r_E}{r} \right)^4 \left(3 - 42 \frac{z^2}{r^2} + 63 \frac{z^4}{r^4} \right) \right] + a_{d_y} \quad (3.14)$$

$$\ddot{z} = -\frac{\mu z}{r^3} \left[1 + J_2 \frac{3}{2} \left(\frac{r_E}{r} \right)^2 \left(3 - 5 \frac{z^2}{r^2} \right) + J_3 \frac{3}{2} \left(\frac{r_E}{r} \right)^3 \left(10 \frac{z}{r} - \frac{35z^3}{3r^3} - \frac{r}{z} \right) - J_4 \frac{5}{8} \left(\frac{r_E}{r} \right)^4 \left(15 - 70 \frac{z^2}{r^2} + 63 \frac{z^4}{r^4} \right) \right] + a_{d_z} \quad (3.15)$$

Now, given initial conditions in position and velocity, **Equations (3.13), (3.14), and (3.15)** can be integrated to obtain the position and velocity for future times. The method of integration used in this study is the Fourth Order Runge-Kutta technique. ^[34]

3.3 GPS Simulation

Once the trajectories have been created the pseudorange and delta-range measurements can be obtained. Most of the GPS related models described in this section are based on a GPS software simulator created by Paul J. Lawrence, Jr., of the C.S. Draper Laboratory. ^[17] An outline of how the components of the simulation are organized is given in **Figure 3.3**.

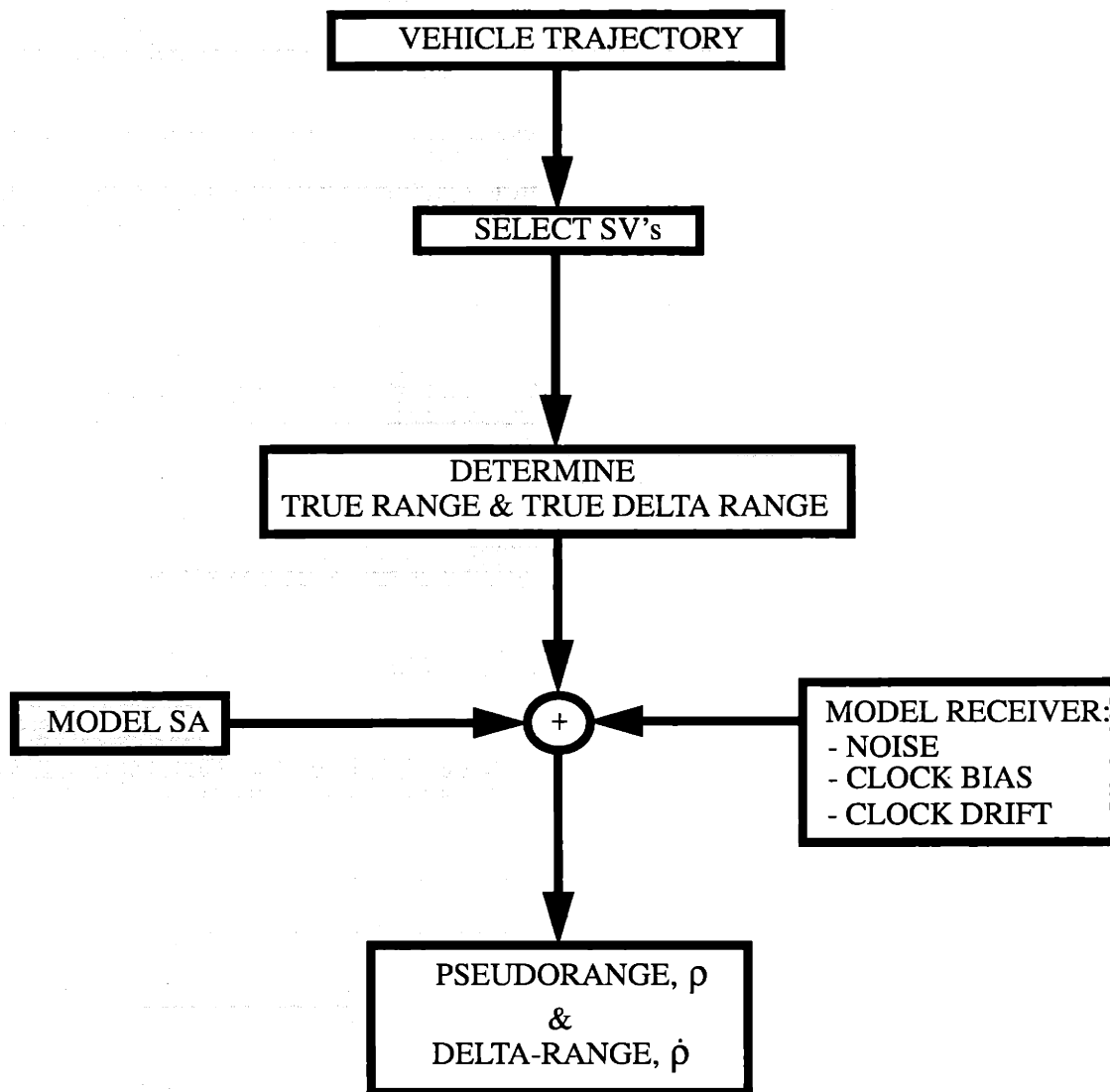


Figure 3.3: Outline of GPS Simulation

The following subsections describe the modeling of these components.

3.3.1 SV Selection and True Range and True Delta-range Determination

The SV trajectories can be determined given their ephemeris data. The ephemeris data transmitted by GPS is updated weekly and data from previous weeks, called almanac data, can be found from various sources. The almanac data from week 889 (third week of January 1997) was used for this study.^[35] A list of the ephemeris data included in this particular almanac is given in **Table 3.2**.

Symbol	Definition
ID	SV identification number
Health	Health status indicator
t_{0e}	Reference time of ephemeris
e	Eccentricity
\sqrt{a}	Square root of semimajor axis
i	Inclination angle
Ω	Longitude of the ascending node
$\dot{\Omega}$	Rate of change of longitude of ascending node
M_0	Mean anomaly at epoch
Af_0	Zero th order clock correction
Af_1	First order clock correction

Table 3.2: GPS Ephemeris Data Definitions^[13, 35]

Given this information the SV's ECEF position vector may be computed using the equations listed in **Table 3.3**.

Equation	Description
$a = (\sqrt{a})^2$	Semimajor axis
$n = \sqrt{\frac{\mu}{a^3}}$	Mean motion
$t_k = t - t_{0e}$	Time from ephemeris epoch
$M_k = M_0 + n(t_k)$	Mean anomaly
$M_k = E_k - e \sin E_k$	Eccentric anomaly (solved iteratively)
$\sin f_k = \frac{\sqrt{1-e^2} \sin E_k}{1 - e \cos E_k}$	True anomaly
$\cos f_k = \frac{\cos E_k - e}{1 - e \cos E_k}$	True anomaly
$\theta_k = f_k + \omega$	Argument of latitude
$r_k = a(1 - e \cos E_k)$	Radius
$\Omega_k = \Omega_0 + (\dot{\Omega} - \dot{\Omega}_e)(t_k) - \dot{\Omega}_e t_{0e}$	Corrected longitude of node
$x_p = r_k \cos \theta_k$	In-plane x position
$y_p = r_k \sin \theta_k$	In-plane y position
$x_{ECEF} = x_p \cos \Omega_k - y_p \sin \Omega_k$	ECEF x-coordinate
$y_{ECEF} = x_p \sin \Omega_k + y_p \cos \Omega_k$	ECEF y-coordinate
$z_{ECEF} = y_p \sin i$	ECEF z-coordinate

Table 3.3: Computation of a Satellite's ECEF Position Vector^[13]

The user's and SV's trajectories are used to select which SV's, from the ones visible, should be used by the user. Many algorithms exist for this purpose including algorithms that choose the SV's based on minimum GDOP and those that base their selection on maximum time of visibility. The SV selection algorithm^[32] used for this study selects the satellites that closely approximate the minimum GDOP selection, which would be the optimum choice as discussed in **Chapter 2**. The algorithm assumes that the receiver antennas are oriented towards the nadir direction and requires the position and velocity of the user, time of measurements, SV ephemeris, number of channels in the receiver, ID's of unhealthy satellites, and mask angle of the receiver. The mask angle is the angle measured from the horizon through which the receiver ignores the SV signal. For this study, this angle was set to 15 degrees which is representative of GPS space-based receivers. The number of channels for the receiver was set to six, which is representative of GPS receivers chosen for the ISS. The algorithm avoids costly and computationally burdensome searches by closely approximating the minimum GDOP selection. A comparison was made between this routine and an algorithm that bases its choice of satellites on minimum GDOP exactly and it was found that the two methods produce similar results despite the approximation.

The SV selection algorithm determines the satellites that the receivers on both the chaser and target vehicles would choose independently. The next step combines the results of the satellites chosen by the target vehicle with those chosen by the chaser vehicle and determines the common SV's which, as discussed in **Section 2.2**, are required for RGPS. It is these common SV's that are finally chosen for use in the relative navigation scheme.

Determining the true range between the vehicles and the selected SV's is done by differencing their respective positions at each time step. The true delta-range is then determined by differencing the successive ranges.

The remaining subsections describe the models of the errors that are added to the true range and true delta-range in order to obtain the simulated pseudoranges and delta-ranges.

3.3.2 SA Model

The technique used to simulate SA in the GPS simulator is an eleventh order model, referred to as the AutoRegressive (AR) model.^[5] In a study of the existing models, Lawrence^[17] showed the AR mode appears to be the most statistically accurate representation of SA. SA is generated in each SV and is uncorrelated between SV's. The amplitude of SA error ranges from 40 to 70 meters maximum with oscillations of periods between 5 to 20 minutes. SA errors result from intentionally producing orbit errors by adding epsilon errors into the broadcast ephemeris and clock errors and by intentionally dithering the satellite clock. The AR model obeys the following equation:

$$y(t) = - \sum_{k=1}^p a(k)y(t-k) + \alpha_{SA}(t) \quad (3.16)$$

where

$y(t)$ = model output

p = model order, or number of poles = 11

$a(k)$ = k^{th} filter coefficient, each given in **Table 3.4**

$\alpha_{SA}(t)$ = white Gaussian noise (variance given in **Table 3.4**)

Note that throughout this study, white noise is generated by multiplying the standard deviation (square root of the variance) by the output of a random number generator.

Term	Value	Term	Value
a(01)	- 1.36192741558063	a(07)	+ 0.10063573000351
a(02)	- 0.15866710938728	a(08)	+ 0.02694677520401
a(03)	+ 0.13545921610672	a(09)	- 0.12898590228866
a(04)	+ 0.21501267664869	a(10)	+ 0.05083106570666
a(05)	+ 0.30061078095966	a(11)	- 0.05600186282898
a(06)	- 0.12390183286070	variance, σ_e^2	$1.6993 \times 10^{-5} m^2$

Table 3.4: Coefficients for AR Model

In his study, Lawrence demonstrated that the AR model was an accurate, robust, and statistically equivalent model of smooth SA collected data. An example of the model output and its standard deviation (1σ) is given in **Figure 3.4**.

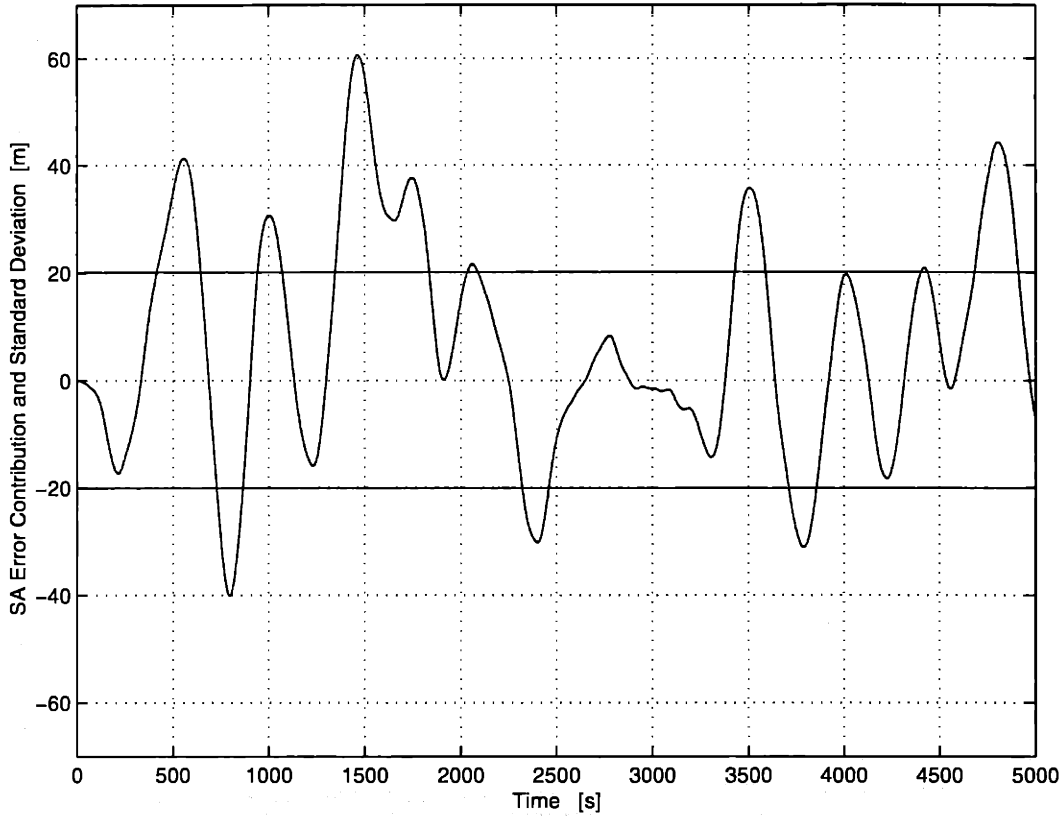


Figure 3.4: Sample Plot of SA Error Contribution to the Pseudorange Measurements

3.3.3 Receiver Clock Errors and White Noise Models

Receiver clock errors include the clock bias, b , and clock drift, d , both of which are required states in any GPS-based navigation estimator.^[28, p. 417] In this study the clock drift is modeled as a random walk, while the clock bias is the integral of this random walk.^[17, 28, pp. 417-419] Mathematically, this is expressed as:

$$d(t) = d(t-1) + \alpha_d(t) \quad (3.17)$$

$$b(t) = b(t-1) + d(t)\Delta t \quad (3.18)$$

where $\alpha_d(t)$ = white noise with variance, $\sigma_d^2 = 2.32 \times 10^{-4} m^2$
 Δt = time increment = 1s

The variance given above corresponds to the 1σ strength, or standard deviation, of the random walk driving noise of $\frac{1}{20} fps$.^[17] Examples of the generated clock drift and clock bias are given in **Figures 3.5** and **3.6**, respectively.

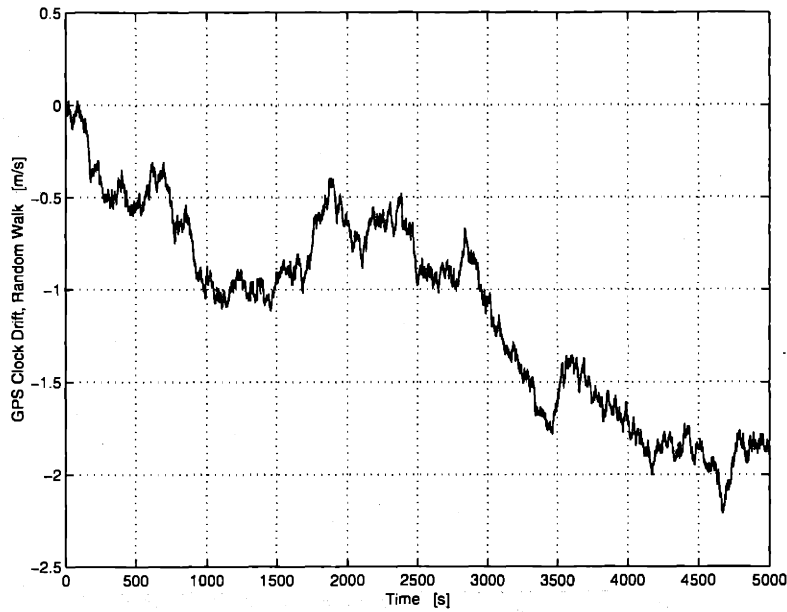


Figure 3.5: GPS Clock Drift, Random Walk

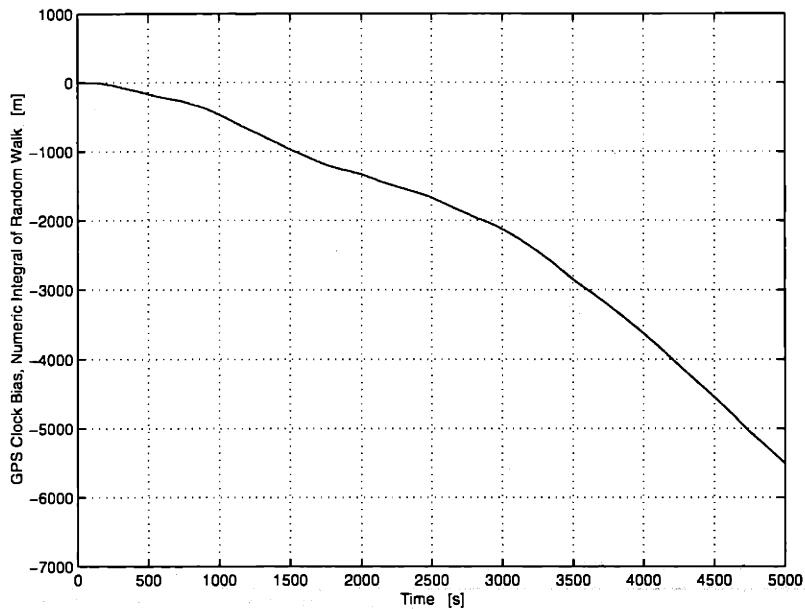


Figure 3.6: GPS Clock Bias, the Integral of Random Walk

The final measurement error modeled is the receiver noise affecting both the pseudorange and delta-range. This was modeled as white Gaussian noise with the variances given in **Table 3.5**

Variance	Value
σ_{ρ}^2	32 m^2
$\sigma_{\dot{\rho}}^2$	$5 \times 10^{-5} \frac{\text{m}^2}{\text{s}^2}$

Table 3.5: Pseudorange and Delta-range White Noise Variances

Since the dominant error in pseudorange is that associated with the clock bias, the total noise contribution looks mostly like **Figure 3.6**. The receiver noise is added to the SA only error, **Figure 3.4**, to demonstrate the effects of this white noise. This is depicted in **Figure 3.7**.

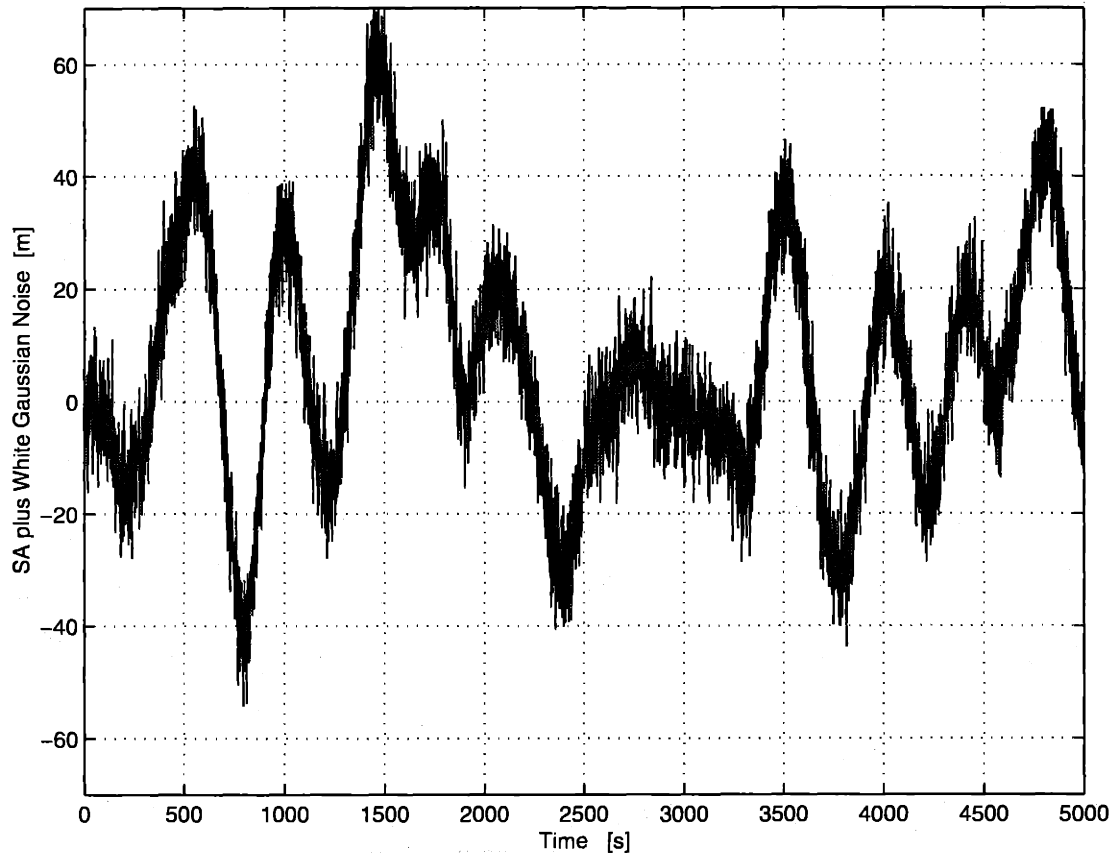


Figure 3.7: GPS Pseudorange Measurement Error Less GPS Clock Bias

3.4 Summary of Models

A summary of the models presented in this chapter is depicted in **Table 3.6**.

Model of	Inputs	Techniques
Vehicle Trajectory	Initial Orbital Elements	4 th Order Runge-Kutta
SV Selection	Vehicle Trajectory Time of Measurements SV Ephemeris Number of Receiver Channels = 6 Unhealthy SV ID's Mask Angle= 15°	Minimum GDOP Approximation
True Range and True Delta-range	Vehicle Orbits SV Orbits	Difference
SA	model order, $p = 11$ $a(k)$ filter coefficients (Table 3.4) white noise, $\sigma_e^2 = 1.6993 \times 10^{-5} m^2$	AR model
Receiver Clock Errors	$\sigma_d^2 = 2.32 \times 10^{-4} m^2$ ($\sigma_d = \frac{1}{20} fps$)	Numeric Integral of Random Walk
Receiver White Noise	$\sigma_p^2 = 32 m^2$ $\sigma_{\dot{p}}^2 = 5 \times 10^{-5} \frac{m^2}{s}$	White Gaussian Noise
Pseudorange and Delta-range	True Range and True Delta-range SA Receiver Clock Errors and White Noise	Summation

Table 3.6: Summary of Models

3.5 GDOP Considerations

Receiving GPS navigation messages from a minimum of four SV's does not ensure an accurate prediction of the relative position and relative velocity. As discussed in **Chapter 2**, the geometry of the selected satellites has a significant effect on the accuracy of the navigation solution. Specifically, GDOP values of greater than six can result in an inaccurate solution.^[12] Therefore, once the common satellites are determined, the corresponding values of GDOP are computed with respect to both the chaser and target vehicles. The method by which GDOP is calculated is summarized below.

The first step is to create a matrix:

$$N = \begin{bmatrix} a_{x1} & a_{y1} & a_{z1} & 1 \\ a_{x2} & a_{y2} & a_{z2} & 1 \\ \dots & \dots & \dots & \dots \\ a_{xs} & a_{ys} & a_{zs} & 1 \end{bmatrix} \quad (3.19)$$

where s = number of selected satellites

and $\hat{a}_i = (a_{xi}, a_{yi}, a_{zi})$ are the unit vectors pointing from the user to the location of the i^{th} satellite, otherwise known as the line of sight vectors. The next step creates another matrix

$$\begin{bmatrix} D_{11} & D_{12} & D_{13} & D_{14} \\ D_{21} & D_{22} & D_{23} & D_{24} \\ D_{31} & D_{32} & D_{33} & D_{34} \\ D_{41} & D_{42} & D_{43} & D_{44} \end{bmatrix} = (N^T N)^{-1} \quad (3.20)$$

and finally the value for GDOP is obtained from

$$GDOP = \sqrt{D_{11} + D_{22} + D_{33} + D_{44}} \quad (3.21)$$

An algorithm using the above equations was used to compute the GDOP for all the cases. An example case is presented in **Figure 3.8**.

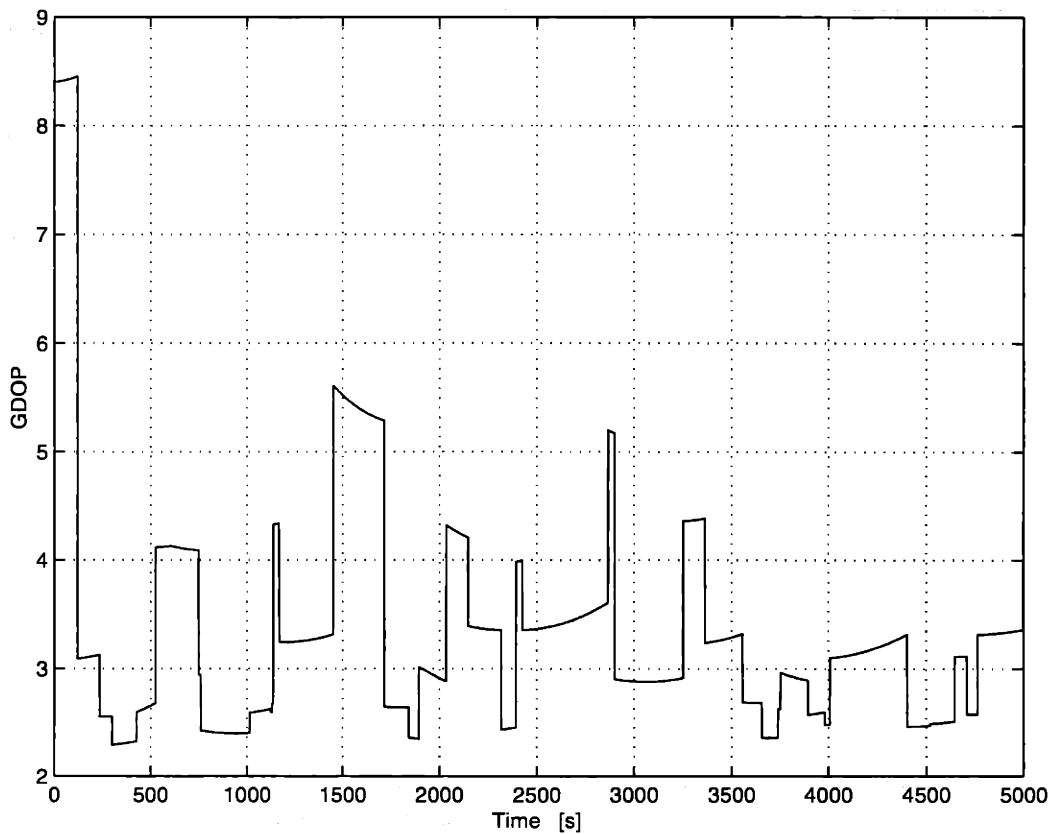


Figure 3.8: Sample Plot of GDOP

Note that the values of GDOP for approximately the first hundred seconds of the sample plot are greater than six. The effects of poor GDOP on the relative navigation filter can be observed during that time period.

3.6 Chapter Summary

The reference frames used throughout this study were presented. This was followed by a description of how the chaser and target orbits were modeled. Specifically, this chapter described the method by which the initial position and velocity of each vehicle were determined. It also described the technique used to propagate these initial values to obtain the vehicle's orbit. Then, the models used to simulate GPS, which included models of SA, receiver clock errors, and white noise were depicted. A summary of all the models was given in **Table 3.6**. Finally, GDOP considerations were addressed and the equations used to determine GDOP were presented. The next chapter presents the design of the relative navigation filter which uses the measurements and orbits modeled in this chapter to estimate the relative position and velocity between the vehicles.

Chapter 4

Filter Design

This chapter delves into the design of the relative navigation (Kalman) filter. Specifically, it describes the state and dynamics of the filter, focusing on the various propagation techniques studied. It also describes how the measurement matrix, H , and the initial covariance matrix, \bar{P}_0 , are obtained, and finally how the covariance is propagated.

4.1 Filter State

Since the intent of relative GPS navigation is to predict the relative position and relative velocity of the chaser vehicle with respect to the target vehicle, the Hill frame depicted in **Figure 3.1** was chosen for describing the relative state. The state, therefore, includes the relative position and velocity in the Hill frame. Since knowledge of the clock bias and clock drift improves the accuracy of position and velocity, these quantities are also included in the state. Mathematically, the state is expressed as

$$x = \begin{bmatrix} x_H \\ y_H \\ z_H \\ u_H \\ v_H \\ w_H \\ \Delta b \\ \Delta d \end{bmatrix} \quad (4.1)$$

where

x_H, y_H, z_H = Chaser-Target relative position
 components in Target centered Hill frame

u_H, v_H, w_H = Chaser-Target relative velocity
 components in Target centered Hill frame

Δb = difference of Chaser/Target GPS receiver clock bias

Δd = difference of Chaser/Target GPS receiver clock drift.

4.2 State Dynamics

The theme of this thesis is to explore the effects of various propagation techniques on RGPS navigation. Therefore, four methods are used to propagate the state. These techniques propagate the state through the use of the following:

- STM based on the Clohessy-Wiltshire (C-W) equations
- Universal Keplerian State Transition Matrix
- First-order equations of relative motion which include J_2 effects and are combined with a second-order conic approximation
- Integration of the equations of motion

These four techniques are described in detail in the following subsections.

Note that the first technique is the only one in which the state is propagated by being pre-multiplied with the STM as described in **Chapter 2**. The remaining techniques require the state to be converted to two independent orbits in the inertial frame, each propagated forward in time, and then converted back to the relative Hill frame of the filter state.

The target vehicle will navigate using absolute GPS; therefore, an estimate of its inertial position and velocity will be known. Combining that knowledge with the estimated state, the inertial position and velocity of the chaser vehicle can be obtained. The conversions between the Hill frame and the inertial frame are presented in **Appendix A**.

4.2.1 The Clohessy and Wiltshire (C-W) Equations of Relative Motion

In 1960, Clohessy and Wiltshire published an article containing the equations of relative motion of two orbiting vehicles.^[8] The C-W equations are also referred to as the Hill equations because of work Hill performed on the Moon's relative motion in 1878. These differential equations describe the motion of small state deviations from a circular orbit, which is assumed to be the target orbit, in a rotating local-vertical coordinate system, the Hill frame.^[4] For the Hill frame described in **Section 3.1**, the C-W equations are

$$\ddot{x} + 2n\dot{z} = 0 \quad (4.2)$$

$$\ddot{y} + 2n^2\dot{y} = 0 \quad (4.3)$$

$$\ddot{z} - 3n^2z + 2\omega\dot{x} = 0 \quad (4.4)$$

where
$$n = \sqrt{\frac{\mu}{r_T^3}} = \text{mean motion of the target vehicle orbit}$$

The system is modeled as

$$\dot{x} = Ax + w \quad (4.5)$$

where A = system matrix

The last two elements of the filter state, Δb and Δd , obey the following equations:

$$\dot{\Delta b} = \Delta d \quad (4.6)$$

$$\dot{\Delta d} = 0 \quad (4.7)$$

Therefore, **Equations (4.2 - 4), (4.6) and (4.7)** form the system matrix, A :

$$A = \begin{bmatrix} 0 & 0 & 0 & 1 & 0 & 0 & 0 & 0 \\ 0 & 0 & 0 & 0 & 1 & 0 & 0 & 0 \\ 0 & 0 & 0 & 0 & 0 & 1 & 0 & 0 \\ 0 & 0 & 0 & 0 & 0 & -2n & 0 & 0 \\ 0 & -n^2 & 0 & 0 & 0 & 0 & 0 & 0 \\ 0 & 0 & 3n^2 & 2n & 0 & 0 & 0 & 0 \\ 0 & 0 & 0 & 0 & 0 & 0 & 0 & 1 \\ 0 & 0 & 0 & 0 & 0 & 0 & 0 & 0 \end{bmatrix} \quad (4.8)$$

The system matrix, A , is converted to the state transition matrix, Φ , of **Equation (2.3)** by using the definition of the state transition matrix^[24, p. 42]:

$$\Phi = e^{At} \quad (4.9)$$

which can be expanded into

$$e^{At} = I + A\Delta t + \frac{1}{2}A^2\Delta t^2 + \dots \quad (4.10)$$

An approximation may be made to the second order, for instance, to simplify calculations. However, for the purpose of this study the transition matrix is obtained exactly using^[24, p. 42]

$$\Phi = [\mathcal{L}^{-1}[(sI - A)^{-1}]]_{t = \Delta t} \quad (4.11)$$

which yields

$$\Phi_{CW} = \begin{bmatrix} 1 & 0 & 6(\sin n\Delta t - n\Delta t) & 4\sin n\Delta t - 3\Delta t & 0 & \frac{2}{n}(1 - \cos n\Delta t) & 0 & 0 \\ 0 & \cos n\Delta t & 0 & 0 & \frac{1}{n}\sin n\Delta t & 0 & 0 & 0 \\ 0 & 0 & 4 - 3\cos n\Delta t & \frac{2}{n}(\cos n\Delta t - 1) & 0 & \frac{1}{n}\sin n\Delta t & 0 & 0 \\ 0 & 0 & 6n(1 - \cos n\Delta t) & 4\cos n\Delta t - 3 & 0 & 2\sin n\Delta t & 0 & 0 \\ 0 & -n\sin n\Delta t & 0 & 0 & \cos n\Delta t & 0 & 0 & 0 \\ 0 & 0 & 3n\sin n\Delta t & -2\sin n\Delta t & 0 & \cos n\Delta t & 0 & 0 \\ 0 & 0 & 0 & 0 & 0 & 0 & 1 & \Delta t \\ 0 & 0 & 0 & 0 & 0 & 0 & 0 & 1 \end{bmatrix} \quad (4.12)$$

4.2.2 Universal Keplerian State Transition Matrix

In 1984 Stanley W. Shepperd published a paper that presented a completely general method for computing the Keplerian STM (KSTM).^[31] It included a new scheme for solving Kepler's problem which is required to compute the KSTM. The equations used to obtain the matrix are presented here. For more detail see [31].

The KSTM linearly propagates state deviations in inertial position and velocity in the following way:

$$\begin{bmatrix} \Delta \dot{r} \\ \Delta \dot{v} \end{bmatrix} = \Phi_K \begin{bmatrix} \Delta \dot{r}_0 \\ \Delta \dot{v}_0 \end{bmatrix} \quad (4.13)$$

where

$$\Phi_K = \begin{bmatrix} \Phi_{11} & \Phi_{12} \\ \Phi_{21} & \Phi_{22} \end{bmatrix} \begin{bmatrix} \frac{\partial}{\partial \dot{r}_0} \dot{r} & \frac{\partial}{\partial \dot{v}_0} \dot{r} \\ \frac{\partial}{\partial \dot{r}_0} \dot{v} & \frac{\partial}{\partial \dot{v}_0} \dot{v} \end{bmatrix} = \text{KSTM} \quad (4.14)$$

and where

$$\Phi_{11} = fI + \begin{bmatrix} \dot{r} & \dot{v} \end{bmatrix} \begin{bmatrix} M_{21} & M_{22} \\ M_{31} & M_{32} \end{bmatrix} \begin{bmatrix} \dot{r}_0 \\ \dot{v}_0 \end{bmatrix} \quad (4.15)$$

$$\Phi_{12} = gI + \begin{bmatrix} \dot{r} & \dot{v} \end{bmatrix} \begin{bmatrix} M_{22} & M_{23} \\ M_{32} & M_{33} \end{bmatrix} \begin{bmatrix} \dot{r}_0 \\ \dot{v}_0 \end{bmatrix} \quad (4.16)$$

$$\Phi_{21} = FI - \begin{bmatrix} \dot{r} & \dot{v} \end{bmatrix} \begin{bmatrix} M_{11} & M_{12} \\ M_{21} & M_{22} \end{bmatrix} \begin{bmatrix} \dot{r}_0 \\ \dot{v}_0 \end{bmatrix} \quad (4.17)$$

$$\Phi_{22} = GI - \begin{bmatrix} \dot{r} & \dot{v} \end{bmatrix} \begin{bmatrix} M_{12} & M_{13} \\ M_{22} & M_{23} \end{bmatrix} \begin{bmatrix} \dot{r}_0 \\ \dot{v}_0 \end{bmatrix} \quad (4.18)$$

I is a (3×3) identity matrix and the state extrapolation coefficients f, g, F, G are defined below:

$$f = 1 - \frac{\mu U_2}{r_0} \quad (4.19)$$

$$g = r_0 U_1 + v_0 U_2 \quad (4.20)$$

$$F = -\frac{\mu U_1}{r r_0} \quad (4.21)$$

$$G = 1 - \frac{\mu U_2}{r} \quad (4.22)$$

The four (2×2) M coefficient matrices are overlapping sub-matrices of the (3×3) M matrix defined by

$$M = \begin{bmatrix} \left(\frac{U_0}{r r_0} + \frac{1}{r_0^2} + \frac{1}{r^2} \right) F - \frac{\mu}{r^3} \frac{\mu}{r_0^3} W & \left| \frac{F U_1}{r} + \frac{G-1}{r^2} \right| & \frac{(G-1)U_1}{r} - \frac{\mu}{r^3} W \\ -\frac{F U_1}{r_0} - \frac{f-1}{r_0^2} & -F U_2 & -(G-1)U_2 \\ \frac{(G-1)U_1}{r_0} - \frac{\mu}{r_0^3} W & (f-1)U_2 & g U_2 - W \end{bmatrix} \quad (4.23)$$

where

$$W = g U_2 + \mu U$$

$$U = \frac{U_2 U_3 + w U_4 - 3 U_5}{3}$$

Even though the M matrix has no obvious physical interpretation it assists in organizing

the coefficients in a compact matrix form. Also note that all the parameters, except for the universal functions, $U_n(w, \beta)$, are obtained from the solution of Kepler's problem. For an explanation of the universal functions refer to [3] or [31].

The KSTM is obtained from the trajectory of the target vehicle. In order to propagate forward, deviations are obtained by differencing the target inertial position and velocity from the respective components of the chaser vehicle. Then **Equation (4.13)** is used to propagate the deviation forward. Since the Kepler problem was already solved for in order to obtain the KSTM, the propagated position and velocity of the target vehicle is known. The propagated deviations are then added to these values to obtain the propagated position and velocity of the chaser vehicle. Finally, these propagated values are converted back to the relative Hill frame of the filter state.

4.2.3 First-order Equations of Relative Motion including J_2 Effects, Combined with a Second-order Conic Approximation

In 1991, Jean A. Kechichian published a paper describing techniques for accurate analytic terminal rendezvous for vehicles in near-circular orbits.^[14] In this paper, Kechichian expanded on the C-W equations by accounting for the perturbation due to the second zonal harmonic, J_2 . He also included a second-order approximation to account for large displacements from the reference orbit. Note that the coordinate frame Kechichian uses is slightly different than the one used in this thesis, such that

$$\begin{aligned}x_K &= -z_H \\y_K &= x_H \\z_K &= -y_H\end{aligned}\tag{4.24}$$

where the subscript, K , annotates Kechichian's frame. Also note that the target position is not assumed to be the center of the relative frame as it was in the Hill frame. Instead, the rotating relative frame is attached to an imaginary, circular orbit, or reference orbit, for each orbiting vehicle. Neither of these differences will pose a problem since the orbits of the vehicles will be propagated separately and the input and output positions and velocities are in the inertial frame. This, of course, means that conversions between the Hill and inertial frame will once again be necessary.

The equations and solutions for the second-order and J_2 corrections are presented below. However, since the equations for the coefficients required in these solutions are lengthy and many, they are included in **Appendix B**. The equations used to obtain the initial conditions and the equations that convert the relative solution to the inertial frame are also included in this appendix.

The second-order corrections to the C-W, or first order, solution are

$$\ddot{x}_2 - 2n\dot{y}_2 - 3n^2 x_2 = \frac{3n^2}{2r_r} (y_1^2 + z_1^2 - 2x_1^2) \quad (4.25)$$

$$\ddot{y}_2 + 2n\dot{x}_2 = \frac{3n^2}{r_r} x_1 y_1 \quad (4.26)$$

$$\ddot{z}_2 + n^2 z_2 = \frac{3n^2}{r_r} x_1 z_1 \quad (4.27)$$

where r_r = radius of the reference of the reference orbit

Note that the forcing terms in the right hand side involve the first-order solution (indicated

with a number "1" in subscript). Also note that in this subsection n refers to the mean motion of the reference orbit, not that of the target. The solution to these differential equations representing the second-order approximation are given by

$$x_2 = \beta_0 + \beta_1 nt + \beta_2 n^2 t^2 + \beta_3 s_{nt} + \beta_4 c_{nt} \quad (4.28)$$

$$+ \beta_5 s_{2nt} + \beta_6 c_{2nt} + \beta_7 nts_{nt} + \beta_8 ntc_{nt}$$

$$\dot{x}_2 = n\beta_1 + 2n\beta_2 nt + n(\beta_8 + \beta_3)c_{nt} + n(\beta_7 - \beta_4)s_{nt} \quad (4.29)$$

$$+ 2n\beta_5 c_{2nt} - 2n\beta_6 s_{2nt} + n\beta_7 ntc_{nt} - n\beta_8 nts_{nt}$$

$$y_2 = -\alpha_0 - \alpha_1 nt - \alpha_2 s_{nt} - \alpha_3 c_{nt} - \alpha_4 s_{2nt} \quad (4.30)$$

$$- \alpha_5 c_{2nt} - \alpha_6 nts_{nt} - \alpha_7 ntc_{nt}$$

$$\dot{y}_2 = -n\alpha_1 - n(\alpha_7 + \alpha_2)c_{nt} - n(\alpha_6 - \alpha_3)s_{nt} \quad (4.31)$$

$$- 2n\alpha_4 c_{2nt} + 2n\alpha_5 s_{2nt} - n\alpha_6 ntc_{nt} + n\alpha_7 nts_{nt}$$

$$z_2 = \gamma_0 + \gamma_1 s_{nt} + \gamma_2 c_{nt} + \gamma_3 s_{2nt} + \gamma_4 c_{2nt} \quad (4.32)$$

$$+ \gamma_5 nts_{nt} + \gamma_6 ntc_{nt}$$

$$\dot{z}_2 = n(\gamma_1 + \gamma_6)c_{nt} + n(\gamma_5 - \gamma_2)s_{nt} + 2n\gamma_3 c_{2nt} \quad (4.33)$$

$$- 2n\gamma_4 s_{2nt} + n\gamma_5 ntc_{nt} - n\gamma_6 nts_{nt}$$

where

$$s_m = \sin m$$

$$c_m = \cos m$$

These equations are combined linearly with the first-order solution to improve the accuracy of the solution for eccentric orbits; that is, orbits that wander great distances from the origin of the rotating frame. The α_i , β_i , and γ_i coefficients are presented in **Appendix B** and are given in terms of the initial relative position and velocity components.

In order to take the second zonal harmonic into account, the relative motion will be given by the solution of

$$\ddot{x} - 2n\dot{y} - 3n^2x = -\frac{3\mu J_2 r_E^2}{2r^4} (1 - 3s_i^2 s_\theta^2) \quad (4.34)$$

$$\ddot{y} + 2n\dot{x} = -\frac{3\mu J_2 r_E^2}{r^4} s_i^2 s_\theta c_\theta \quad (4.35)$$

$$\ddot{z} + n^2z = -\frac{3\mu J_2 r_E^2}{r^4} s_i c_i c_\theta \quad (4.36)$$

Retaining only the first-order terms in **Equations (4.34 - 36)**, the analytic solutions in relative position and velocity component forms are

$$\begin{aligned} x = & \frac{\dot{x}_0}{n} s_{nt} + x_0 c_{nt} + \frac{1}{2} (c_0 + 2nK) (1 - c_{nt}) \\ & + \frac{2b_0}{n^2} (nt - s_{nt}) + \frac{1}{2n} (2b'_1 + c_1) s_{nt} \\ & - \frac{1}{2n} (2b'_1 + c_1) t c_{nt} - \frac{1}{2n} (2b_1 - c'_1) t s_{nt} \\ & + \sum_{j=2}^5 \left(\frac{2b'_j}{j} + c_j \right) \frac{(j s_{nt} - s_{jnt})}{n^2 (j^2 - 1)} \\ & - \sum_{j=2}^5 \left(\frac{2b_j}{j} - c'_j \right) \frac{(c_{nt} - c_{jnt})}{n^2 (j^2 - 1)} \end{aligned} \quad (4.37)$$

$$\begin{aligned}
\dot{x} = & \dot{x}_0 c_{nt} - n x_0 s_{nt} + \frac{1}{n} (c_0 + 2nK) s_{nt} & (4.38) \\
& + \frac{2b_0}{n} (1 - c_{nt}) + \frac{1}{2} (2b'_1 + c_1) t s_{nt} \\
& - \frac{1}{2n} (2b_1 - c'_1) s_{nt} - \frac{1}{2} (2b_1 - c'_1) t c_{nt} \\
& + \sum_{j=2}^5 \left(\frac{2b'_j}{j} + c_j \right) \frac{(j c_{nt} - j c_{jnt})}{n(j^2 - 1)} \\
& + \sum_{j=2}^5 \left(\frac{2b_j}{j} - c'_j \right) \frac{(s_{nt} - j s_{jnt})}{n(j^2 - 1)}
\end{aligned}$$

$$\begin{aligned}
y = & 2 \frac{\dot{x}_0}{n} c_{nt} - 2 x_0 s_{nt} - \frac{2}{n} (c_0 + 2nK) (nt - s_{nt}) & (4.39) \\
& - \frac{3b_0}{2} t^2 - \frac{4b_0}{n^2} c_{nt} + \frac{2}{n} (2b'_1 + c_1) c_{nt} \\
& + \frac{1}{n} (2b'_1 + c_1) t s_{nt} + \frac{1}{2} (2b_1 - c'_1) (s_{nt} - n t c_{nt}) \\
& + \sum_{j=2}^5 2 \left(\frac{2b'_j}{j} + c_j \right) \frac{\left(j c_{nt} - \frac{c_{jnt}}{j} \right)}{n^2 (j^2 - 1)} \\
& + \sum_{j=2}^5 2 \left(\frac{2b_j}{j} - c'_j \right) \frac{\left(s_{nt} - \frac{s_{jnt}}{j} \right)}{n^2 (j^2 - 1)} \\
& - \sum_{j=1}^5 \frac{b_j}{j^2 n^2} s_{jnt} - \sum_{j=1}^5 \frac{b'_j}{j^2 n^2} c_{jnt} + Kt + K'
\end{aligned}$$

$$\dot{y} = -2\dot{x}_0 s_{nt} - 2nx_0 c_{nt} - \frac{2}{n}(c_0 + 2nK)(1 - c_{nt}) \quad (4.40)$$

$$- \frac{4b_0}{n}(nt - s_{nt}) - \frac{1}{n}(2b'_1 + c_1)s_{nt}$$

$$+ (2b'_1 + c_1)tc_{nt} + (2b_1 - c'_1)ts_{nt}$$

$$- \sum_{j=2}^5 2 \left(\frac{2b'_j}{j} + c_j \right) \frac{(js_{nt} - s_{jnt})}{n(j^2 - 1)}$$

$$+ \sum_{j=2}^5 2 \left(\frac{2b_j}{j} - c'_j \right) \frac{(c_{nt} - c_{jnt})}{n(j^2 - 1)}$$

$$+ b_0 t - \sum_{j=1}^5 \frac{b_j}{jn} c_{jnt} + \sum_{j=1}^5 \frac{b'_j}{jn} s_{jnt} + K$$

$$z = \frac{\dot{z}_0}{n} s_{nt} + z_0 c_{nt} + \frac{d_1}{2n} (s_{nt} - ntc_{nt}) + \frac{d_0}{2} (1 - c_{nt}) \quad (4.41)$$

$$+ \frac{d'_1}{2n} ts_{nt} + \sum_{j=2}^4 \frac{d_j (js_{nt} - s_{jnt})}{n^2 (j^2 - 1)}$$

$$+ \sum_{j=2}^4 \frac{d'_j (c_{nt} - c_{jnt})}{n^2 (j^2 - 1)}$$

$$\dot{z} = \dot{z}_0 c_{nt} - nz_0 s_{nt} + \frac{d_1}{2} ts_{nt} + \frac{d_0}{n} s_{nt} \quad (4.42)$$

$$+ \frac{d'_1}{2n} (s_{nt} + ntc_{nt}) + \sum_{j=2}^4 \frac{d_j (jc_{nt} - jc_{jnt})}{n(j^2 - 1)}$$

$$+ \sum_{j=2}^4 \frac{d'_j (-s_{nt} + js_{jnt})}{n(j^2 - 1)}$$

where $x_0, y_0, z_0, \dot{x}_0, \dot{y}_0, \dot{z}_0 =$ initial conditions

Once again, the equations for the coefficients associated with the **Equations (4.37 - 42)** are presented in **Appendix B**.

The second-order approximations are now added to the perturbed first-order solution to provide a more accurate representation of the motion of the spacecraft relative to the reference frame which is perturbed by the J_2 harmonic

$$\begin{aligned}x_f &= x + x_2 \\ \dot{x}_f &= \dot{x} + \dot{x}_2 \\ y_f &= y + y_2 \\ \dot{y}_f &= \dot{y} + \dot{y}_2 \\ z_f &= z + z_2 \\ \dot{z}_f &= \dot{z} + \dot{z}_2\end{aligned}\tag{4.43}$$

Once the final relative positions and velocities are determined, they are converted to the inertial frame with equations given in **Appendix B**. This process is done independently for each vehicle. The results are then converted to the Hill frame to obtain the propagated filter state.

4.2.4 Integration of the Equations of Motion

The inertial positions and velocities obtained from the filter state can be considered as initial conditions of two separate orbits and propagated forward by integrating the equations of motion described in **Subsection 3.2.2**. Once the orbits are propagated indepen-

dently, the results are converted back to the relative Hill frame to become the propagated state.

4.3 Measurement Matrix

The measurement matrix, H , as described in **Chapter 2**, relates the states to the measurements. For a set of pseudorange and delta-range measurements from each SV, an (8×2) measurement matrix can be formed

$$H = \frac{\partial z}{\partial x} = \begin{bmatrix} \frac{\partial \rho}{\partial \hat{r}_H} & \frac{\partial \rho}{\partial \hat{v}_H} & \frac{\partial \rho}{\partial \Delta b} & \frac{\partial \rho}{\partial \Delta d} \\ \frac{\partial}{\partial \hat{r}_H} \dot{\rho} & \frac{\partial}{\partial \hat{v}_H} \dot{\rho} & \frac{\partial}{\partial \Delta b} \dot{\rho} & \frac{\partial}{\partial \Delta d} \dot{\rho} \end{bmatrix} \quad (4.44)$$

Since the measurements are in the inertial frame and the filter states are in the Hill frame a conversion must be made. However, to simplify calculations, an approximation is made such that the inertial frame is converted to a target local (L) frame, rather than the Hill frame. The main difference between the L frame, depicted in **Figure 4.1**, and the Hill frame is that the former is not a curvilinear frame.

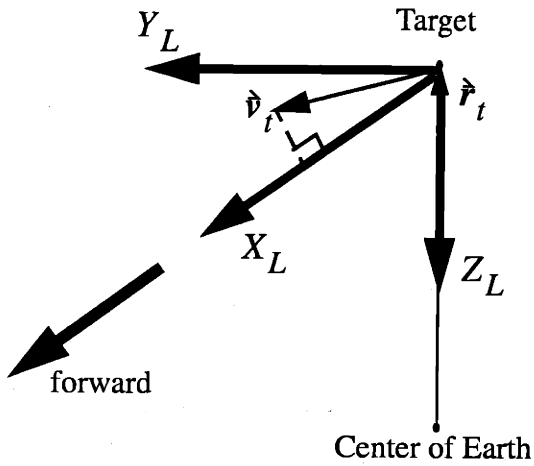


Figure 4.1: Target Local Frame

Given this frame, a transformation matrix from the target local frame to the inertial frame can be defined as

$$C_L^I = [X_L \ Y_L \ Z_L] \quad (4.45)$$

where

$$X_L = \frac{Y_L \times Z_L}{|Y_L \times Z_L|}$$

$$Y_L = \frac{\hat{v}_t \times \hat{r}_t}{|\hat{v}_t \times \hat{r}_t|}$$

$$Z_L = -\frac{\hat{r}_t}{|\hat{r}_t|}$$

\hat{r}_t = target vehicle position

\hat{v}_t = target vehicle velocity

Note that the transformation matrix for a transformation from the inertial frame to the local frame is simply the transpose of **Equation (4.45)**

$$C_I^L = (C_L^I)^T \quad (4.46)$$

Now that the transformation matrix has been defined, the measurement matrix can be obtained from

$$H = \begin{bmatrix} H_1 & O_{1 \times 3} & 1 & 0 \\ H_2 & H_1 & 0 & 1 \end{bmatrix} \quad (4.47)$$

where

$$H_1^T = C_I^H \frac{\dot{\hat{r}}_t - \dot{\hat{r}}_{GPS}}{\rho_t} \cong C_I^L \frac{\dot{\hat{r}}_t - \dot{\hat{r}}_{GPS}}{\rho_t}$$

$$H_2^T \cong C_I^L \frac{\dot{\hat{v}}_t - \dot{\hat{v}}_{GPS}}{\rho_t} - \frac{\dot{\rho}_t}{\rho_t} C_I^L (\hat{r}_t - \hat{r}_{GPS}) - \Omega_{IL}^L H_1^T$$

$$\Omega_{IL}^L = \begin{bmatrix} 0 & 0 & -n \\ 0 & 0 & 0 \\ n & 0 & 0 \end{bmatrix}$$

$$O_{1 \times 3} = [0 \ 0 \ 0]$$

$$\rho_t = |\hat{r}_t - \hat{r}_{GPS}|$$

$$\dot{\rho}_t = \frac{(\hat{r}_t - \hat{r}_{GPS})(\dot{\hat{v}}_t - \dot{\hat{v}}_{GPS})^T}{\rho_t}$$

Note that for this study, GPS measurements are taken at 1 second intervals.

4.4 Covariance Matrix

This section focuses on the covariance matrix. Specifically, it presents the means by which the initial covariance, \bar{P}_0 , is obtained and concludes with a description of how the covariance matrix is propagated.

4.4.1 Initial Covariance

Stanley W. Shepperd also published a paper on the topic of covariance matrices for near-circular orbits.^[30] This paper included solutions that are useful for initializing a filter simulation. Shepperd's solution was adapted for the Hill frame defined in this thesis and follows

$$\bar{P}_0 = \begin{bmatrix} X_0^2 + 2b^2 & 0 & 0 & 0 & 0 & nb^2 & 0 & 0 \\ 0 & \frac{c^2}{2} & 0 & 0 & 0 & 0 & 0 & 0 \\ 0 & 0 & Z_0^2 + \frac{b^2}{2} & -n\left(\frac{3}{2}Z_0^2 + b^2\right) & 0 & 0 & 0 & 0 \\ 0 & 0 & -n\left(\frac{3}{2}Z_0^2 + b^2\right) & n^2\left(\frac{9}{4}Z_0^2 + 2b^2\right) & 0 & 0 & 0 & 0 \\ 0 & 0 & 0 & 0 & \frac{n^2 c^2}{2} & 0 & 0 & 0 \\ nb^2 & 0 & 0 & 0 & 0 & \frac{n^2 b^2}{2} & 0 & 0 \\ 0 & 0 & 0 & 0 & 0 & 0 & \sigma_{\Delta b}^2 & 0 \\ 0 & 0 & 0 & 0 & 0 & 0 & 0 & \sigma_{\Delta d}^2 \end{bmatrix} \quad (4.48)$$

where

$$X_0 = x_0 - \frac{2}{n}\dot{z}_0$$

$$Z_0 = 4z_0 + \frac{2}{n}\dot{x}_0$$

$$b \sin \phi = -3z_0 - \frac{2}{n}\dot{x}_0$$

$$b \cos \phi = \frac{\dot{z}_0}{n}$$

$$c \sin \psi = \frac{\dot{y}_0}{n}$$

$$c \cos \psi = y_0$$

$$b = \sqrt{b(\sin \phi)^2 + b(\cos \phi)^2}$$

$$\phi = \text{atan}\left(\frac{b \sin \phi}{b \cos \phi}\right)$$

$$c = \sqrt{c(\sin \psi)^2 + c(\cos \psi)^2}$$

$$\psi = \text{atan}\left(\frac{c \sin \psi}{c \cos \psi}\right)$$

The parameter b is the semi-minor axis of the ellipse, the parameter c is the magnitude of the simple oscillator out-of-plane motion, and the parameters ϕ and ψ are the phase angles for the in-plane and out-of-plane motions, respectively. The elements $\sigma_{\Delta b}^2$ and $\sigma_{\Delta d}^2$ of the matrix represent the standard deviations of the clock bias and clock drift differences, respectively.

4.4.2 Covariance Propagation

In **Chapter 2, Equation (2.18)** was given as the method of propagating the covariance matrix. For completeness, this equation is given again here

$$\bar{P}_{i+1} = \Phi_i P_i \Phi_i^T + Q_i \quad (4.49)$$

A more rigorous form of obtaining the covariance matrix is^[24, p. 165]

$$\bar{P}_{i+1} = \Phi_i P_i \Phi_i^T + \int_{t_i}^{t_{i+1}} \Phi(t_i, \tau) G(\tau) Q(\tau) G^T(\tau) \Phi^T(t_i, \tau) d\tau \quad (4.50)$$

where

$G(\tau)$ = noise input matrix

$Q(\tau)$ = spectral density matrix

Since position is obtained exactly from integrating the velocity, there is no modeling error in position. However, since there are other perturbations that are not accounted for in acceleration, integrating the acceleration introduces errors in the system modeling. Therefore, the $Q(\tau)$ matrix is given by

$$Q(\tau) = \begin{bmatrix} q_{v_x} & 0 & 0 & 0 & 0 \\ 0 & q_{v_y} & 0 & 0 & 0 \\ 0 & 0 & q_{v_z} & 0 & 0 \\ 0 & 0 & 0 & q_{\Delta b} & 0 \\ 0 & 0 & 0 & 0 & q_{\Delta d} \end{bmatrix} \quad (4.51)$$

where q_i = is the strength, or spectral, of i

The corresponding $G(\tau)$ matrix is

$$G(\tau) = \begin{bmatrix} 0 & 0 & 0 & 0 & 0 \\ 0 & 0 & 0 & 0 & 0 \\ 0 & 0 & 0 & 0 & 0 \\ 1 & 0 & 0 & 0 & 0 \\ 0 & 1 & 0 & 0 & 0 \\ 0 & 0 & 1 & 0 & 0 \\ 0 & 0 & 0 & 1 & 0 \\ 0 & 0 & 0 & 0 & 1 \end{bmatrix} \quad (4.52)$$

The integral portion of **Equation (4.50)** is redefined as

$$Q' = \int_{t_{i-1}}^{t_i} \Phi(t_i, \tau) G(\tau) Q(\tau) G^T(\tau) \Phi^T(t_i, \tau) d\tau \quad (4.53)$$

and yields the following elements of an (8×8) matrix:

$$Q'(1, 1) = \left(\frac{8}{n^2} \Delta t + 3 \Delta t^3 + \frac{24}{n^2} c_{n\Delta t} \Delta t - \frac{4}{n^3} s_{2n\Delta t} - \frac{24}{n^3} s_{n\Delta t} \right) q_{v_x} \quad (4.54)$$

$$+ \left(\frac{6}{n^2} \Delta t + \frac{1}{n^3} s_{2n\Delta t} - \frac{8}{n^3} s_{n\Delta t} \right) q_{v_z}$$

$$Q'(1, 3) = \left(-\frac{2}{n^3} c_{n\Delta t} + \frac{2}{n^3} - \frac{3}{n} \Delta t^2 - \frac{4}{n^3} s_{n\Delta t}^2 + \frac{6}{n^2} s_{n\Delta t} \Delta t \right) q_{v_x} \quad (4.55)$$

$$+ \left(\frac{1}{n^3} s_{n\Delta t}^2 + \frac{2}{n^3} c_{n\Delta t} - \frac{2}{n^3} \right) q_{v_z}$$

$$Q'(1, 4) = \left(\frac{8}{2} s_{n\Delta t}^2 - \frac{12}{n} s_{n\Delta t} \Delta t + \frac{9}{2} \Delta t^2 \right) q_{v_x} \quad (4.56)$$

$$- \left(\frac{2}{n} s_{n\Delta t}^2 + \frac{4}{n} c_{n\Delta t} - \frac{4}{n} \right) q_{v_z}$$

$$Q'(1, 6) = \left(\frac{4}{n} \Delta t - \frac{2}{n} s_{2n\Delta t} - \frac{6}{n} s_{n\Delta t} + \frac{6}{n} c_{n\Delta t} \Delta t \right) q_{v_x} \quad (4.57)$$

$$+ \left(\frac{1}{n} \Delta t + \frac{1}{2n} s_{2n\Delta t} - \frac{2}{n} s_{n\Delta t} \right) q_{v_z}$$

$$Q'(2, 2) = \left(\frac{1}{2n} \Delta t - \frac{1}{4n} s_{2n\Delta t} \right) q_{v_y} \quad (4.58)$$

$$Q'(2, 5) = \left(\frac{1}{2n} s_{n\Delta t}^2 \right) q_{v_y} \quad (4.59)$$

$$Q'(3, 3) = \left(\frac{6}{n} \Delta t - \frac{8}{n} s_{n\Delta t} + \frac{1}{n} s_{2n\Delta t} \right) q_{v_x} \quad (4.60)$$

$$+ \left(\frac{1}{2n} \Delta t - \frac{1}{4n} s_{2n\Delta t} \right) q_{v_z}$$

$$Q'(3, 4) = \left(\frac{14}{n} s_{n\Delta t} - \frac{10}{n} \Delta t - \frac{2}{n} s_{2n\Delta t} \right) q_{v_x} \quad (4.61)$$

$$+ \left(-\frac{1}{n} \Delta t + \frac{1}{2n} s_{2n\Delta t} \right) q_{v_z}$$

$$Q'(3, 6) = \left(-\frac{4}{n} c_{n\Delta t} + \frac{4}{n} - \frac{2}{n} s_{n\Delta t}^2 \right) q_{v_x} \quad (4.62)$$

$$+ \left(\frac{1}{2n} s_{n\Delta t}^2 \right) q_{v_z}$$

$$Q'(4, 4) = \left(17\Delta t + \frac{4}{n} s_{2n\Delta t} - \frac{24}{n} s_{n\Delta t} \right) q_{v_x} \quad (4.63)$$

$$+ \left(2\Delta t - \frac{1}{n} s_{2n\Delta t} \right) q_{v_z}$$

$$Q'(4, 6) = \left(\frac{4}{n} s_{n\Delta t}^2 + \frac{6}{n} c_{n\Delta t} - \frac{6}{n} \right) q_{v_x} \quad (4.64)$$

$$+ \left(-\frac{1}{n} s_{n\Delta t}^2 \right) q_{v_z}$$

$$Q'(5, 5) = \left(\frac{\Delta t}{2} + \frac{1}{4n} s_{2n\Delta t} \right) q_{v_y} \quad (4.65)$$

$$Q'(6, 6) = \left(2\Delta t - \frac{1}{n} s_{2n\Delta t} \right) q_{v_x} \quad (4.66)$$

$$+ \left(\frac{\Delta t}{2} + \frac{1}{4n} s_{2n\Delta t} \right) q_{v_z}$$

$$Q'(7, 7) = \Delta t q_{\Delta b} + \frac{\Delta t^3}{3} q_{\Delta d} \quad (4.67)$$

$$Q'(7, 8) = \frac{\Delta t^2}{2} q_{\Delta d} \quad (4.68)$$

$$Q'(8, 8) = \Delta t q_{\Delta d} \quad (4.69)$$

where $\Delta t = t_{i+1} - t_i$

Since the covariance matrix is symmetric, all the off-diagonal elements from the equations above will have the same value at its corresponding transpose. All the remaining elements are zero.

The results were validated by comparing them to the corresponding results obtained by numerically integrating **Equation (4.50)** with Fourth Order Runge Kutta method.

4.5 Chapter Summary

This chapter presented the design of the relative navigation filter used for this study. It began with a description of the filter state. Then, the four techniques used to propagate the filter state were presented. These techniques included propagation by (1) integration of the equations of motion, (2) first-order equations of relative motion which include effects of J_2 combined with a second-order conic approximation, (3) the Universal Keplerian state transition matrix, and finally, (4) the state transition matrix based on the Clohessy-Wiltshire equations. This was followed by a description of how the measurement matrix and initial covariance matrix were obtained, as well as how the covariance matrix was propagated. The following chapter presents the results of propagating and estimating the state with the four techniques described in this chapter.

Chapter 5

Results

This chapter summarizes the results of the modeling and filter estimation described in the previous chapters. Three cases are studied in which the eccentricity of the chaser orbit is varied. The parameters used for these cases are presented first, along with a sample of the true state for the first case. This is followed by a comparison of the different propagation techniques as well as the effects these techniques have when used as methods of propagating the state in a relative navigation filter. Effects of eccentricity, the number of common satellites, and GDOP. A brief summary on the computation costs associated with each propagation technique and a general summary of each technique concludes the chapter.

5.1 Description of Cases

The initial orbital parameters of the target vehicle are the same for all the cases tested. Orbital parameters similar to those of the ISS were chosen and are given in **Table 5.1**.

Parameter	Value
a	6785136 m
e	0.001
i	51.6°
Ω	57.4°
ω	247.6°

Table 5.1: Orbital Parameters of Target Vehicle

Note that the semimajor axis, a , corresponds to an altitude of 407 km, which is representative of the ISS orbit.

The chaser vehicle orbit is designed such that initially it is approximately 25 km away from the target vehicle, midway through the run it is within a few meters of the target, and at the end it is approximately 25 km away. This choice of design was made because RGPS navigation will only be used within approximately 20 km of the target. The orbits are illustrated in **Figure 5.1**.

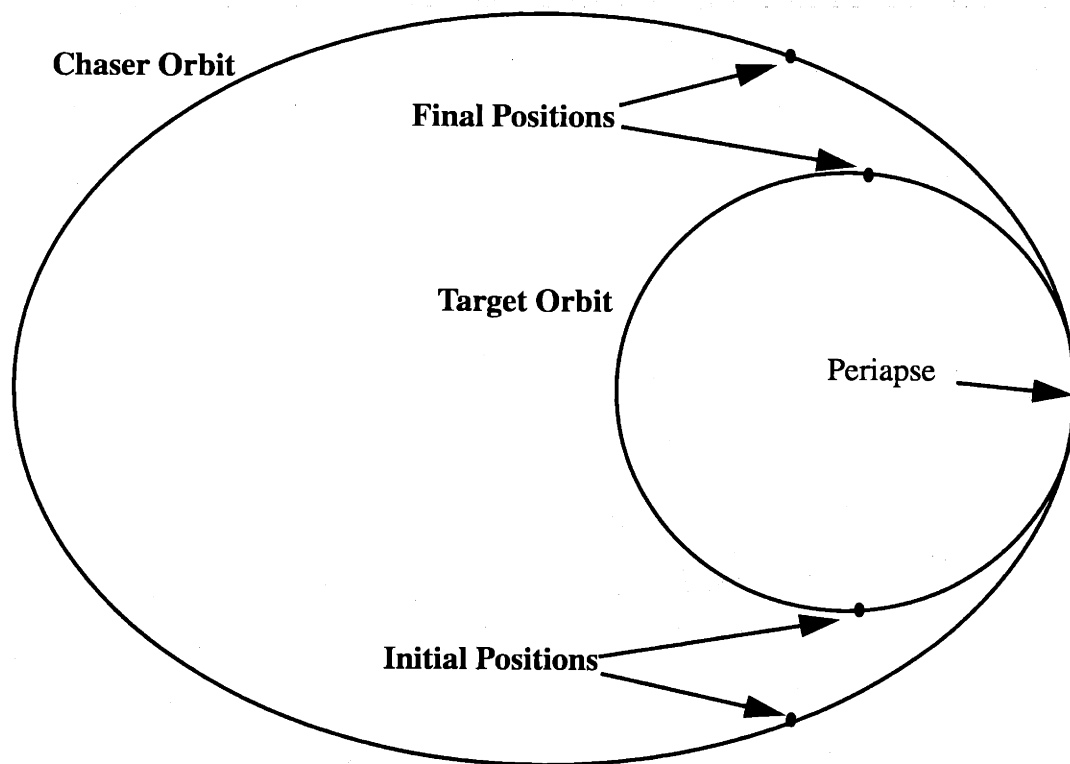


Figure 5.1: Orbit Design of Cases Studied

The initial inclination, argument of ascending node, and argument of periapse of the

chaser vehicle are the same as those of the target. The semimajor axis, however, depends on the choice of eccentricity. That is, for a choice of eccentricity, the semimajor axis is chosen such that the periapsis altitude of both orbits are equal. Therefore, without perturbations the target and chaser vehicles would “meet” at the periapse. The initial true anomalies of both vehicles also vary with each case to adjust for the initial 25 km separation. These values are summarized in **Table 5.2**.

Parameter	Case 1 Values	Case 2 Values	Case 3 Values
e_{chaser}	0.015	0.010	0.005
a_{chaser}	6881574.5 m	6846819.1 m	6812412.9 m
$f_{0_{chaser}}$	327.32°	311.17°	275.74°
$f_{0_{target}}$	327.50°	311.29°	275.67°

Table 5.2: Remaining Orbital Parameters

These cases were chosen in order to study the effects of eccentricity on each of the state propagation techniques. The highest value of eccentricity, Case 1, was limited by the periapsis altitude of the chaser (300 km).

These orbital elements are used to obtain the initial vehicle position and velocity which are integrated to obtain the vehicle’s trajectory. The GPS software simulator is then used to obtain the pseudorange and delta-range measurements. The true relative position and velocity states are determined by converting the inertial position and velocities into the Hill frame. Since the clock bias and clock drift of each vehicle are obtained from the GPS simulator, the true states of the clock bias and clock drift differences are obtained by simply differencing the target clock bias and clock drift from the corresponding values of

the chaser. The true states, or the truth, for Case 1 are presented in **Figures 5.2, 5.3** and **5.4**, corresponding to the relative position, relative velocity, and clock bias and clock drift differences, respectively. Notice that the vehicles are closest to each other at approximately 500 seconds into the run.

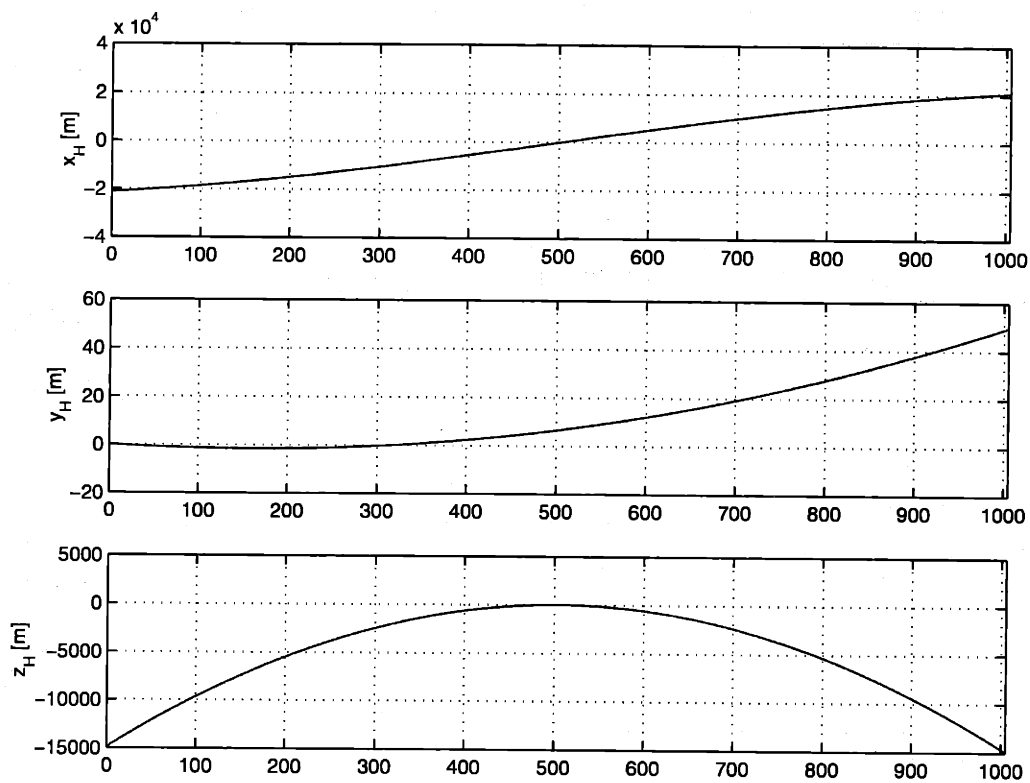


Figure 5.2: Relative Position Truth (Case 1)

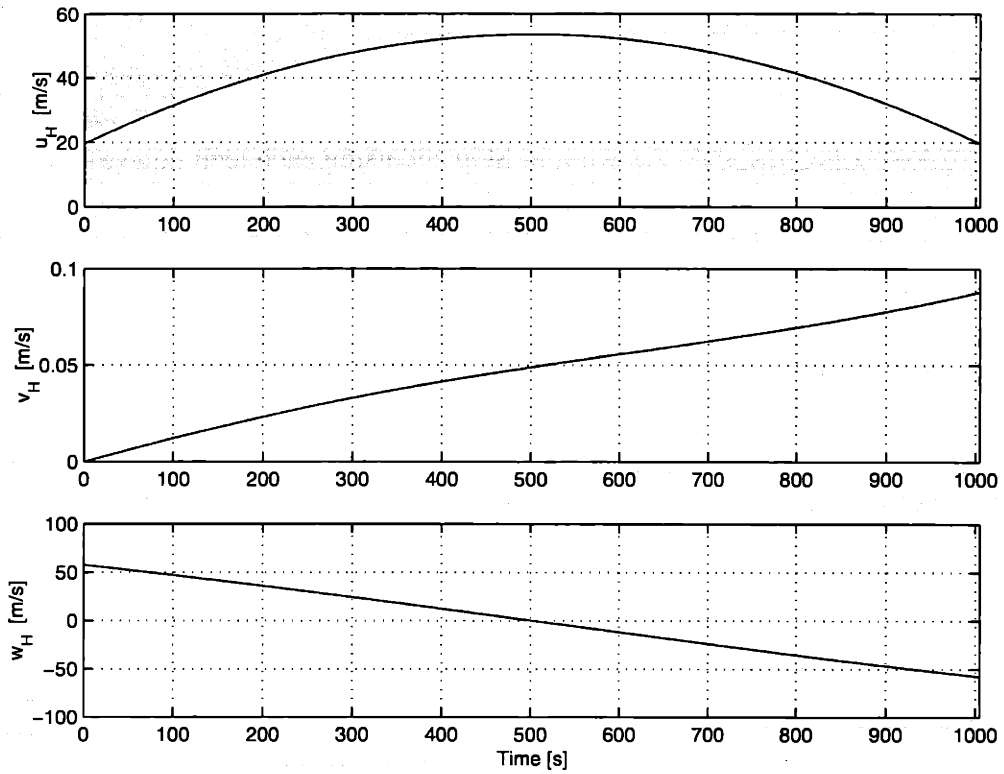


Figure 5.3: Relative Velocity Truth (Case 1)

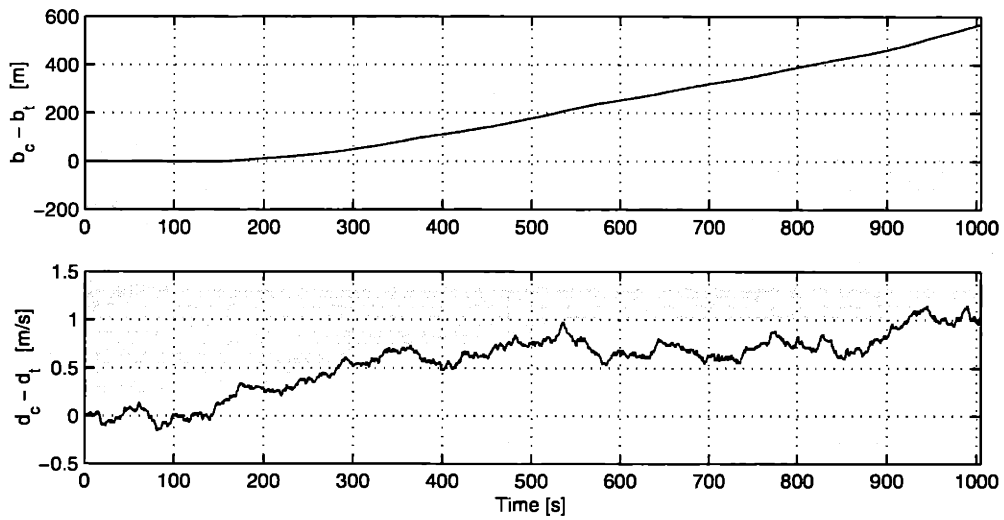


Figure 5.4: GPS Clock Error Differences Truth (Case 1)

5.2 Effects of Propagation Techniques

For Case 1, one run is made in which the states are propagated and not estimated. This is done by taking the true state at each time step and using each technique to propagate the state forward one time step (1 second). This process is repeated for each time step and the results are differenced from the truth to obtain the propagation errors over an integration step. These errors are given in **Figures 5.5 - 5.6**, and magnified in **Figures 5.7 - 5.8** to show more detail. **Table 5.3** summarizes the notation used to depict the propagation techniques in this chapter.

Notation	Propagation with:
CW-STM	State Transition Matrix based on the C-W equations
KSTM	Universal Keplerian State Transition Matrix
KECH	Kechichian's Equations of Relative Motion accounting for J_2
INT	Integration of Equations of Motion

Table 5.3: Notation for Propagation Techniques

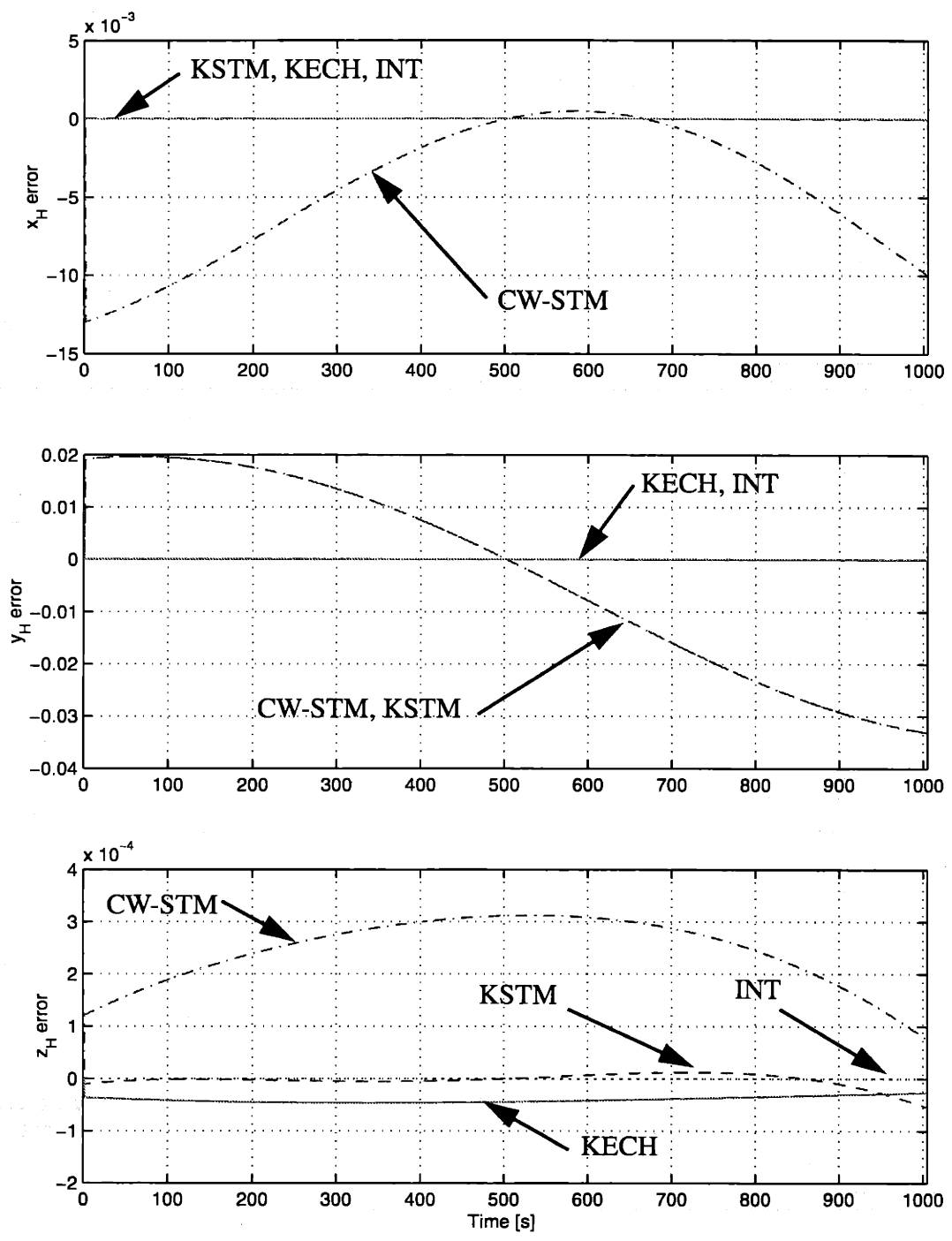


Figure 5.5: Relative Position Propagation Errors

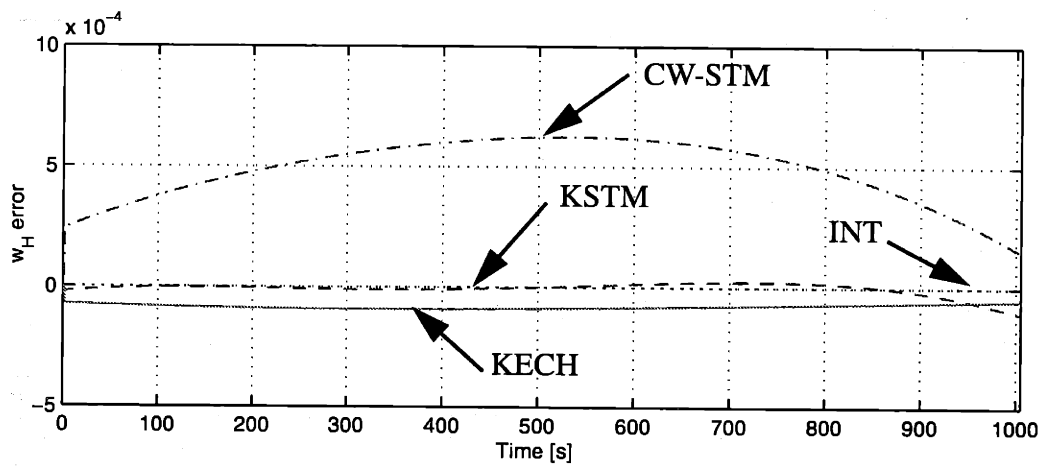
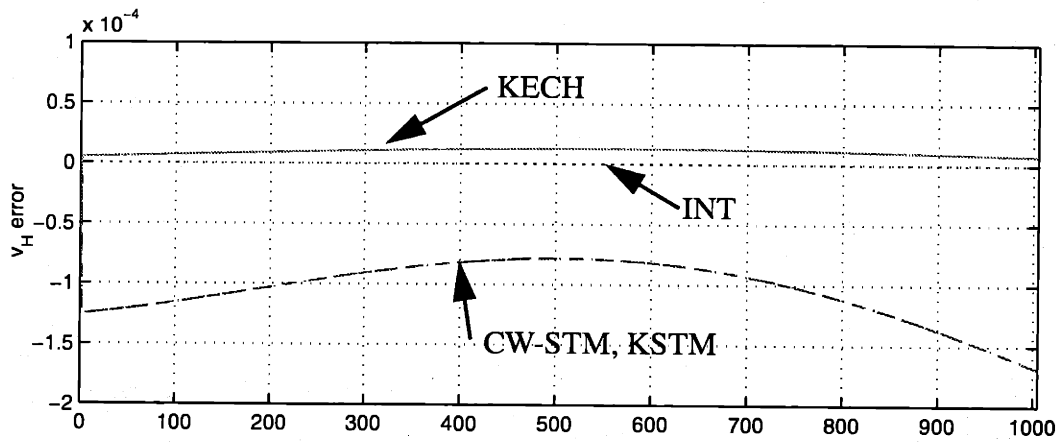
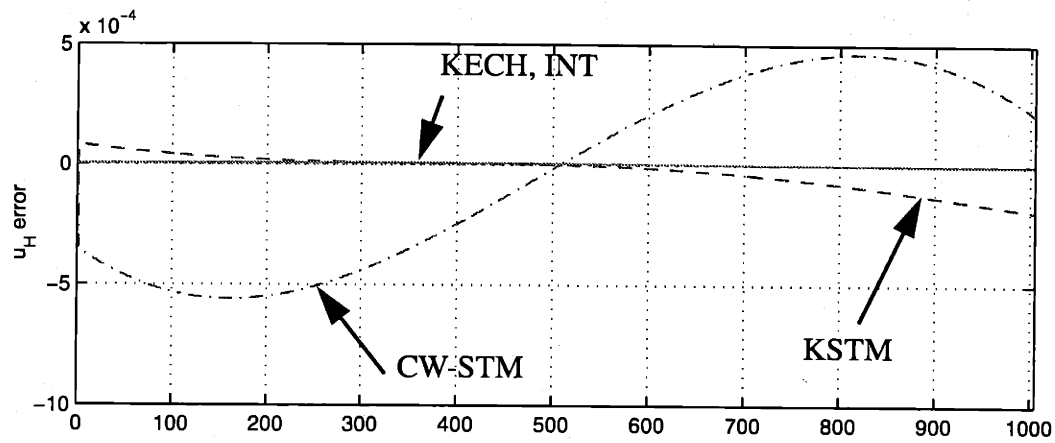


Figure 5.6: Relative Velocity Propagation Errors

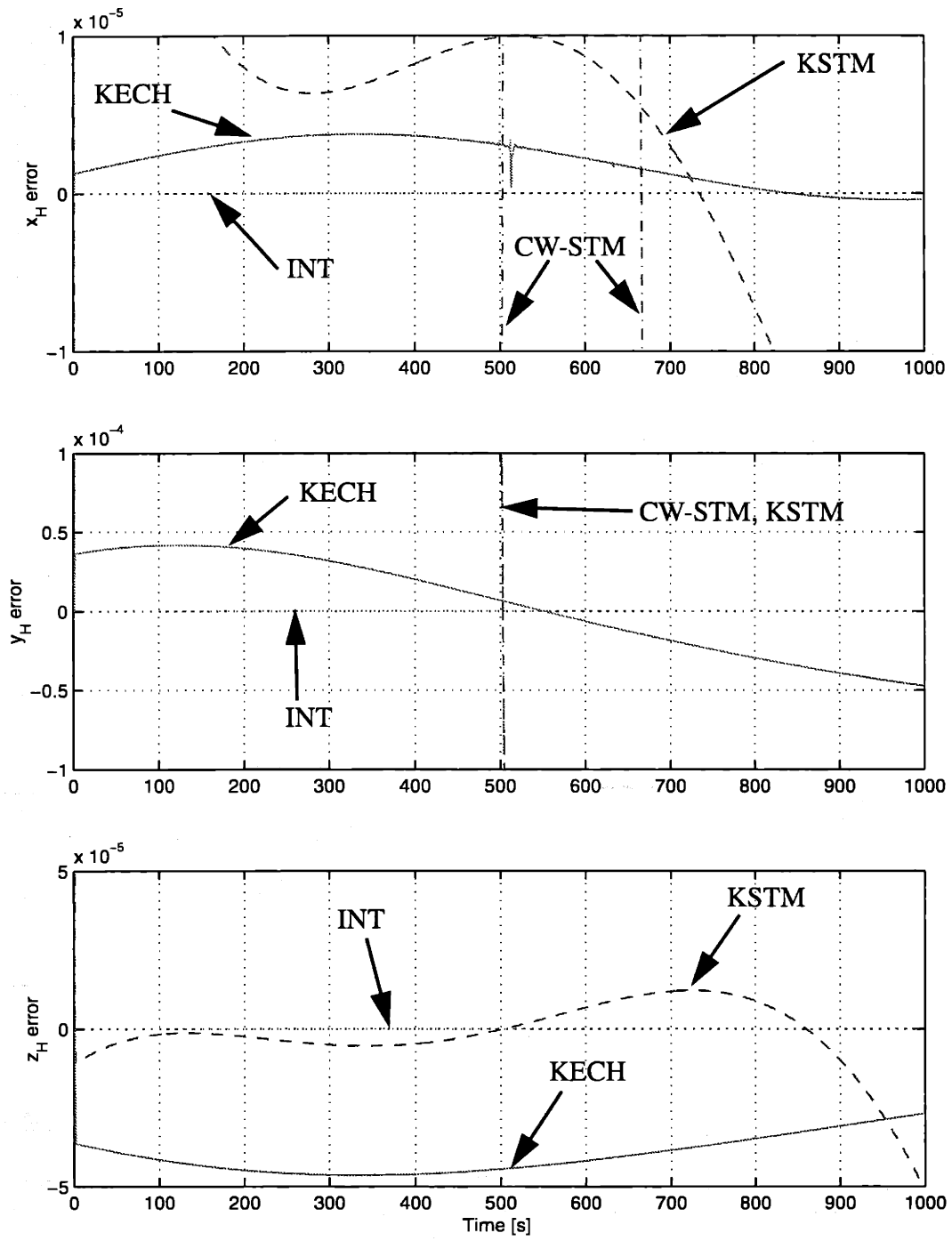


Figure 5.7: Relative Position Propagation Errors (magnified)

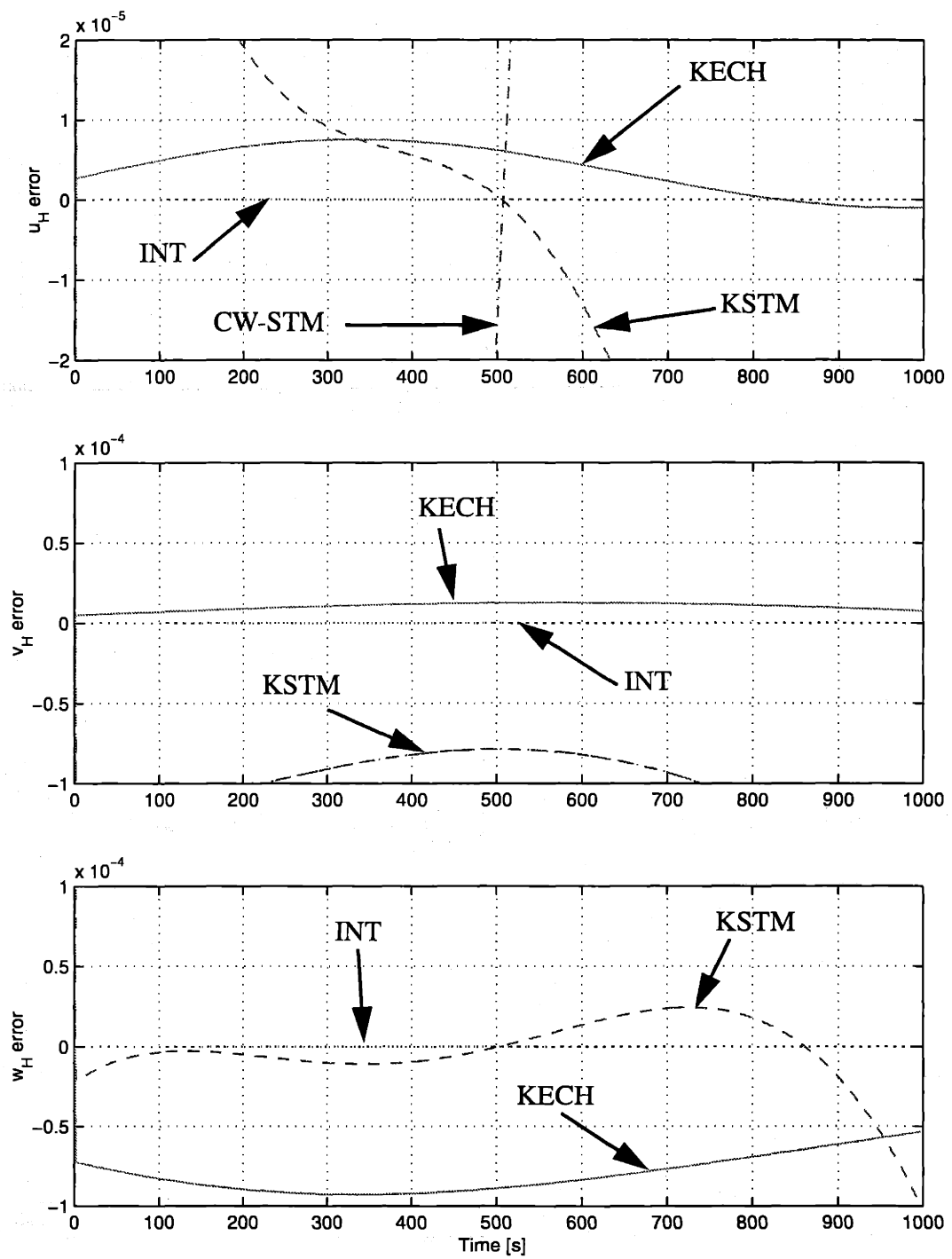


Figure 5.8: Relative Velocity Propagation Errors (magnified)

Overall, the CW-STM method has the worst performance. The solution to the C-W equations are an approximation to small deviations from a circular orbit. This method breaks down with increasing eccentricity and larger separation between vehicles, which is further explored in the next section. It does not account for any of the perturbations nor for the eccentricity of the target orbit. Note that the largest error occurs in the y-component of the position. This is primarily due to the effects of J_2 at the inclination of the orbits.

The KSTM method improves upon the CW-STM as it accounts for the eccentricity of the orbits. However, it does not account for J_2 and, therefore, has the same errors in the y-components, in both position and velocity, as the CW-STM method. Significant improvements are made in the corresponding x-components; however, the KECH and INT methods are better. In the z-components, the KSTM method appears to be better than the KECH method. This is attributed to the fact that the KECH method includes only a second approximation to correct for eccentricity, whereas the KSTM accounts for it fully. As the separation increases, as noted in the last 50 seconds of the run, the KSTM errors become greater than that of the KECH method. This is due to the increase in separation between the vehicles. Another reason is that in the early portions of the propagated orbits, the effects of the perturbations, such as J_2 , have not significantly deviated the orbits from two-body orbits. With time, the precessions from the initial orbital elements, will have a greater effect, which begins to appear during the last 50 seconds of the run.

Aside from the anomaly just discussed, the KECH method improves upon the CW-STM and KSTM techniques. The KECH method compensates for the J_2 effects which are especially apparent in the y-components. The significant decrease in these errors relative to the aforementioned methods indicates that the J_2 perturbation has the greatest

effect of all the perturbations, since of these three methods, KECH is the only method that takes J_2 into account.

The INT method obviously has negligible errors since the models were based on integrating the equations of motion.

To see the effects of the propagation techniques in RGPS navigation, Case 1 is implemented in the Kalman filter, varying only the propagation technique. Note that the filter was tuned using the INT method for propagation. The corresponding strengths, or spectral values, of the process noise are given in **Table 5.4**.

Strength	Value	Units
q_{v_x}	5×10^{-4}	$\frac{m^2}{s^3}$
q_{v_y}	5×10^{-9}	$\frac{m^2}{s^3}$
q_{v_z}	1×10^{-14}	$\frac{m^2}{s^3}$
$q_{\Delta b}$	9	$\frac{m}{s}$
$q_{\Delta d}$	9×10^{-4}	$\frac{m^2}{s^3}$

Table 5.4: Spectral Values of the Process Noise

The results from the each filter run is illustrated with three figures: the position filter

errors, velocity filter errors, and clock state filter errors, respectively. The following figures correspond to the indicated propagation techniques:

- CW-STM: **Figures 5.9 - 11**
- KSTM: **Figures 5.12 - 14**
- KECH: **Figures 5.15 - 17**
- INT: **Figures 5.18 - 20**

Note that the figures include plots of the 3σ covariance bounds.

The filter performance using each propagation technique parallels the same observations that are made when the techniques were used to just propagate the state. Overall the CW-STM method has the worst performance with the filter state errors exceeding the covariance bounds in all eight states. The KSTM method showed significant improvement in all states except for the y-components, once again due to the effects of J_2 . The KECH technique improves the results even further with the exception of the z-component in velocity due to the limit of the second-order approximation. Finally, as expected, the filter errors associated with the INT method of propagation give the best results, with all state errors remaining within the covariance bounds.

An interesting effect is observed in the velocity filter errors of the CW-STM method, **Figure 5.10**. The velocity errors seem to follow a cyclic pattern, while the position errors do not. This can be accounted for by the propagation errors for the CW-STM method, where a similar cyclic pattern occurs in the position errors. Since the propagation occurs over a one second time step, position propagation errors are directly reflected in the delta-range. The delta-range, in turn, is directly correlated to filter velocity errors. Therefore, position propagation errors are reflected in the filter velocity errors.

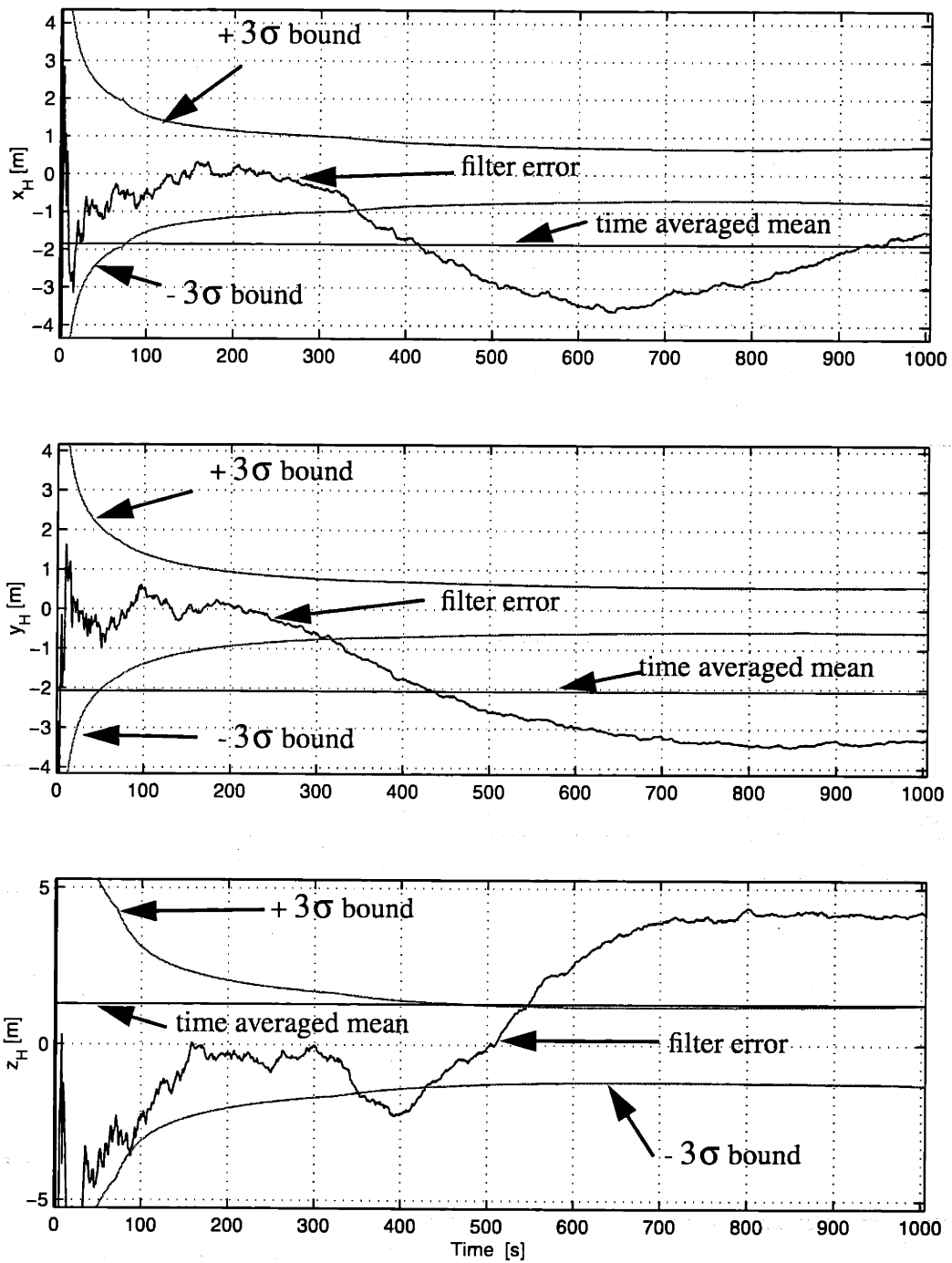


Figure 5.9: Position Filter Errors when Propagating with the Clohessy-Wiltshire State Transition Matrix (Case 1)

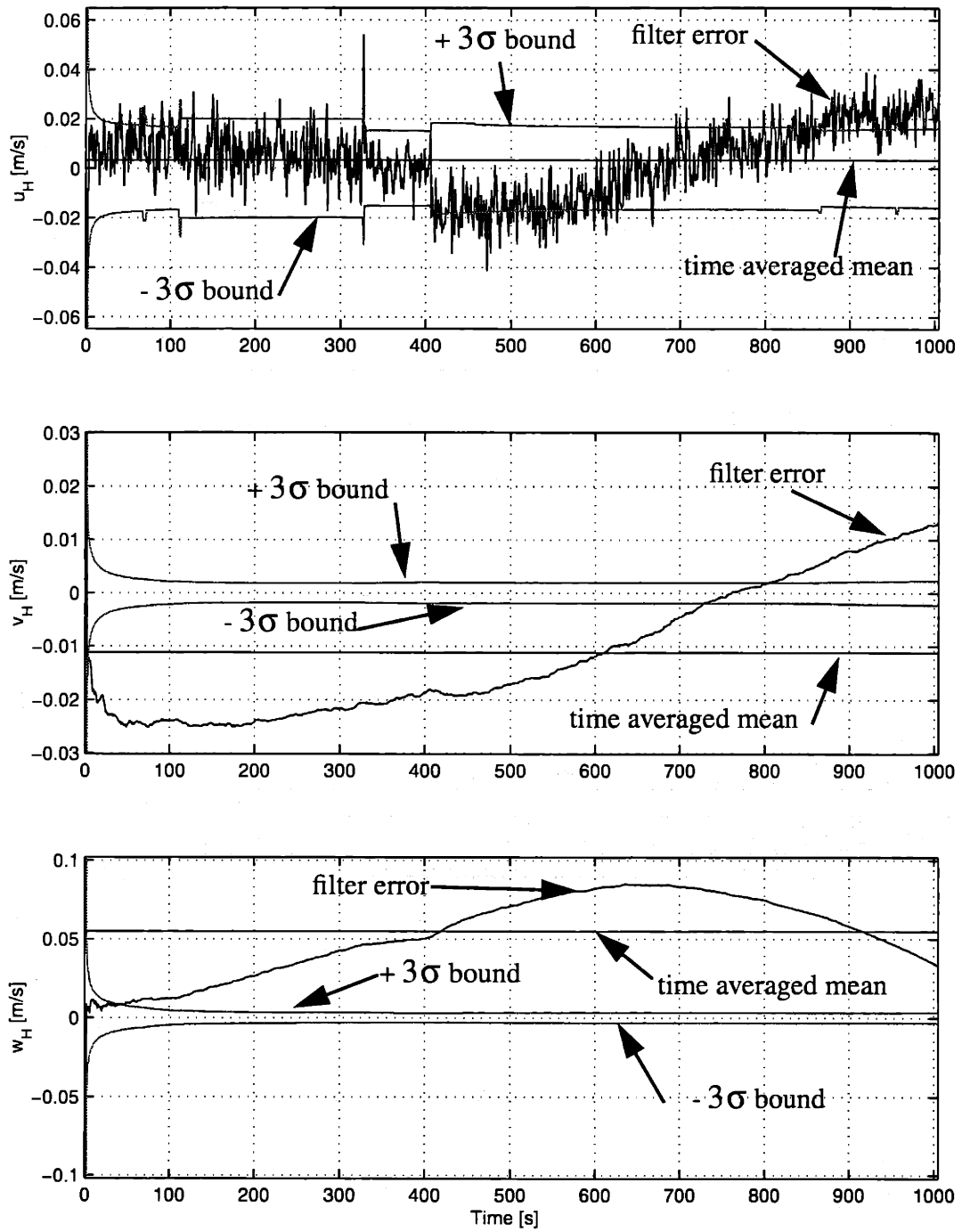


Figure 5.10: Velocity Filter Errors when Propagating with the Clohessy-Wiltshire State Transition Matrix (Case 1)

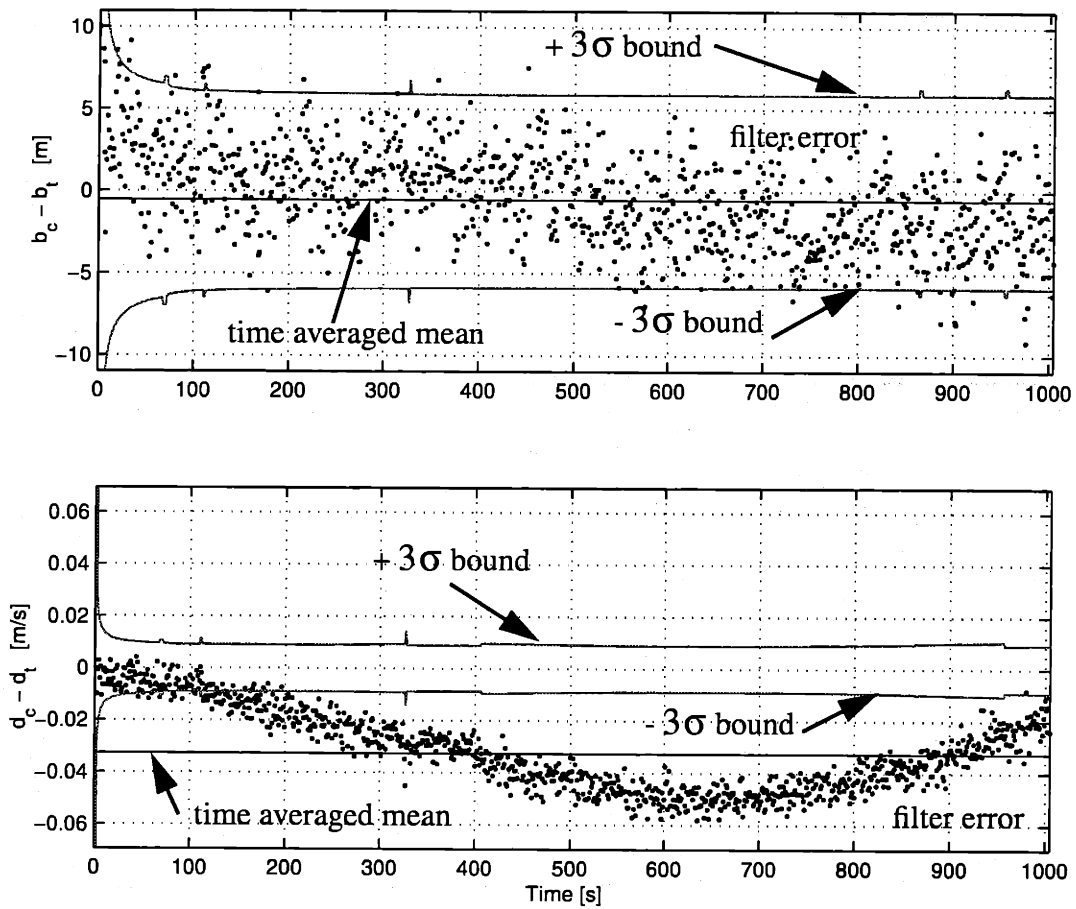


Figure 5.11: Clock Filter Errors when Propagating with the Clohessy-Wiltshire State Transition Matrix (Case 1)

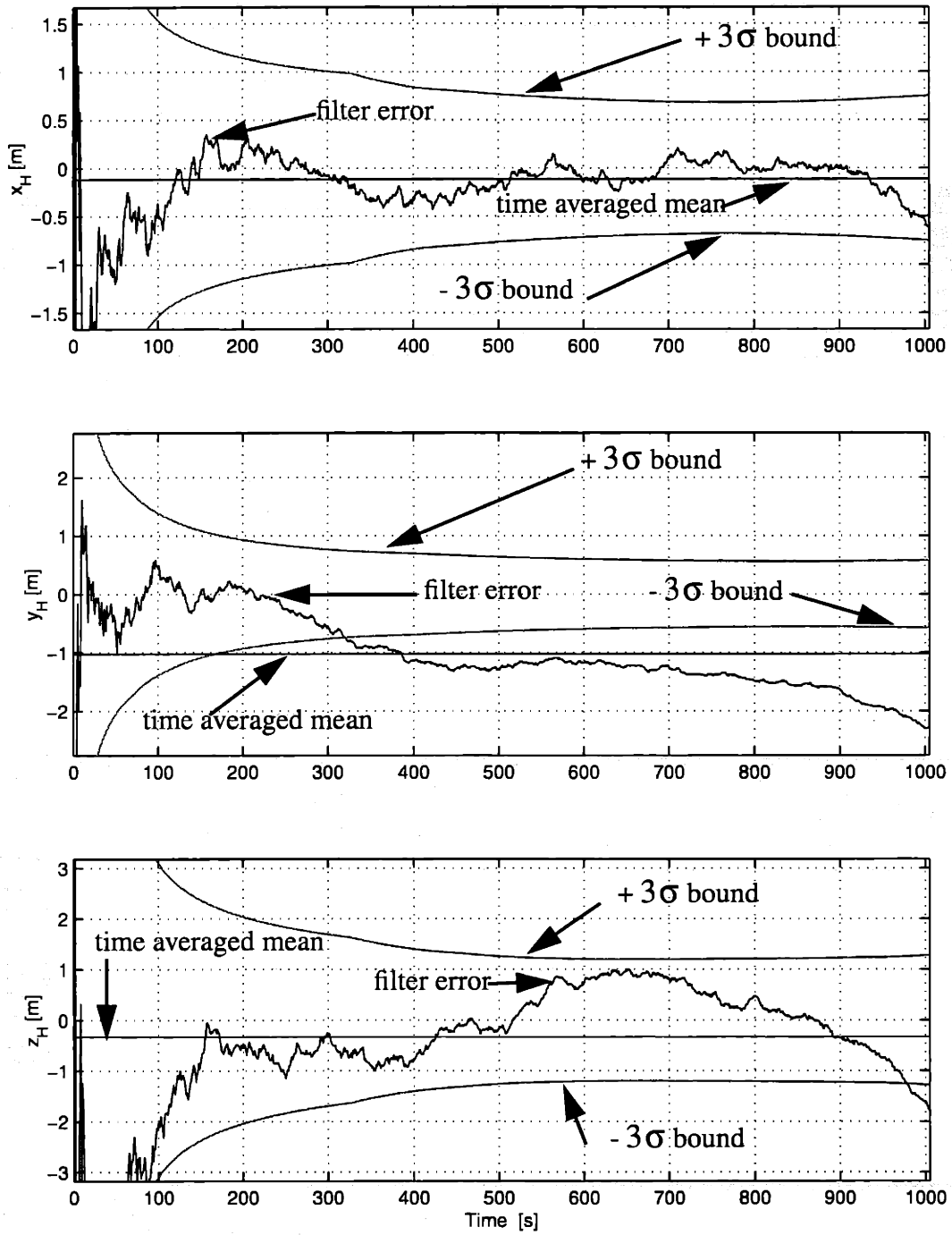


Figure 5.12: Position Filter Errors when Propagating with the Keplerian State Transition Matrix (Case 1)

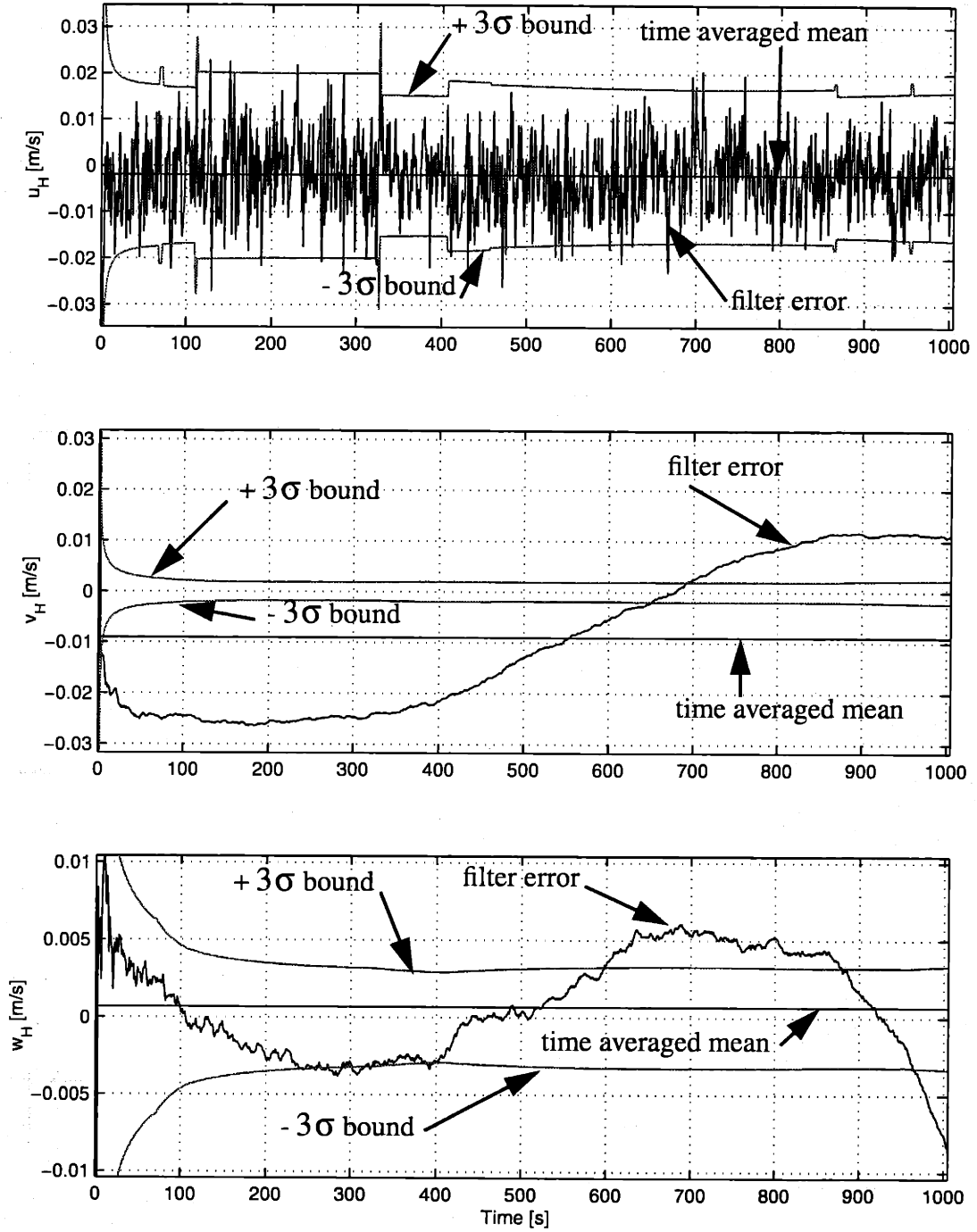


Figure 5.13: Velocity Filter Errors when Propagating with the Keplerian State Transition Matrix (Case 1)

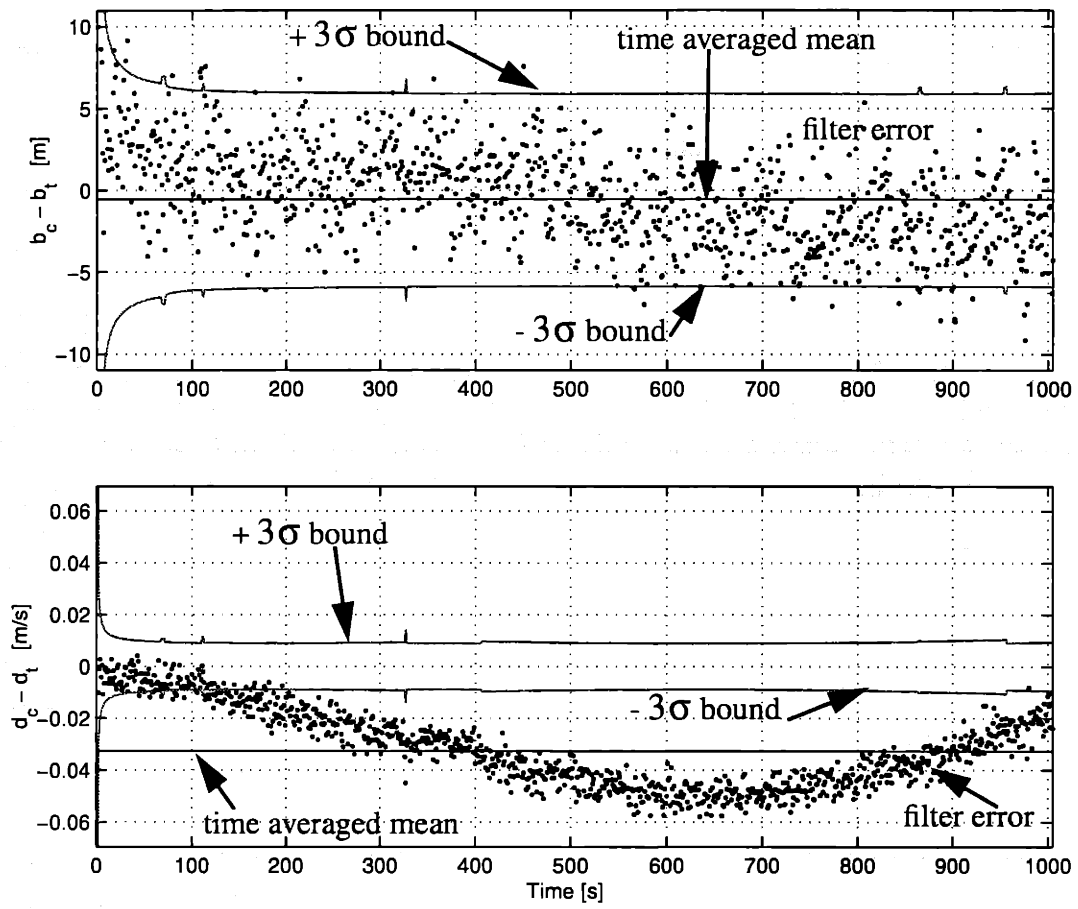


Figure 5.14: Clock Filter Errors when Propagating with the Keplerian State Transition Matrix (Case 1)

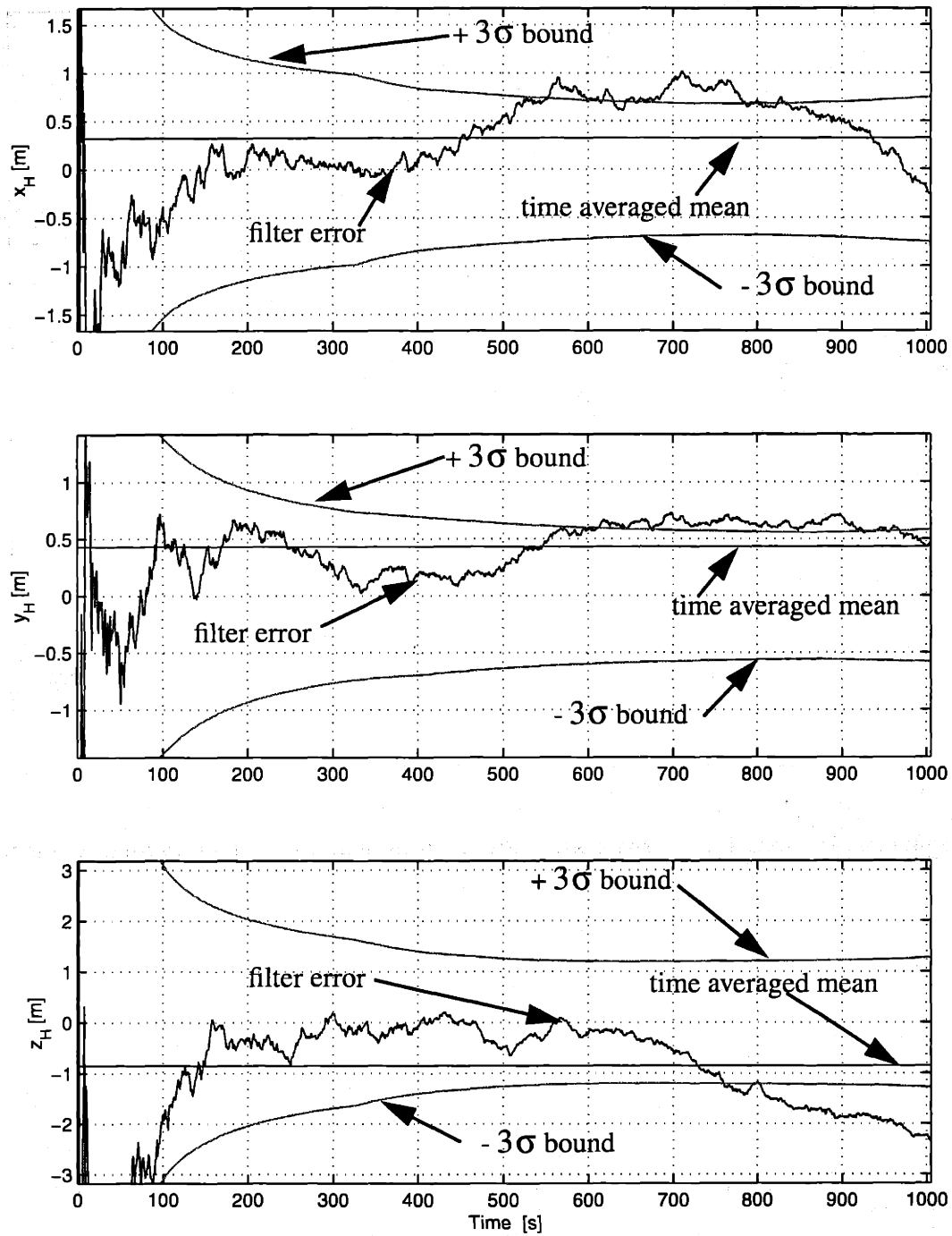


Figure 5.15: Position Filter Errors when Propagating with Kechichian's Analytic Method (Case 1)

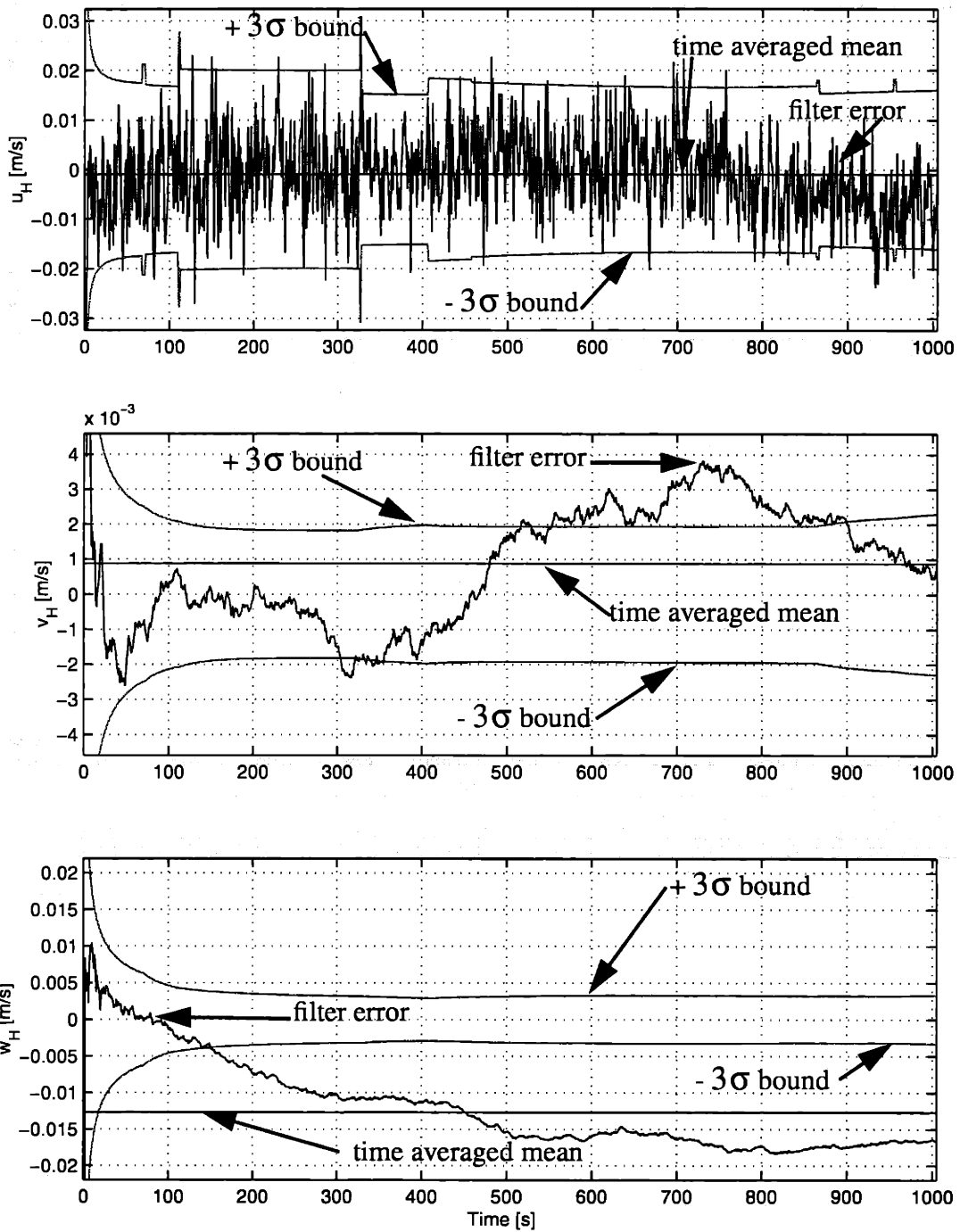


Figure 5.16: Velocity Filter Errors when Propagating with Kechichian's Analytic Method (Case 1)

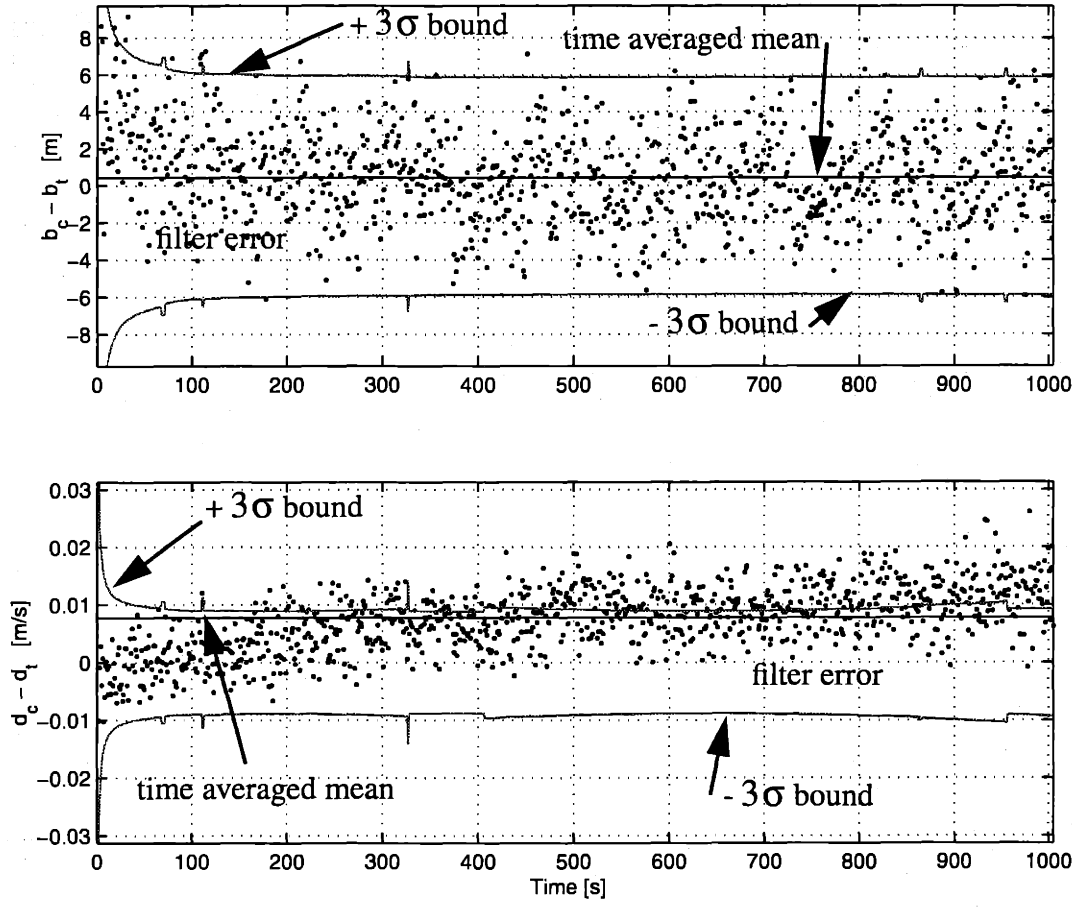


Figure 5.17: Clock Filter Errors when Propagating with Kechichian's Analytic Method (Case 1)

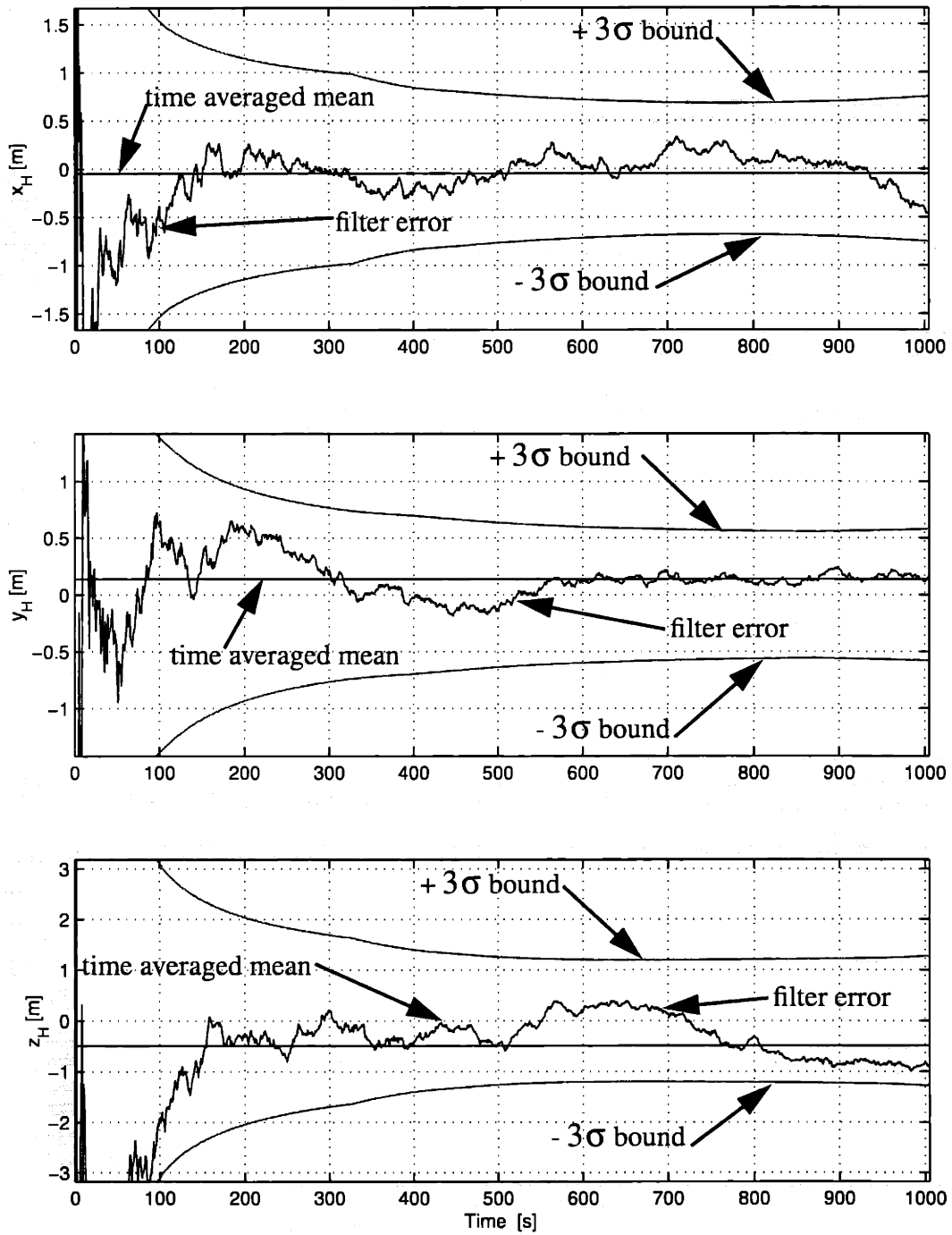


Figure 5.18: Position Filter Errors when Propagating by Integrating the Equations of Motion (Case 1)

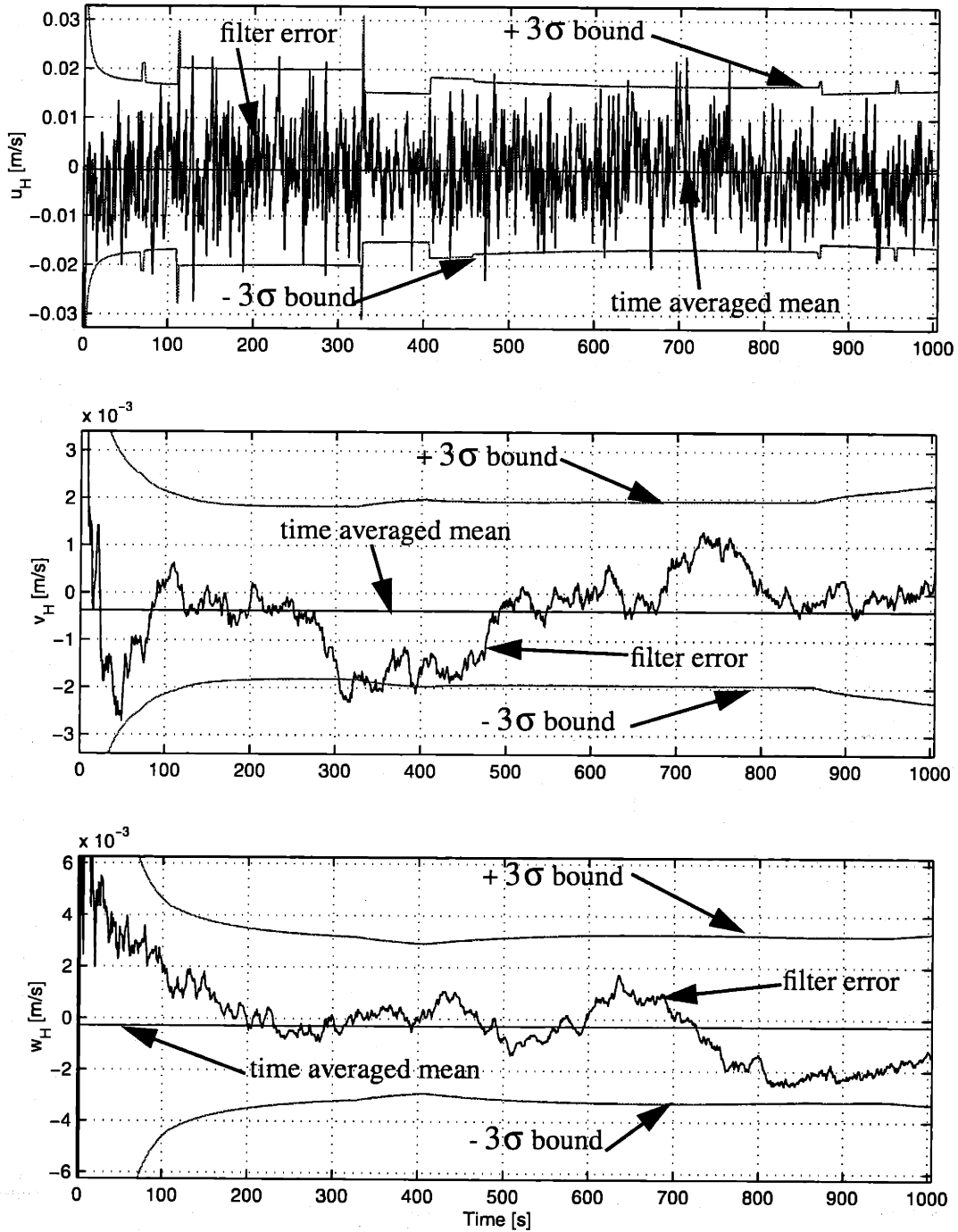


Figure 5.19: Velocity Filter Errors when Propagating by Integrating the Equations of Motion (Case 1)

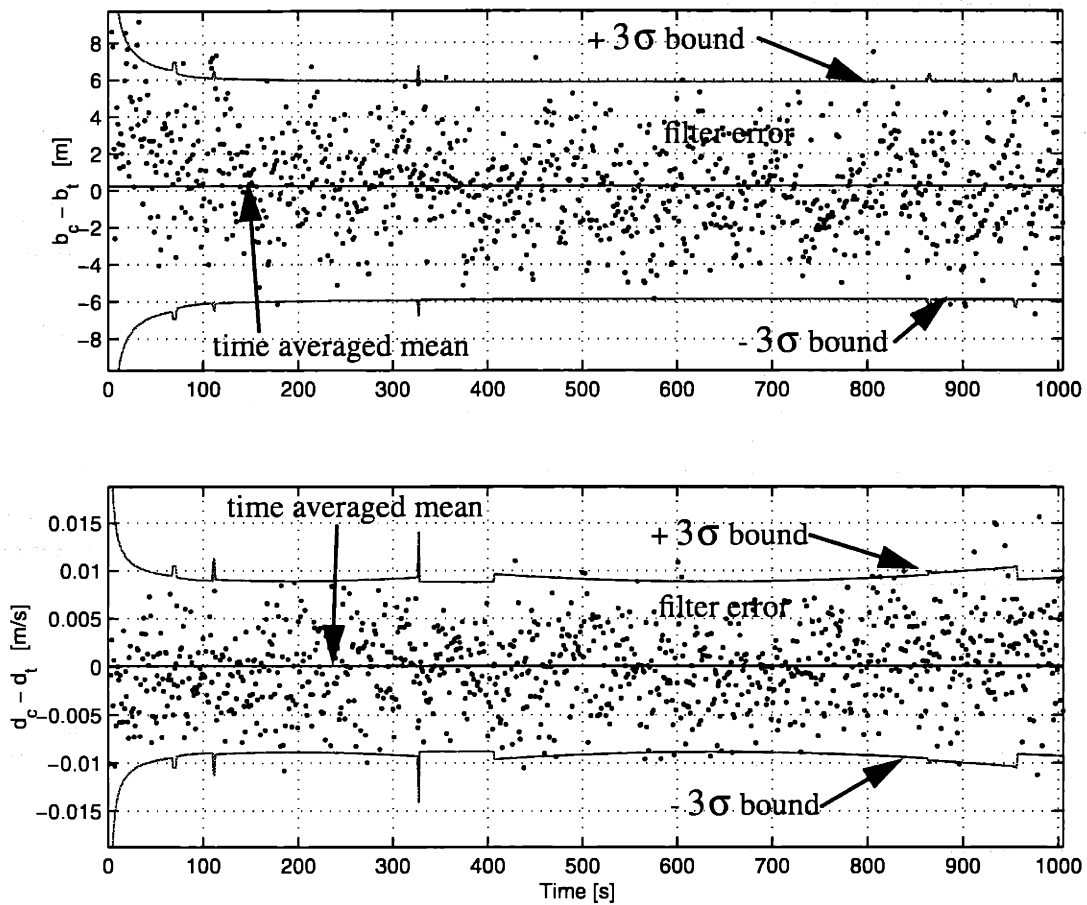


Figure 5.20: Clock Filter Errors when Propagating by Integrating the Equations of Motion (Case 1)

The filter, as stated in the previous section, was tuned using the INT method of propagation. If the filter were to be re-tuned using the other methods, the filter state errors of these methods could be made to fall within the covariance bounds, which would be larger. However, this re-tuning would also have the effect of making the filter errors more noise-like since the filter would weight the measurements more than the propagation.

5.3 Effects of Eccentricity on Propagation with the Clohessy-Wiltshire State Transition Matrix

Filter results for Cases 2 and 3, in which the eccentricity of the chaser orbit was varied, are illustrated in this section to show the effects of eccentricity on the C-W STM propagation method. For comparison, the same cases are run using integration as the propagation technique. The results are given in **Figures 5.21 - 32**.

These figures along with the figures in the first section that correspond to the CW-STM method indicate that as the eccentricity of the chaser orbit decreases, the filter state errors for propagation done with the CW-STM method improve. This most significant improvements are in the x and z-components; whereas, the y-components are dominated by errors due to the effects of J_2 . No noticeable effects due to eccentricity are observed with the INT method.

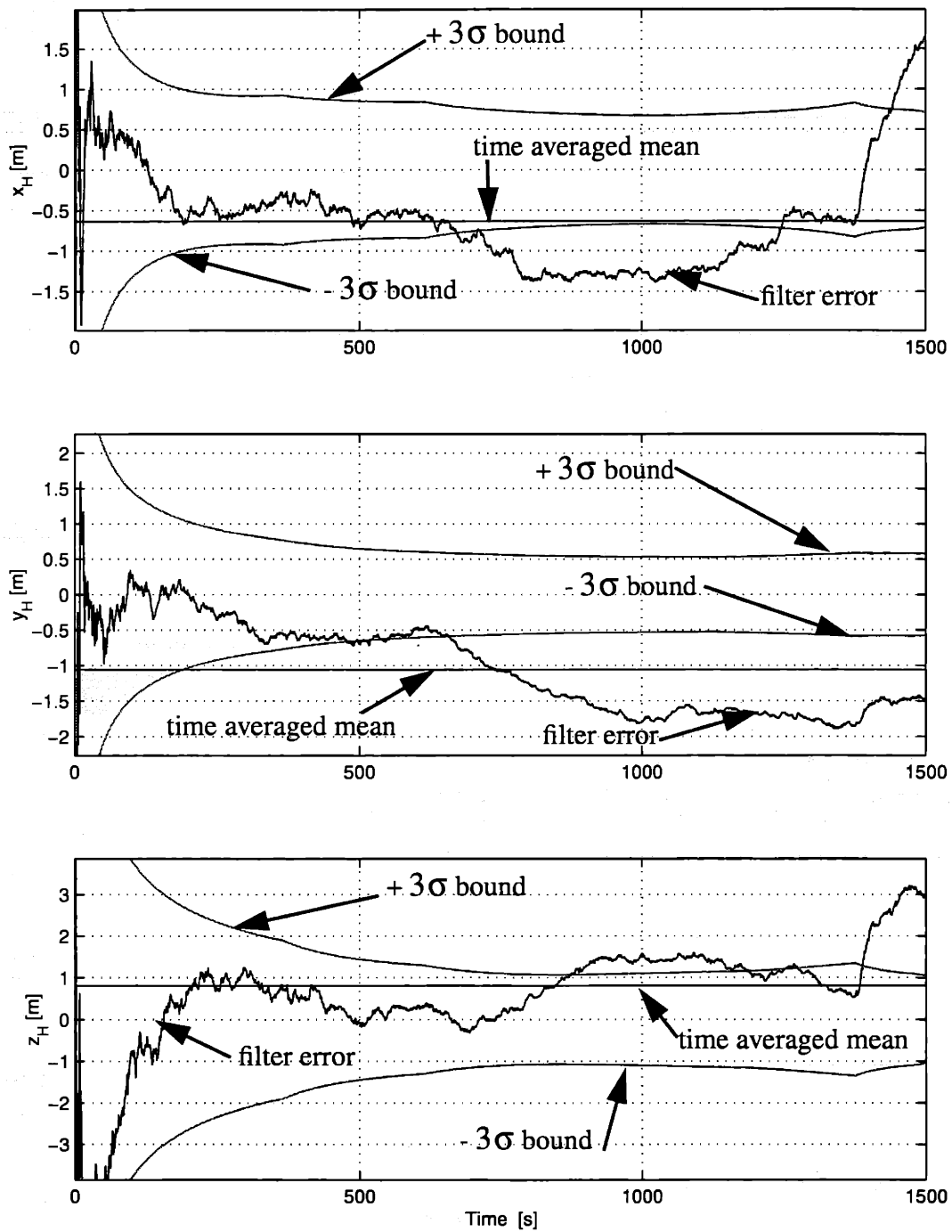


Figure 5.21: Position Filter Errors when Propagating with the Clohessy-Wiltshire State Transition Matrix (Case 2)

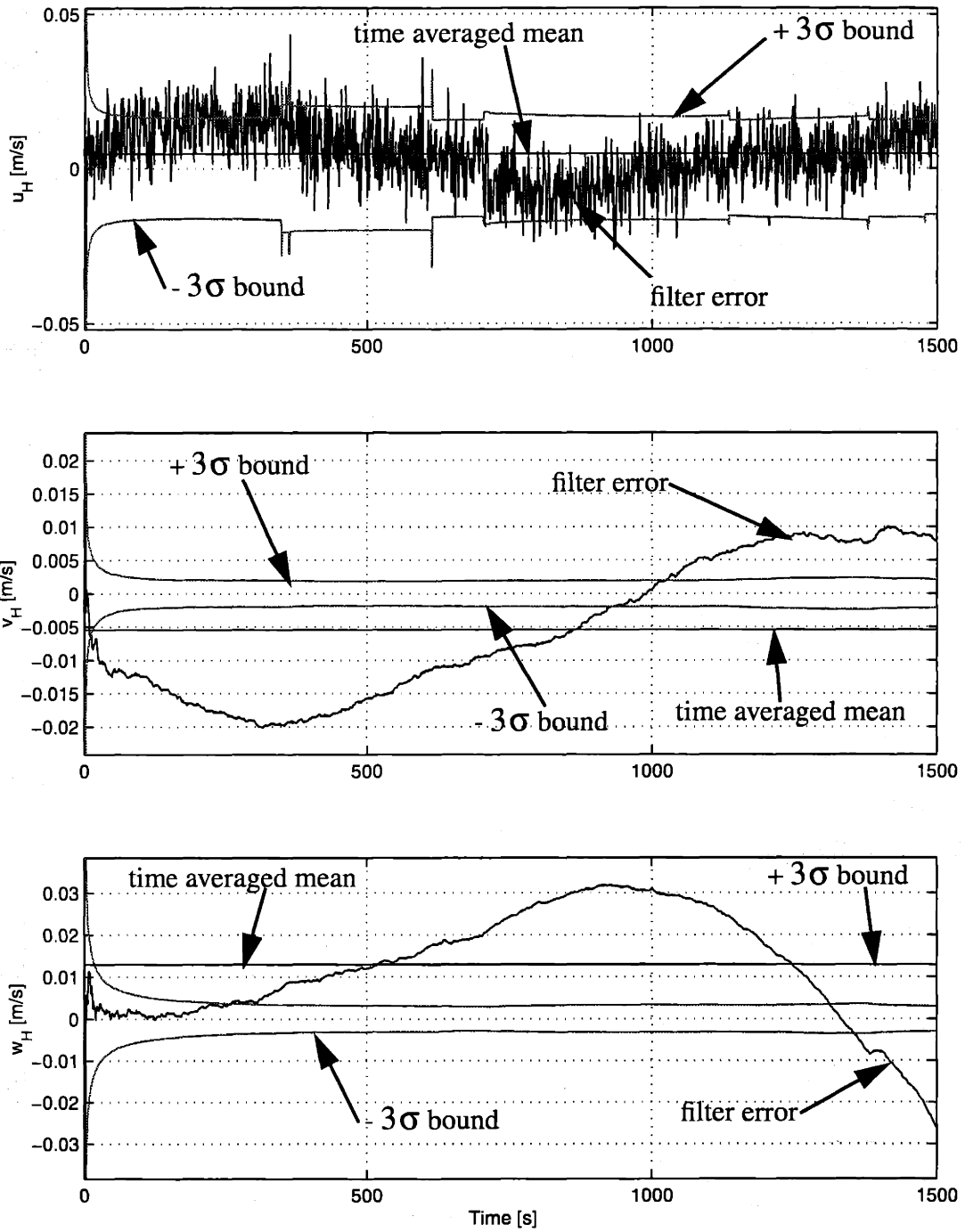


Figure 5.22: Velocity Filter Errors when Propagating with the Clohessy-Wiltshire State Transition Matrix (Case 2)

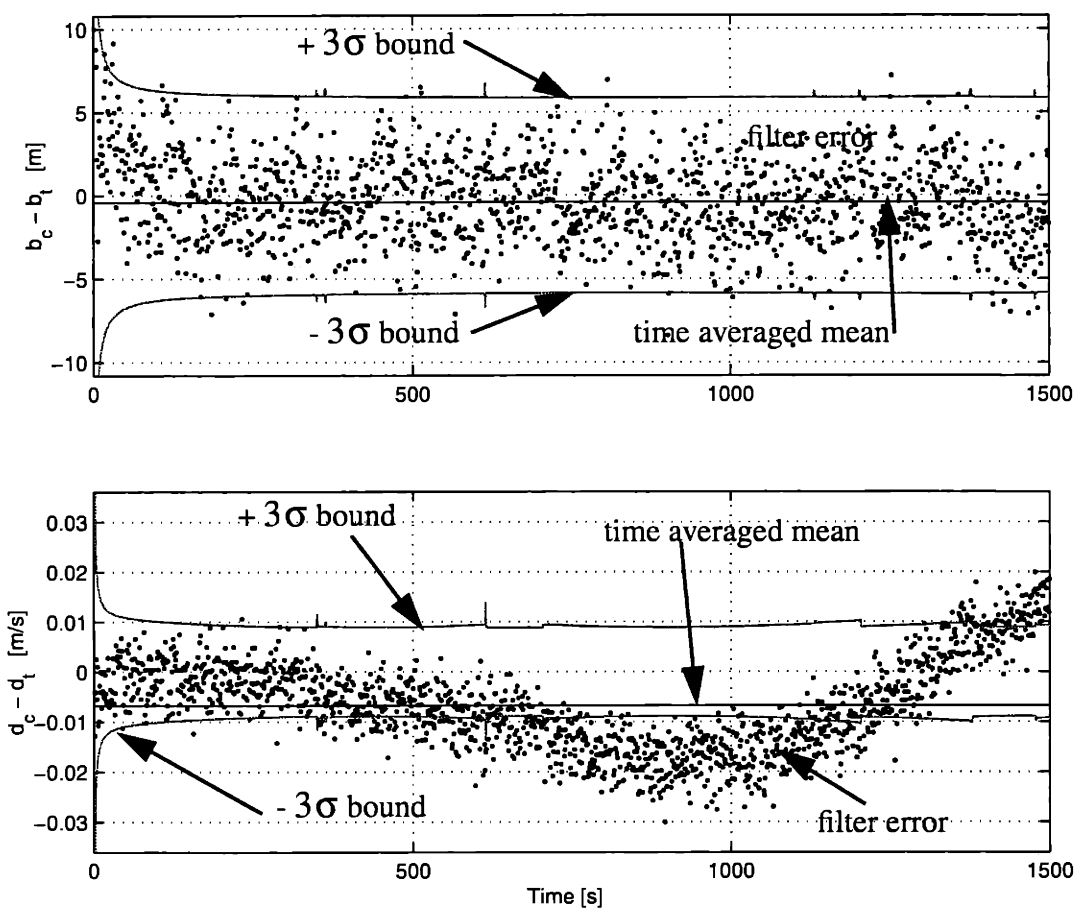


Figure 5.23: Clock Filter Errors when Propagating with the Clohessy-Wiltshire State Transition Matrix (Case 2)

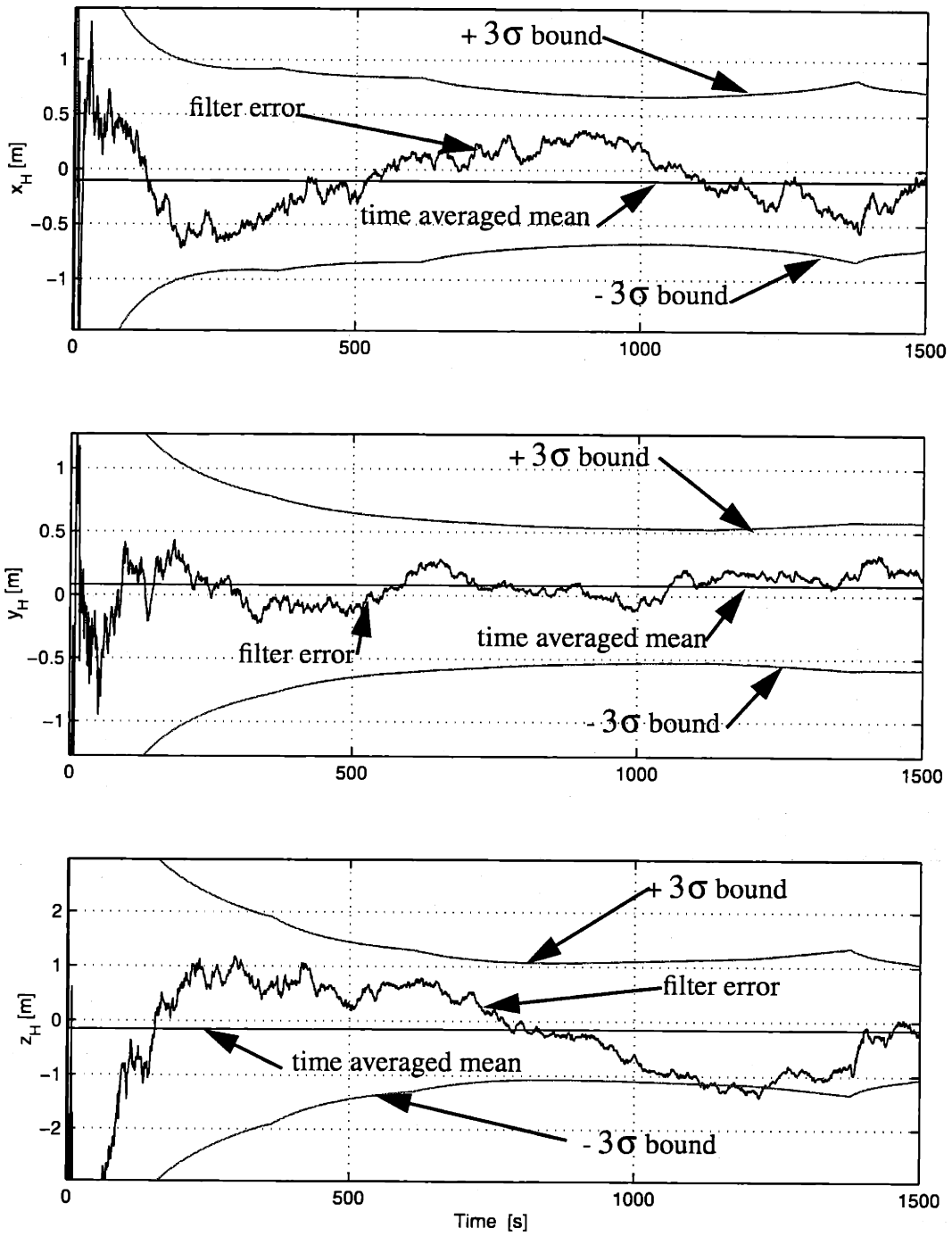


Figure 5.24: Position Filter Errors when Propagating by Integrating the Equations of Motion (Case 2)

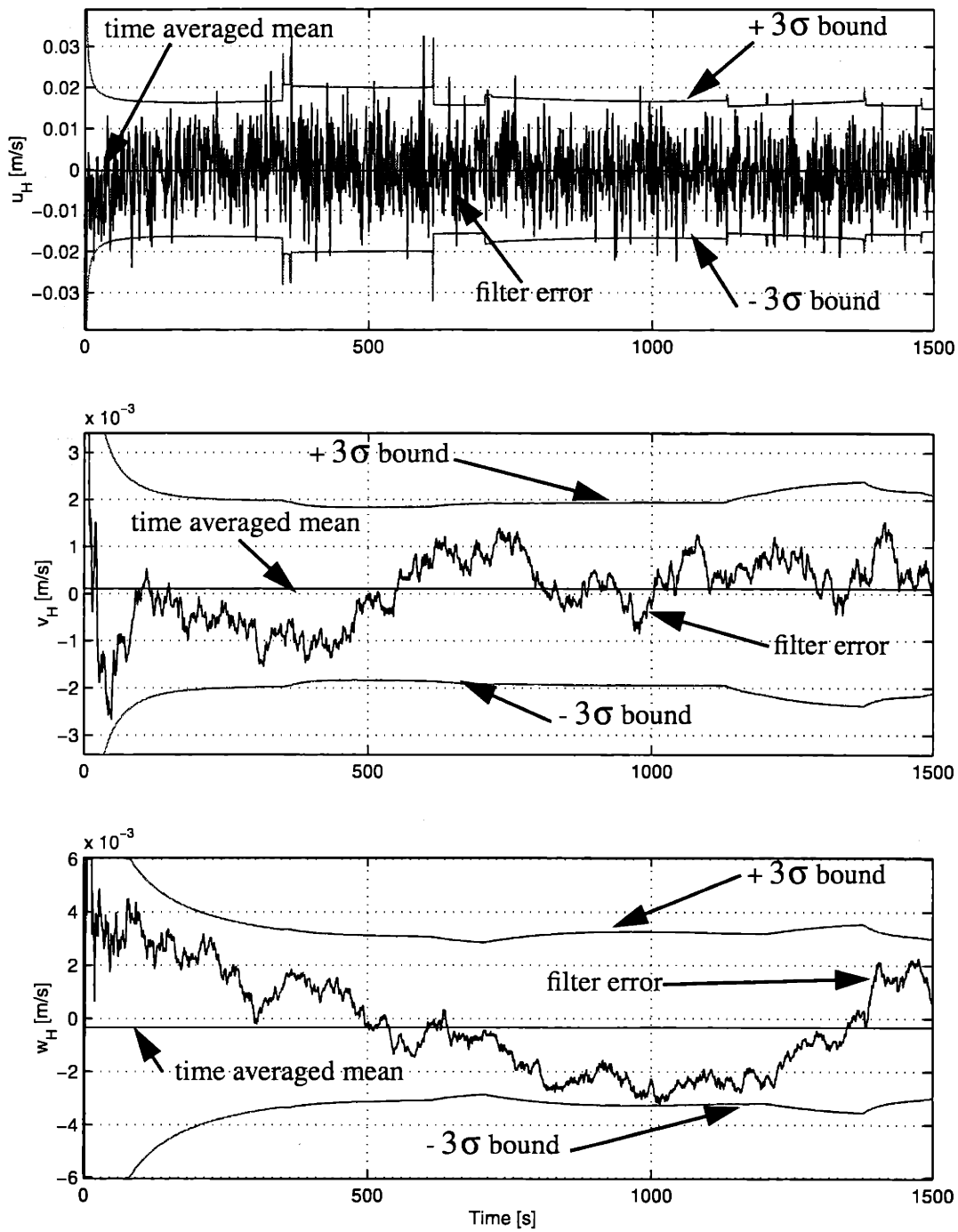


Figure 5.25: Velocity Filter Errors when Propagating by Integrating the Equations of Motion (Case 2)

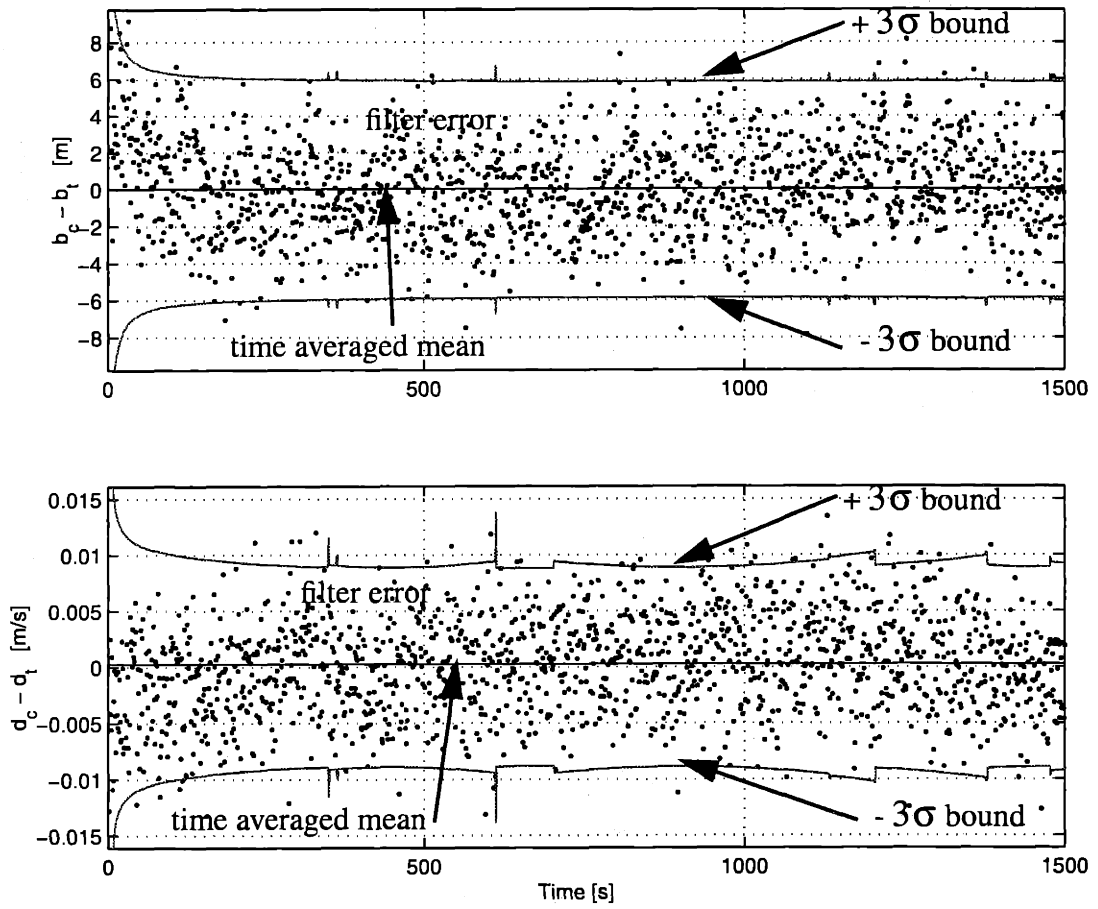


Figure 5.26: Clock Filter Errors when Propagating by Integrating the Equations of Motion (Case 2)

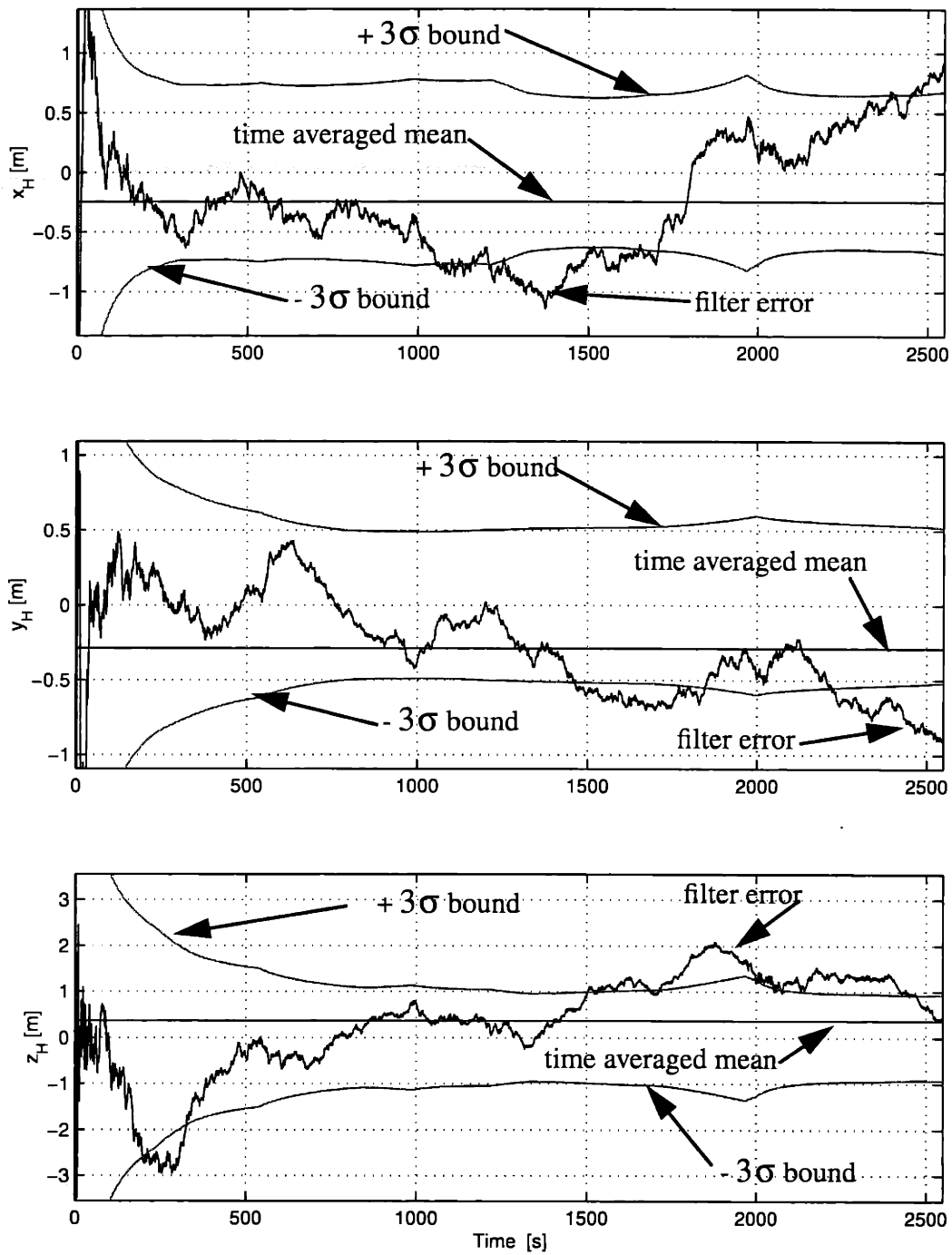


Figure 5.27: Position Filter Errors when Propagating with the Clohessy-Wiltshire State Transition Matrix (Case 3)

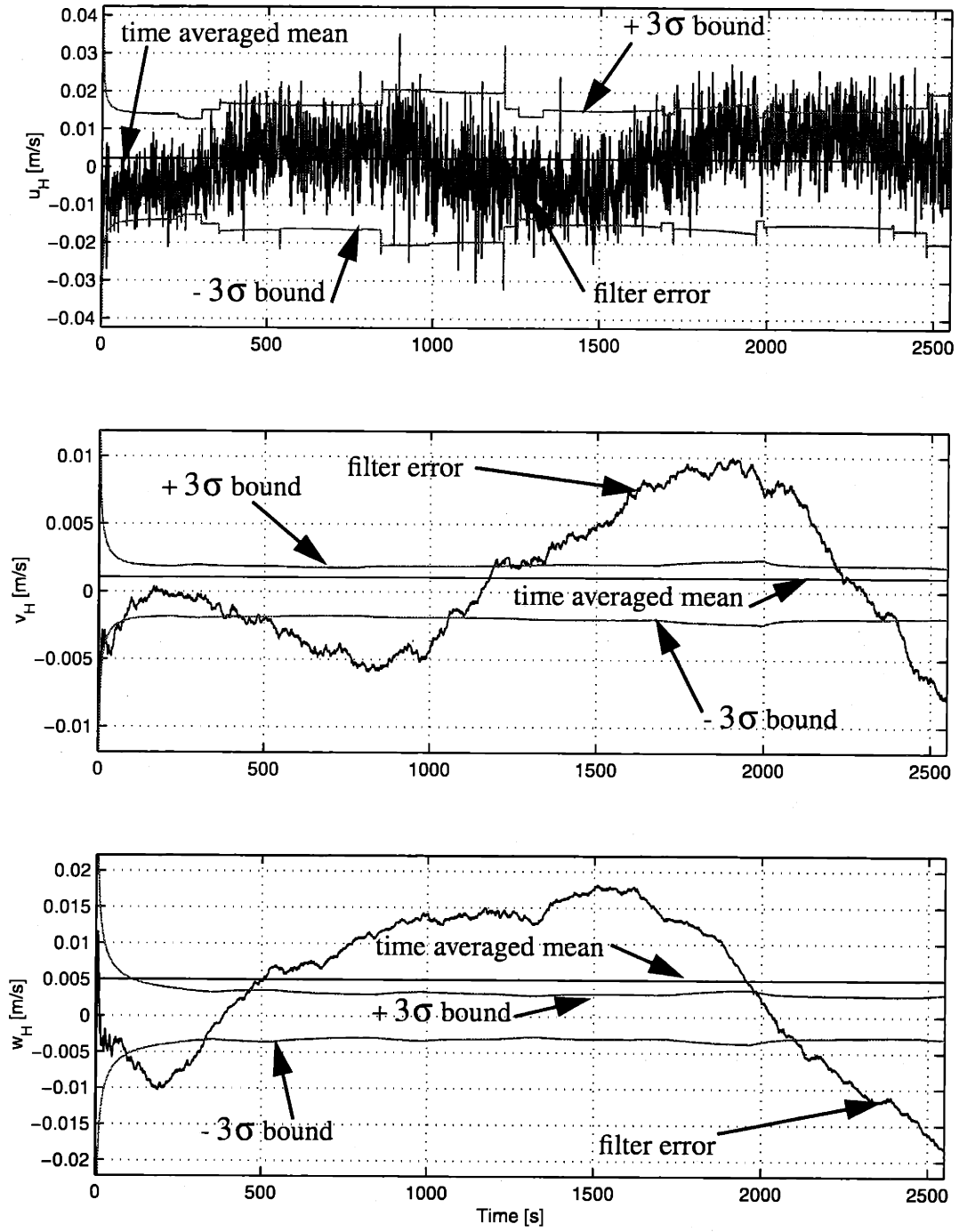


Figure 5.28: Velocity Filter Errors when Propagating with the Clohessy-Wiltshire State Transition Matrix (Case 3)

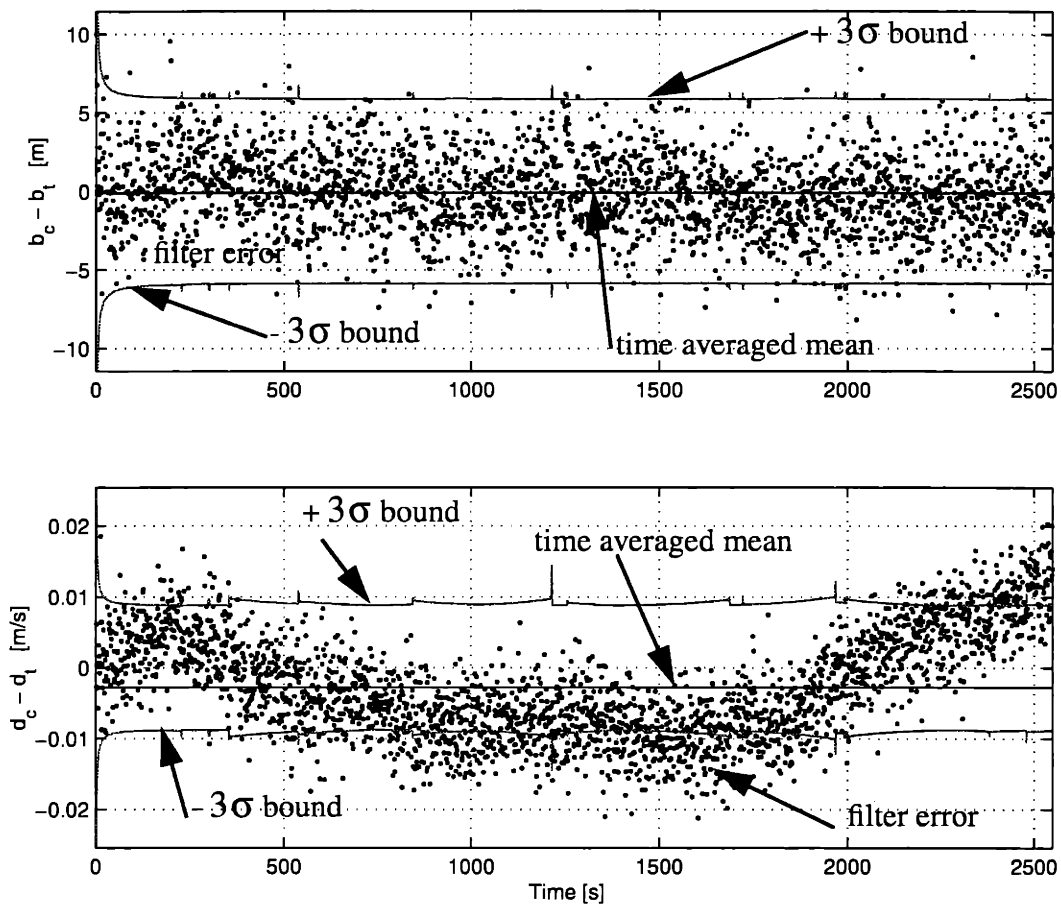


Figure 5.29: Clock Filter Errors when Propagating with the Clohessy-Wiltshire State Transition Matrix (Case 3)

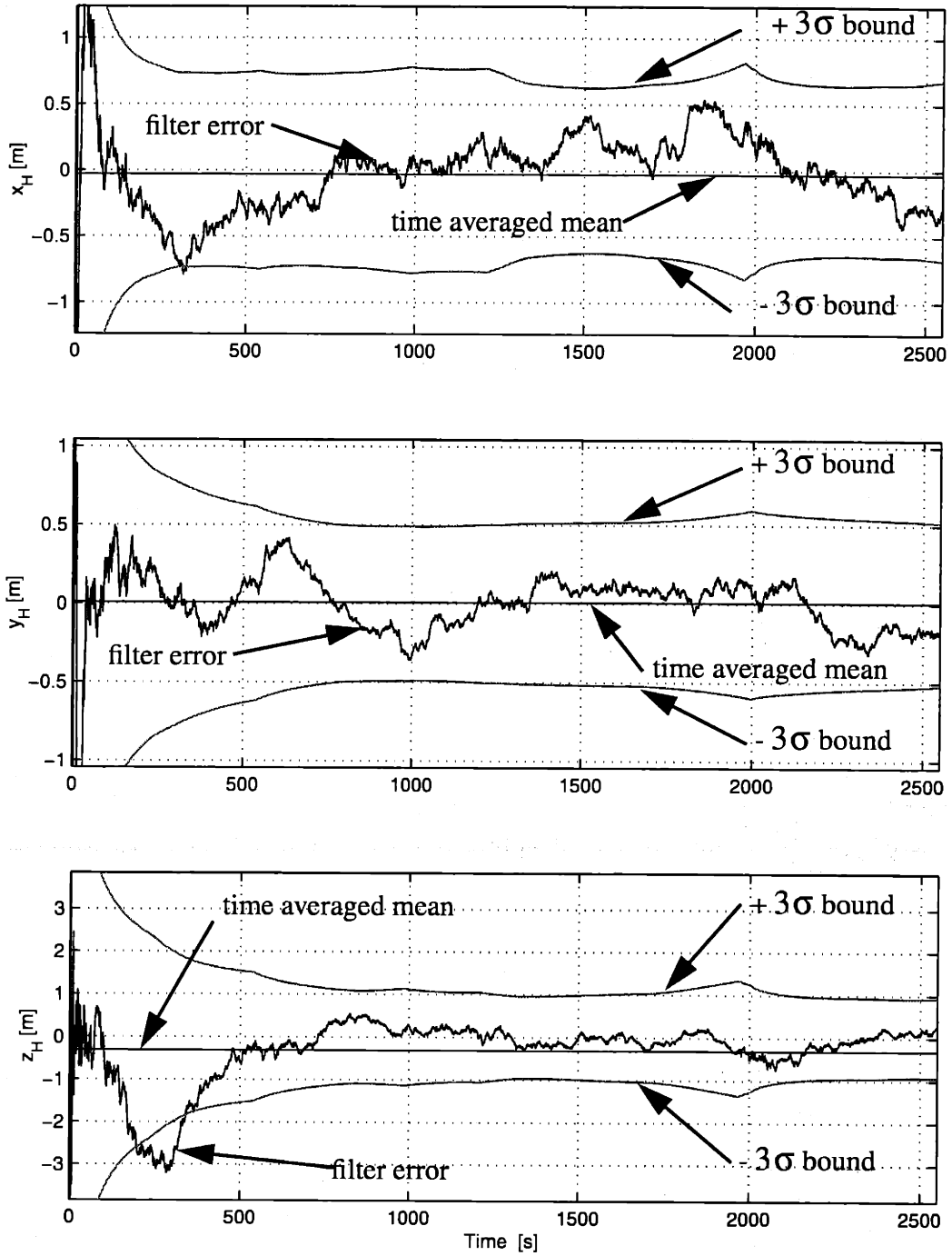


Figure 5.30: Position Filter Errors when Propagating by Integrating the Equations of Motion (Case 3)

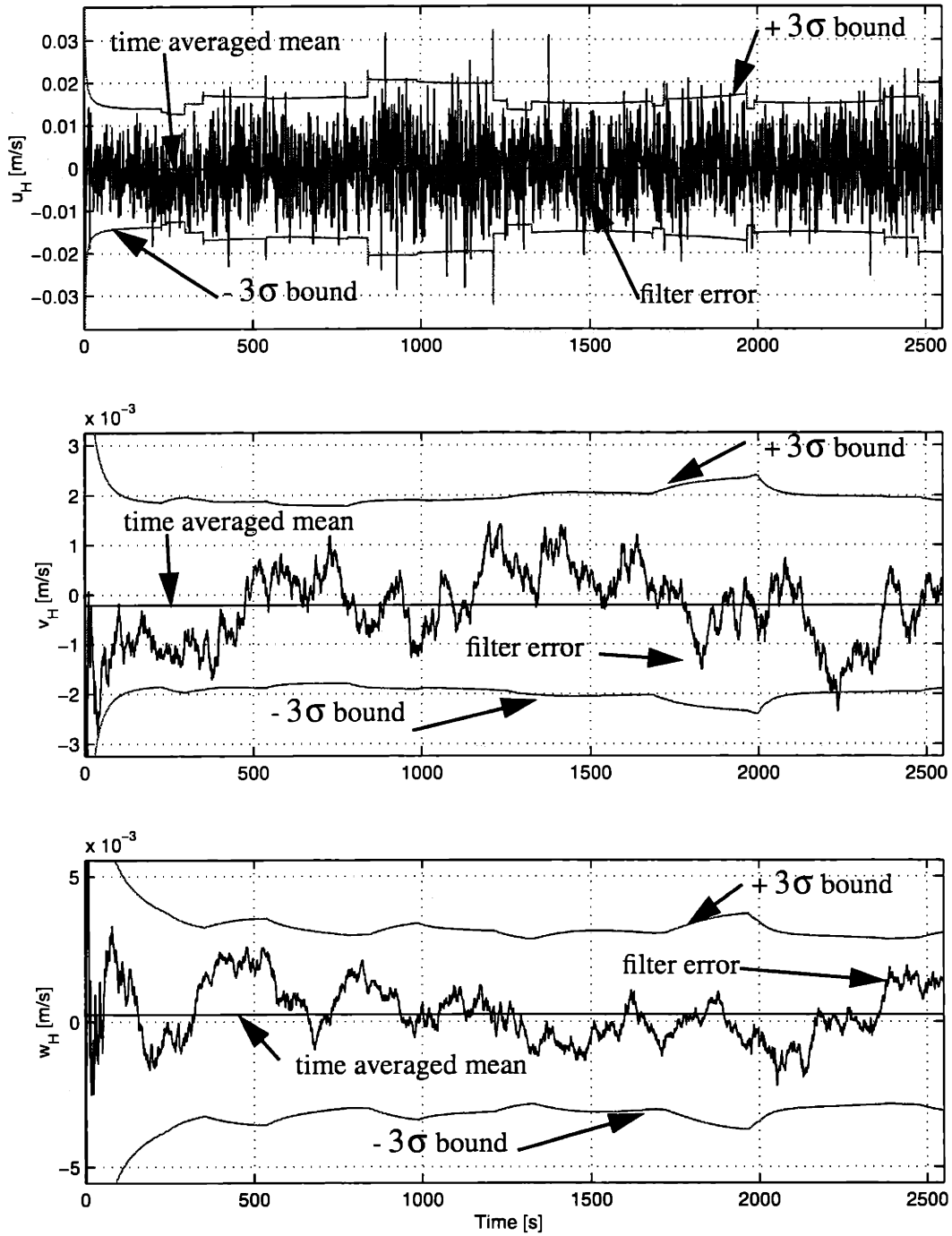


Figure 5.31: Velocity Filter Errors when Propagating by Integrating the Equations of Motion (Case 3)

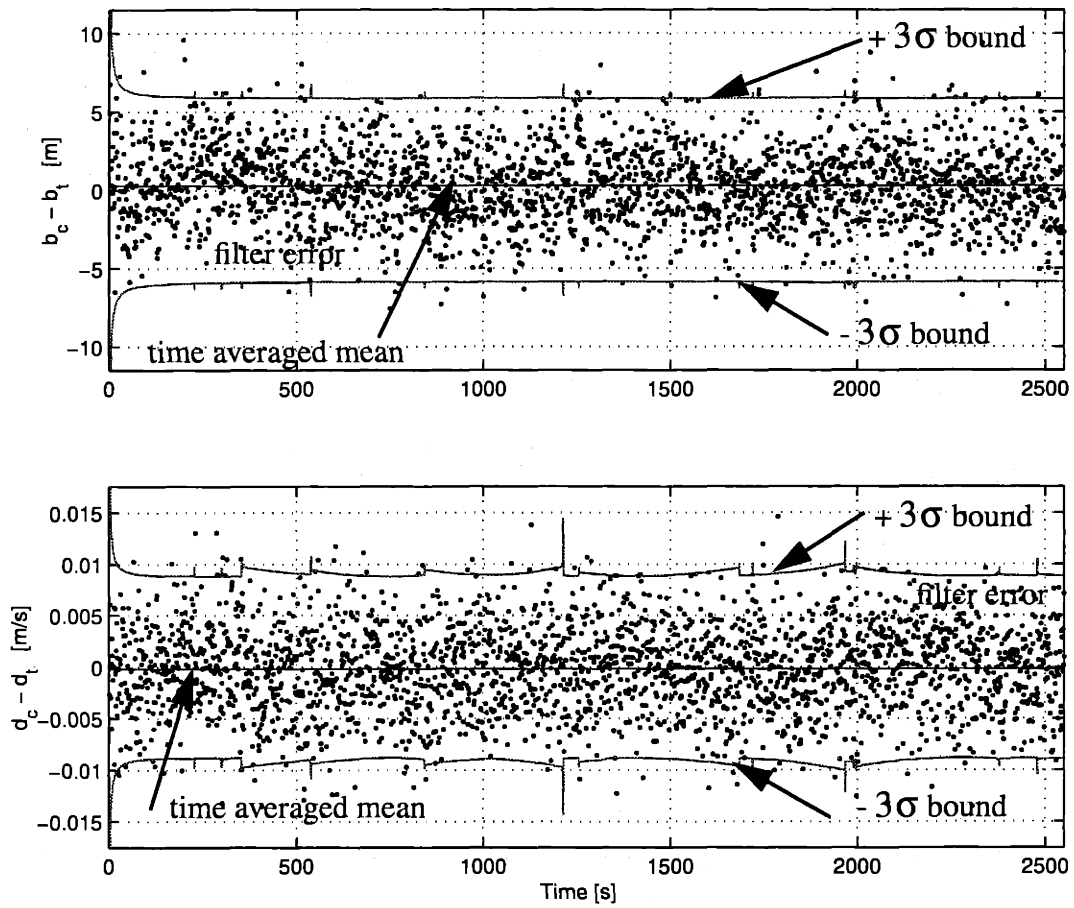


Figure 5.32: Clock Filter Errors when Propagating by Integrating the Equations of Motion (Case 3)

The effects of eccentricity and the separation between the vehicles on the CW-STM propagation are studied further with additional cases. For these cases the chaser and target vehicles are placed in the same orbit and at the same initial separation (approximately 15 km) for each case. The eccentricity of the orbit is varied and the maximum filter state error for the u_H error is recorded. Note that the receiver noise and SA are not included in the measurement errors for this study. The results are depicted in **Figure 5.33**.

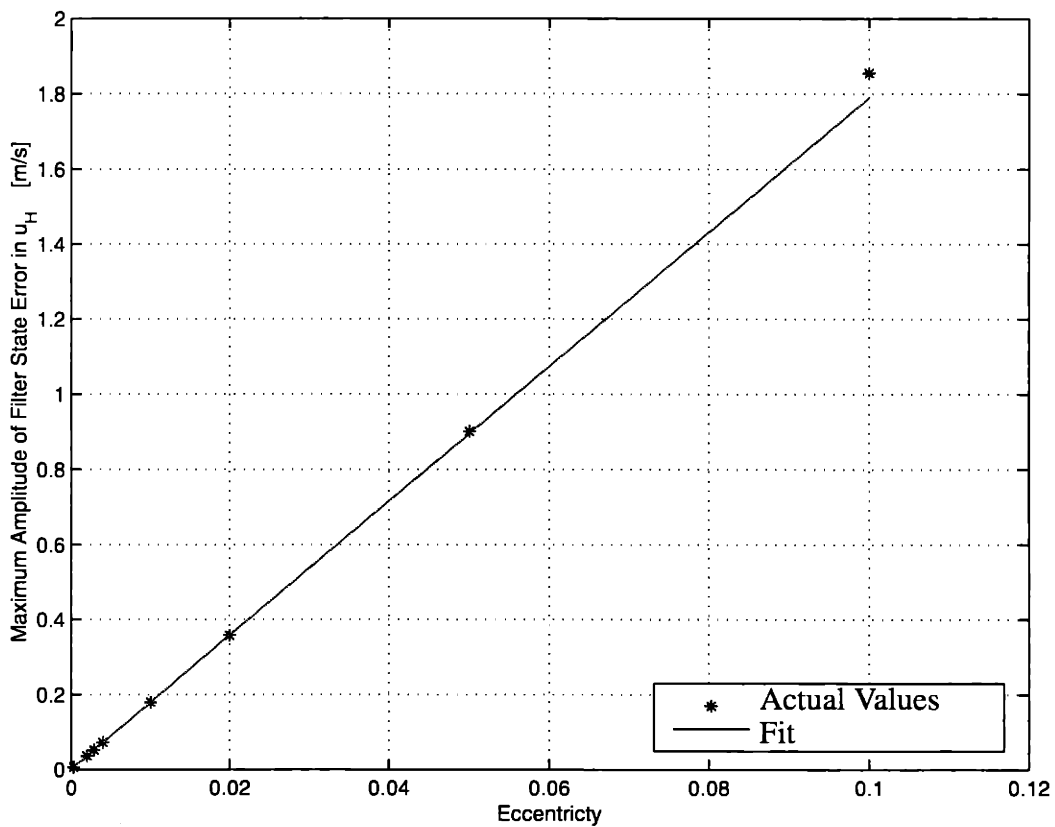


Figure 5.33: Relationship between Filter State Error and Eccentricity when Propagating with the Clohessy-Wiltshire State Transition Matrix

There appears to be a linear relationship between the errors and eccentricity. This linearity begins to deteriorate as eccentricity increases which is noticed in the value of the error corresponding to the eccentricity of 0.1.

In a study on the effects of separation, the eccentricity is held constant ($e = 0.002$), while the initial separation between the vehicles is varied. The results are illustrated in **Figure 5.34**.

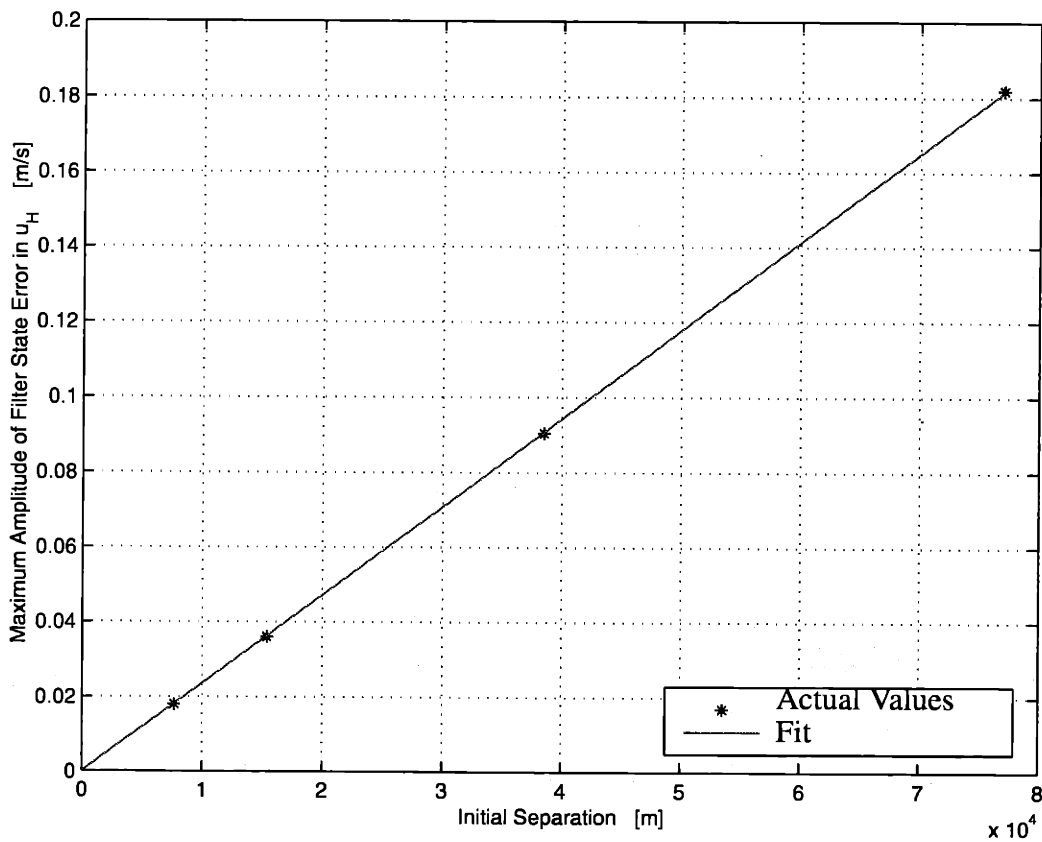


Figure 5.34: Relationship between Filter State Error and Separation when Propagating with the Clohessy-Wiltshire State Transition Matrix

Once again, a linearity is observed between the separation of the vehicles and the filter state error.

Similar relationships are observed with the z-component of the velocity, though the magnitude of the errors are significantly less than those observed in the x-component shown in **Figures 5.33 - 34**.

5.4 Effects of GDOP and Number of Common Satellites

To show the effects that the number of common satellites between the vehicles and GDOP have on the filter performance, plots of both are presented in **Figures 5.35** and **5.36**, respectively, for Case 3.

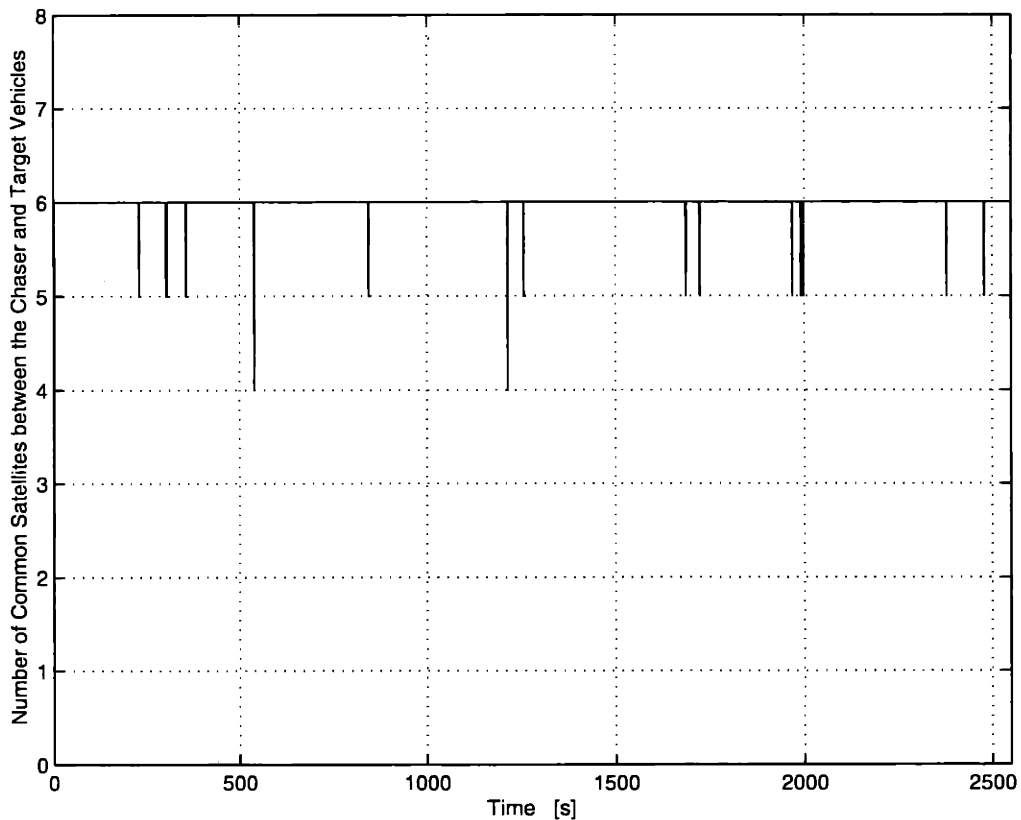


Figure 5.35: Number of Common GPS Satellites between the Chaser Vehicle and the Target Vehicle (Case 3)

Note that though there were six common satellites for most of the run, at two different instances there were only four. The effect these drops have can be easily identified in the filter results with peaks in the covariance bounds. For instance, the drop to four satellites which occurs at time, $t = 1214$ s, corresponds to the peaks in the covariance bounds of the x-component in velocity, clock bias difference, and clock drift differences in **Figures 5.31 - 32.**

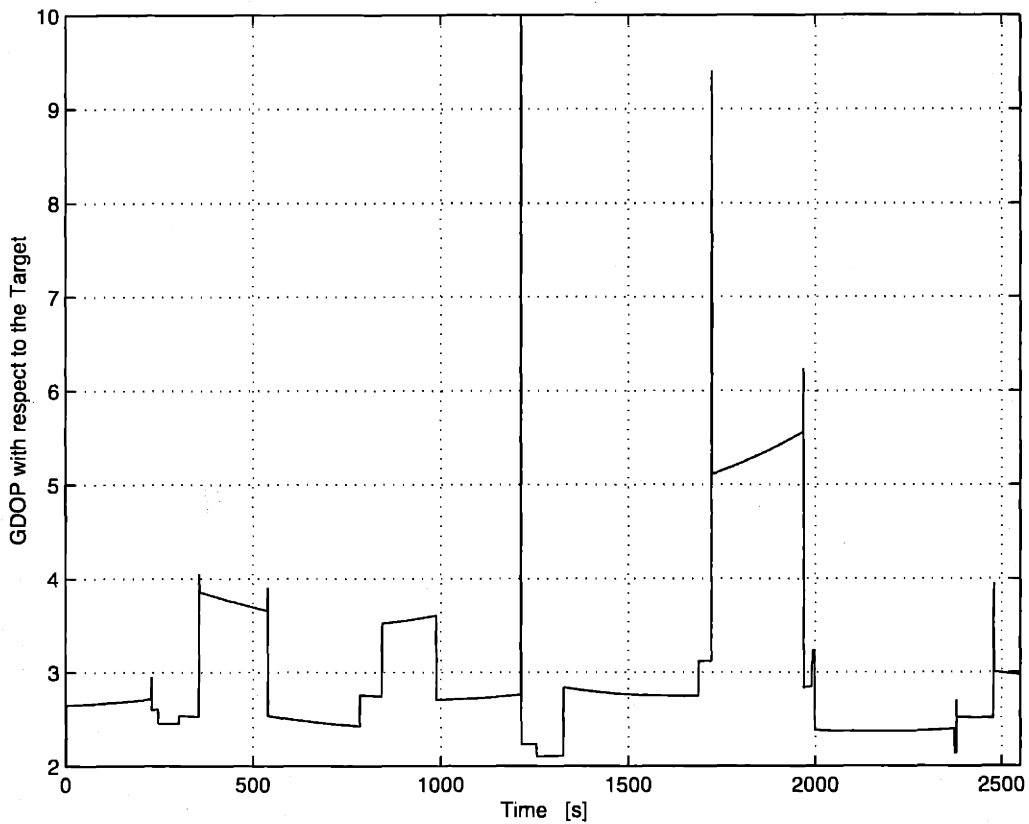


Figure 5.36: GDOP Values with respect to the Target (Case 3)

The effects of GDOP are also important. Notice that one of the drops in the number of common satellites (at $t = 1214$ s) corresponds to an excessively high value of GDOP (22.7). This also explains why the covariance peaks associated with this drop were higher

than the other ones. In comparing the plot of GDOP to the filter state errors of **Figures 5.30 - 32**, it appears that the size of the covariance bounds is directly related to the values of GDOP. For instance, the values of GDOP are highest on average within the 1700 to 1900 second time range. This directly corresponds to the growth in covariance bounds in all the states during the same time range.

5.5 Computation Costs

The number of computations each propagation technique requires is important since it is directly related to the time required to complete the task as well as the required software and hardware. All coding related to this thesis was done on MATLABTM which has the ability to estimate the number of computations with a function called FLOPS (FLOating Point OPerationS count). FLOPS provides an estimate because it is not feasible to count absolutely all operations in MATLABTM. However, it provides a relative scale in which to compare the propagation techniques used. The number of computations each technique required for each propagation step are given in **Table 5.5**.

Propagation Technique	Computations
CW-STM	128
KSTM	1834
KECH	4883
INT	1788

Table 5.5: Computations Required for Each Propagation Technique

Notice that the number of computations of each method is not directly related to the performance.

5.6 Summary of Propagation Methods

Propagating the state with the state transition matrix based on the Clohessy-Wiltshire relative equations of motion was the simplest method in that conversions between frames were not required. This is supported by the fact that the C-W STM technique was, by a significant margin, the lowest computationally intensive method. The CW-STM method is limited by the separation of the vehicles and the eccentricity of their orbits. Despite this, the performance of the filter, when propagating with this technique, still met the performance requirements set in **Chapter 1**. Nonetheless, use of the C-W equations are mostly useful when the orbit of the target is nearly circular, the chaser vehicle is near the target, and the chaser is on a low eccentric orbit.

The Universal Keplerian State Transition Matrix is an excellent analytic method in that it accounts for eccentric orbits. Though frame conversions were required, it was easily adapted to the requirements of this situation and relatively fast in computation. This was primarily due to Shepperd's^[31] new scheme for solving Kepler's problem, which is a required step in computing the transition matrix.

Kechichian's technique^[14] was the only method found that analytically accounted for the J_2 perturbation. As shown in the propagation and filter results, the effects of J_2 were significant, especially in the y-component of the Hill frame. In his paper, Kechichian dem-

onstrates that his technique used in this study, combined with the Newton-Raphson iteration, can be used as a highly accurate analytic two-impulse rendezvous predictor.

Finally, even though integrating the equations of motion was more computationally intensive than using the Clohessy-Wiltshire equations, this method accounted for all the perturbations. Integrating the equations of motion also provides more flexibility since additional models, such as higher gravitational harmonics, can be added if desired.

5.7 Chapter Summary

The results of the study were presented in this chapter. The first section, described the three cases tested and gave a sample of the true states. The following section summarized the effects of propagating and estimating the states with the four techniques described in the previous chapter. The method in which the state is propagated by integrating the equations of motion had the best performance with the smallest propagation and filter state errors. The next section showed the effects of eccentricity on propagating with the Clohessy-Wiltshire State Transition Matrix. A linearity between the x-component velocity error and eccentricity, as well as separation, was observed. The integration method proved to be robust with varying eccentricity. The following section demonstrated the effects of GDOP and number of common satellite on the covariance bounds of the filter state errors. This was followed by an analysis of the computation costs, which showed that the Clohessy-Wiltshire method was the least computationally intensive. Finally, a summary of all the propagation methods was presented.

The following chapter presents the conclusions based on these results, as well as recommendations for future work.

Chapter 6

Conclusions and Recommendations

The goal of this thesis was to analyze a relative GPS navigation filter through the study of various state propagation techniques. The conclusion of this study and recommendations for future work are presented in this chapter.

6.1 Conclusions

The main objective of this thesis was to ensure that the chaser vehicle could efficiently navigate to the target. The performance requirements were taken from current studies performed by the ESA^[9] and were presented in **Chapter 1**. For completeness, they are given again here:

position error < 10 m (3 σ)

velocity error < 0.05 m/s (3 σ)

The results indicate that all four propagation techniques studied surpassed these performance requirements.

Results also indicate that if performance is solely based on overall propagation and filter state errors, the following priority could be assigned with the first indicating the best performance:

1. Integration of the equations of motion
2. Kechichian's analytic method accounting for J_2
3. Universal Keplerian State Transition Matrix
4. State Transition Matrix based on the Clohessy-Wiltshire equations

Note that the numbered rank of this list is used to identify the propagation method for the remainder of this chapter

The factors that affected the performance and, therefore, had a direct role in this prioritization included effects due to perturbations, the eccentricity of the orbits, and the separation between the vehicles.

It was determined that of all the modeled perturbations, which included, J_2 , J_3 , J_4 , and aerodynamic drag, J_2 had the greatest effect. Propagation methods (3) and (4) did not account for J_2 and displayed significant errors in propagating and estimating the y-component position and velocities in the Hill frame. Methods (1) and (2), which did take J_2 into account had the overall best performance.

The effects of eccentricity and separation were observed in propagation methods (2), (3), and (4). Method (2) performed slightly worse than (3) in the z-components because it only included a second-order approximation in eccentricity. This, however, changed as separation between the vehicles increased in which case method (3) began to break down. Further study of method (4) indicated that the maximum errors in the x-component of velocity were linearly related to the eccentricity of the orbits and the separation of the vehicles.

The best performance was observed in propagation method (1), which was expected since the same technique was used to create the orbits. Nonetheless, in a real situation, this

would remain the best propagation technique as it accounts for more perturbations than the other three techniques.

It was determined that GDOP and the number of common satellites had a direct effect on the covariance bounds of the filter state errors.

A study of the computation cost was also performed and if the number of computations were the sole basis in prioritizing the methods, with the first being the least computationally expensive, the priority would be

- State Transition Matrix based on the Clohessy-Wiltshire equations (128)
- Integration of the equations of motion (1788)
- Universal Keplerian State Transition Matrix (1834)
- Kechichian's analytic method accounting for J_2 (4883)

Note that the amount of relative computations per propagation are given in parenthesis in order to depict how each method compares relative to the others.

In conclusion, even though all the propagation techniques met the performance requirements and despite the fact that the C-W technique had the lowest amount of computations, the recommended propagation method is to integrate the equations of motion. In all the cases run, this method was the most robust with the filter errors always remaining within the 3σ covariance bounds. With today's technology, the almost 14-fold increase in computations over the C-W method should not be a significant software or hardware hindrance. Also note that despite the high number of computations, integration required fewer computations than methods (2) and (3).

This study has demonstrated that RGPS navigation can be efficiently used as a method for space rendezvous for long-range operations (20 km to 500 m). In combination with a laser radar, a navigation scheme can be developed to automate a docking and/or berthing operation in space. Current work is being done and tested to implement such systems for service vehicles that will dock with the International Space Station.

6.2 Recommendations for Future Work

Several issues were raised during the course of this study which would be appropriate for future work.

One area of future work could include a study on the effects of chaser vehicle maneuvers on the techniques. Future study could also look into the effects of having less than four GPS satellites in view. This could occur due to view blockage by either vehicle when they are close to each other, unhealthy or loss of SV's, and large vehicle separation. Finally, since propagation method (2) was overall the second best performer in filter state errors, but the worst in number of computations, further study could be conducted to determine if the computations can be decreased. One possibility would be to allow the propagation within the algorithm to go beyond the one second time-step and re-initialize when the state errors reach a pre-defined bound.

More flight experiments, like the ones currently being conducted by NASDA, are also strongly recommended to ensure proper operations when this technology is used for docking and/or berthing with the International Space Station.

6.3 Chapter Summary

The final chapter presented the conclusions of this study. The main one was that although all the propagation techniques met the performance requirements, the technique which integrates the equations of motion had the overall best performance. This was shown by the fact that it had the smallest propagation and filter state errors, which remained within the covariance bounds for all the cases tested. The thesis concluded with recommendations for future work.

Appendix A

Converting between the Hill Frame and the Inertial Frame

Throughout this study, conversions between the relative Hill frame and the inertial frame are required. The purpose of this appendix is to outline how these conversions are made. The method used was developed by J. Arnold Soltz, the author of reference [32].

The conversion from the inertial position and velocities to the Hill frame are presented first. The appendix concludes with the inverse.

A.1 Converting from the Inertial Frame to the Hill Frame

One way to think about the Hill frame, first defined in **Chapter 3**, is as a Forward-Right-Down (FRD) frame. “Down” represents the direction of a vector pointing from the target vehicle to the center of mass of the Earth, “forward” represents the direction of the horizontal component of the target vehicle’s velocity, and “right” represents the direction to the right, perpendicular to down and forward. **Figure A.1** depicts example orbits with this frame.

The first step is to determine the unit vectors of the FRD frame

$$\hat{d} = -\frac{\vec{r}_t}{r_t} \quad (\text{A.1})$$

$$\hat{r} = \frac{\hat{d} \times \vec{v}_t}{|\hat{d} \times \vec{v}_t|} \quad (\text{A.2})$$

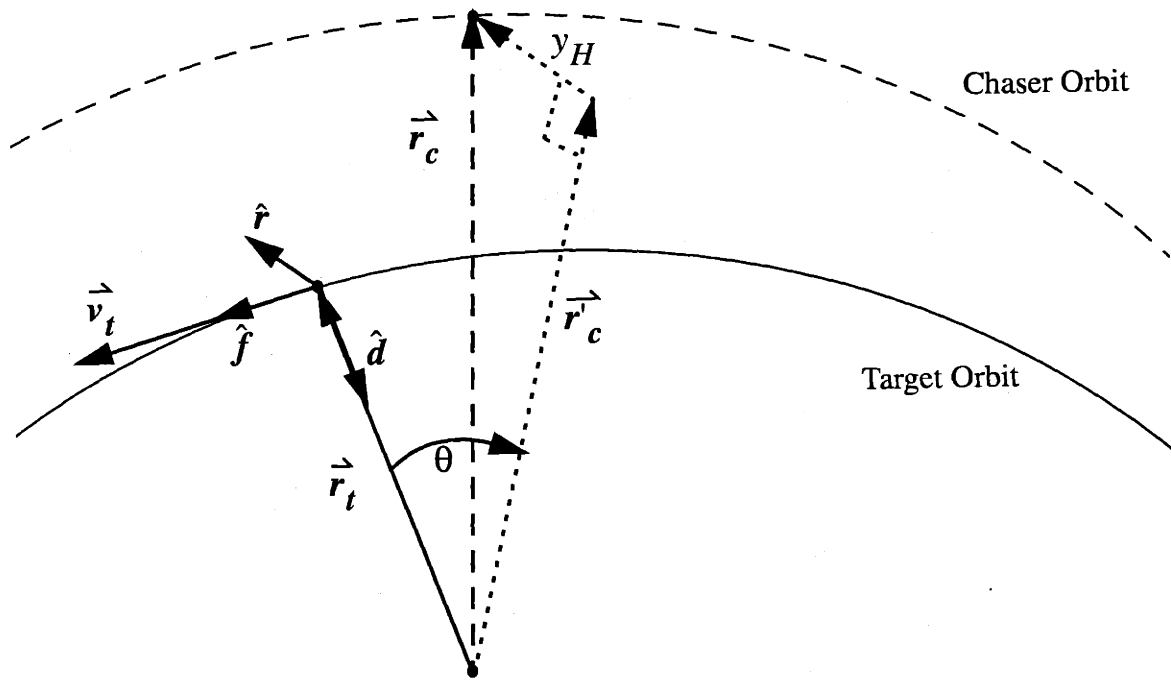


Figure A.1: The Hill Frame Redefined as the FRD Frame

$$\hat{f} = \hat{r} \times \hat{d} \quad (\text{A.3})$$

where \vec{r}_t, \vec{v}_t = position and velocity of the target vehicle in the inertial frame
 $\hat{f}, \hat{r}, \hat{d}$ = forward, right, down unit vectors, respectively

Note that the $\hat{\mathbf{f}}$ and $\hat{\mathbf{d}}$ vectors are in the orbital plane of the target.

Given these unit vectors, a matrix, C_{I2FRD} , can be constructed which converts vectors in the inertial frame to vectors in the FRD frame

$$C_{I2FRD} = \begin{bmatrix} \hat{\mathbf{f}} & \hat{\mathbf{r}} & \hat{\mathbf{d}} \end{bmatrix} \quad (\text{A.4})$$

The inertial positions and velocities of the target and chaser, $\vec{\mathbf{r}}_t$, $\vec{\mathbf{v}}_t$, $\vec{\mathbf{r}}_c$, and $\vec{\mathbf{v}}_c$, are required to make the transformation to the Hill frame. Each of these vectors is first converted to the FRD frame by

$$\vec{\mathbf{w}}_{i_{FRD}} = C_{I2FRD} \vec{\mathbf{w}}_i \quad (\text{A.5})$$

where $\vec{\mathbf{w}}$ represents either the position or velocity vector, and i represents the corresponding target or chaser vehicle

Note that because of the definition of the FRD frame

$$\vec{\mathbf{r}}_{t_{FRD}} = \begin{bmatrix} 0 \\ 0 \\ r_t \end{bmatrix} \quad (\text{A.6})$$

and

$$\vec{\mathbf{v}}_{t_{FRD}} = \begin{bmatrix} v_{t_x} \\ 0 \\ v_{t_z} \end{bmatrix} \quad (\text{A.7})$$

The components of the chaser position and velocity in the target plane can now be easily formed by

$$\vec{r}'_c = \begin{bmatrix} (r_{c_{FRD}})_f \\ 0 \\ (r_{c_{FRD}})_d \end{bmatrix} \quad (\text{A.8})$$

$$\vec{v}'_c = \begin{bmatrix} (v_{c_{FRD}})_f \\ 0 \\ (v_{c_{FRD}})_d \end{bmatrix} \quad (\text{A.9})$$

Since the Hill frame is curvilinear, the length of the arc from the target, along the target orbit, to \vec{r}'_c will be the magnitude of \hat{x}_H . In order to obtain that arc-length, the angle between \vec{r}'_t and \vec{r}'_c , shown as θ in **Figure A.1** must be obtained. This angle must be positive if the chaser is “ahead” of the target and negative if it is “behind.” MATLABTM has a function called ATAN2 which is the four quadrant inverse tangent. It ensures that the proper sign, according to the numerator and denominator of the argument, is assigned. This angle, θ , is obtained by

$$\theta = \text{atan2} \left(\frac{(r_{c_{FRD}})_f}{-(r_{c_{FRD}})_d} \right) \quad (\text{A.10})$$

Note the negative sign in the denominator of the argument to ensure the proper sign of θ .

The x-component of the position can now be easily obtained from

$$x_H = r_t \theta \quad (\text{A.11})$$

The y and z-components of position are obtained with

$$y_H = (r_{c_{FRD}})_r \quad (\text{A.12})$$

and

$$z_H = r_t - r'_c \quad (\text{A.13})$$

Both of these equations can be confirmed with **Figure A.1**.

Kepler's Second Law is helpful in obtaining the x-component of the velocity in the Hill frame

$$\dot{\theta} = \frac{h}{r^2} \quad (\text{A.14})$$

where h = magnitude of angular momentum

The time derivative of **Equation (A.11)** is

$$u_H = r_t \dot{\theta} + \dot{r}_t \theta \quad (\text{A.15})$$

where $\dot{\theta} = \dot{\theta}_{c'} - \dot{\theta}_t$

The last term in **Equation (A.15)** is zero since the Hill frame assumes that the target is in a circular orbit. That is, r_t is constant with time and, therefore, its derivative is zero.

The target's velocity along the x direction is already known

$$(v_{t_{FRD}})_f = r_t \dot{\theta}_t \quad (\text{A.16})$$

Therefore, the only remaining element to find is $\dot{\theta}_{c'}$. Using **Equation (A.14)**

$$\dot{\theta}_{c'} = \frac{|\dot{\mathbf{r}}_{c_{FRD}} \times \dot{\mathbf{v}}_{c_{FRD}}|}{r_{c_{FRD}}^2} \quad (\text{A.17})$$

Finally, the x-component of velocity in the Hill frame is

$$u_H = r_t \frac{|\dot{\mathbf{r}}_{c_{FRD}} \times \dot{\mathbf{v}}_{c_{FRD}}|}{r_{c_{FRD}}^2} - (v_{t_{FRD}})_f \quad (\text{A.18})$$

The y-component of the velocity is

$$v_H = (v_{c_{FRD}})_r \quad (\text{A.19})$$

since there is no y-component term from the target

Finally, the z-component of velocity is obtained by differencing the z-components

$$w_H = v_{c_z} - v_{t_z} = v_{c_z} - \left(\frac{\vec{r}'_c}{r'_c} \cdot \vec{v}'_c \right) \quad (\text{A.20})$$

A.2 Converting from the Hill Frame to the Inertial Frame

In order to convert from the Hill frame to the inertial frame, the inertial position and velocity of the target, \vec{r}_t and \vec{v}_t , and the relative position and velocity of the chaser, x_H , y_H , z_H , u_H , v_H , and w_H , are required.

Since \vec{r}_t and \vec{v}_t are known, the unit vectors of the FRD frame, \hat{f} , \hat{r} , and \hat{d} , can once again be obtained, which yields C_{I2FRD} . To obtain the matrix that converts vectors in the FRD frame to vectors in the inertial frame, the transform is taken

$$C_{FRD2I} = C_{I2FRD}^T \quad (\text{A.21})$$

First, however, $\hat{r}_{t_{FRD}}$ and $\hat{v}_{t_{FRD}}$ are obtained from **Equation (A.5)**, or **Equations (A.6)** and **(A.7)**.

Solving for r'_c in **Equation (A.13)** yields

$$r'_c = r_t - z_H \quad (\text{A.22})$$

and solving for θ in **Equation (A.11)** yields

$$\theta = \frac{x_H}{r_t} \quad (\text{A.23})$$

From the geometry of **Figure A.1** and **Equation (A.12)** the FRD position coordinates of the chaser can be constructed by

$$(r_{c_{\text{FRD}}})_f = r'_c \sin \theta \quad (\text{A.24})$$

$$(r_{c_{\text{FRD}}})_r = y_H \quad (\text{A.25})$$

$$(r_{c_{\text{FRD}}})_d = -r'_c \cos \theta \quad (\text{A.26})$$

Note that since the magnitude of position vectors do not change in frame transformations

$$r_c = r_{c_{\text{FRD}}} \quad (\text{A.27})$$

In order to obtain the FRD velocity coordinates of the chaser, **Equations (A.15 - 20)** are used to determine the values for v_c and φ with

$$v_c \cos \varphi = \frac{(r_{c_{\text{FRD}}})_r v_H - r'_c (w_H + (v_{t_{\text{FRD}}})_d)}{r_c} \quad (\text{A.28})$$

$$v_c \sin \varphi = \frac{r_c}{r_t} (u_H + (v_{t_{\text{FRD}}})_f) \quad (\text{A.29})$$

$$v_c^2 = (v_c \cos \varphi)^2 + (v_c \sin \varphi)^2 \quad (\text{A.30})$$

and

$$v'_c = \sqrt{v_c^2 - v_H^2} \quad (\text{A.31})$$

$$\sin \psi = \frac{(w_H + (v_{t_{FRD}})_d)}{v'_c} \quad (\text{A.32})$$

$$\varphi = \theta + \text{asin}(\sin \psi) \quad (\text{A.33})$$

Now, the FRD velocity coordinates of the chaser can be constructed

$$(v_{c_{FRD}})_f = v'_c \cos \varphi \quad (\text{A.34})$$

$$(v_{c_{FRD}})_r = v_H \quad (\text{A.35})$$

$$(v_{c_{FRD}})_d = v'_c \sin \varphi \quad (\text{A.36})$$

Finally, In order to obtain the inertial coordinates, the C_{FRD2I} transformation matrix is used

$$\vec{r}_c = C_{FRD2I} \hat{r}_{c_{FRD}} \quad (\text{A.37})$$

$$\vec{v}_c = C_{FRD2I} \hat{v}_{c_{FRD}} \quad (\text{A.38})$$

Appendix B

Equations for Constants in Kechichian's Algorithm

Chapter 4 outlined the equations of relative motion obtained by Jean Kechichian.^[14] The intent of this appendix is to describe the algorithm in more detail. The routine includes a basic solution which accounts for J_2 effects, as well as a second approximation which accounts for eccentricity. This appendix supplements the equations presented in **Subsection 4.2.3**. It includes the equations used to obtain the initial conditions, all the required coefficients, and the equations which are used to convert the solution from the local frame to the inertial frame.

B.1 Initial Conditions

The initial conditions are based on the classical orbital elements $(a, e, i, \Omega, \omega, f_0)$ and the argument of latitude (θ_0) at the initial time, or epoch. The reference circular orbit is defined to have an eccentricity of zero and a semimajor axis, a_r , equal to that of the orbit's at epoch. Recall that the orbital elements of the vehicle orbit will not be constant because of the effects of J_2 .

The relative initial position components are obtained from

$$x_0 = r_0 - a_r \tag{B.1}$$

$$y_0 = 0 \tag{B.2}$$

$$z_0 = 0 \quad (\text{B.3})$$

where $r_0 = \frac{a(1-e^2)}{(1+ec_{f0})} = \text{radial distance at epoch}$

The relative initial velocity components are obtained from

$$\begin{bmatrix} \dot{x}_0 \\ \dot{y}_0 \\ \dot{z}_0 \end{bmatrix} = R_{\Omega i \theta_0}^T \begin{bmatrix} \dot{x}_0(I) \\ \dot{y}_0(I) \\ \dot{z}_0(I) \end{bmatrix} \quad (\text{B.4})$$

where

$$R_{\Omega i \theta_0} = \begin{bmatrix} c_{\Omega} c_{\theta_0} - s_{\Omega} c_i s_{\theta_0} & -c_{\Omega} s_{\theta_0} - s_{\Omega} c_i c_{\theta_0} & s_{\Omega} s_i \\ s_{\Omega} c_{\theta_0} + c_{\Omega} c_i s_{\theta_0} & -s_{\Omega} s_{\theta_0} + c_{\Omega} c_i c_{\theta_0} & -c_{\Omega} s_i \\ s_i s_{\theta_0} & s_i c_{\theta_0} & c_i \end{bmatrix}$$

$$\begin{aligned} \dot{x}_0(I) = & \frac{\mu}{h_{sc}} [-c_{\Omega}(s_{\theta_0} + es_{\omega}) - s_{\Omega}(c_{\theta_0} + ec_{\omega})c_i] \\ & - \frac{\mu}{h_{ref}} (-c_{\Omega} s_{\theta_0} - s_{\Omega} c_i c_{\theta_0}) \\ & + \frac{h_{ref}}{2a_r} (c_{\Omega} s_i \rho_z^0 + c_i \rho_y^0) \end{aligned}$$

$$\begin{aligned} \dot{y}_0(I) = & \frac{\mu}{h_{sc}} [-s_{\Omega}(s_{\theta_0} + es_{\omega}) + c_{\Omega}(c_{\theta_0} + ec_{\omega})c_i] \\ & - \frac{\mu}{h_{ref}} (-s_{\Omega}s_{\theta_0} + c_{\Omega}c_i c_{\theta_0}) \\ & + \frac{h_{ref}}{2} (s_{\Omega}s_i \rho_{\hat{z}}^0 - c_i \rho_{\hat{x}}^0) \\ & a_r \end{aligned}$$

$$\begin{aligned} \dot{z}_0(I) = & \frac{\mu}{h_{sc}} (c_{\theta_0} + ec_{\omega})s_i - \frac{\mu}{h_{ref}} s_i c_{\theta_0} \\ & - \frac{h_{ref}}{2} (s_{\Omega}s_i \rho_{\hat{y}}^0 + c_{\Omega}s_i \rho_{\hat{x}}^0) \\ & a_r \end{aligned}$$

and where

$$\begin{bmatrix} 0 \\ \rho_{\hat{x}}^0 \\ 0 \\ \rho_{\hat{y}}^0 \\ 0 \\ \rho_{\hat{z}}^0 \end{bmatrix} = \begin{bmatrix} (R_{\Omega i \theta_0})_{11} \\ (R_{\Omega i \theta_0})_{21} \\ (R_{\Omega i \theta_0})_{31} \end{bmatrix} x_0$$

$$\begin{aligned} h_{ref} &= \sqrt{\mu a_r} \\ h_{sc} &= \sqrt{\mu a (1 - e^2)} \end{aligned}$$

$(R)_{mn}$ = element from matrix R (m^{th} row and n^{th} column)

B.2 Coefficients

Once the initial conditions have been obtained, all the coefficients required for the algorithm may be obtained. Note that these coefficients remain constant since they are

dependent on the initial conditions. Also note that the mean motion used in the equations for the coefficients is the mean motion for the reference orbit

$$n = \sqrt{\frac{\mu}{a_r^3}} \quad (\text{B.5})$$

B.2.1 Coefficients for the Second-Order Approximation

The α coefficients are obtained from

$$\alpha_0 = \frac{3}{a_r} \left(-x_0 y_0 + \frac{\dot{x}_0 \dot{y}_0}{n^2} + \frac{5x_0 \dot{x}_0}{2n} + \frac{z_0 \dot{z}_0}{2n} \right) \quad (\text{B.6})$$

$$\alpha_1 = \frac{3}{a_r} \left(y_0^2 + \frac{11}{2} x_0^2 + \frac{z_0^2}{2} + 2 \frac{\dot{y}_0^2}{n^2} + \frac{\dot{x}_0^2}{2n^2} + \frac{\dot{z}_0^2}{2n^2} + 7 \frac{\dot{y}_0}{n} x_0 - y_0 \frac{\dot{x}_0}{n} \right) \quad (\text{B.7})$$

$$\alpha_2 = \frac{1}{a_r} \left(-36x_0 \frac{\dot{y}_0}{n} - 30x_0^2 - 10 \frac{\dot{y}_0^2}{n^2} + 3y_0 \frac{\dot{x}_0}{n} - 2 \frac{\dot{x}_0^2}{n^2} - 3y_0^2 - z_0^2 - 2 \frac{\dot{z}_0^2}{n^2} \right) \quad (\text{B.8})$$

$$\alpha_3 = \frac{1}{a_r} \left(3x_0 y_0 - 2 \frac{\dot{x}_0 \dot{y}_0}{n^2} - 6x_0 \frac{\dot{x}_0}{n} - 2z_0 \frac{\dot{z}_0}{n} \right) \quad (\text{B.9})$$

$$\alpha_4 = \frac{1}{a_r} \left(\frac{\dot{x}_0^2}{4n^2} - \frac{\dot{y}_0^2}{n^2} - 3x_0 \frac{\dot{y}_0}{n} - \frac{9}{4} \dot{x}_0^2 + \frac{\dot{z}_0^2}{4n^2} - \frac{z_0^2}{4} \right) \quad (\text{B.10})$$

$$\alpha_5 = \frac{1}{a_r} \left(-\frac{\dot{x}_0 \dot{y}_0}{n^2} - \frac{3}{2} x_0 \frac{\dot{x}_0}{n} + \frac{z_0 \dot{z}_0}{2n} \right) \quad (\text{B.11})$$

$$\alpha_6 = \frac{3}{a_r} \left(-\frac{\dot{x}_0 \dot{y}_0}{n^2} - 2x_0 \frac{\dot{x}_0}{n} \right) \quad (\text{B.12})$$

$$\alpha_7 = \frac{3}{a_r} \left(7x_0 \frac{\dot{y}_0}{n} + 6x_0^2 + 2 \frac{\dot{y}_0^2}{n^2} \right) \quad (\text{B.13})$$

The β coefficients are obtained from

$$\beta_0 = \frac{3}{a_r} \left(\frac{y_0^2}{2} + \frac{\dot{y}_0^2}{n^2} + \frac{7}{2} x_0^2 - \frac{\dot{x}_0^2}{2n^2} + 4 \frac{\dot{y}_0}{n} x_0 + \frac{z_0^2}{4} + \frac{\dot{z}_0^2}{4n^2} \right) \quad (\text{B.14})$$

$$\beta_1 = -\frac{3}{a_r} \left(-2x_0 y_0 - y_0 \frac{\dot{y}_0}{n} + 4x_0 \frac{\dot{x}_0}{n} + 2\dot{x}_0 \frac{\dot{y}_0}{n^2} \right) \quad (\text{B.15})$$

$$\beta_2 = -\frac{9}{2a_r} \left(4x_0^2 + 4x_0 \frac{\dot{y}_0}{n} + \frac{\dot{y}_0^2}{n^2} \right) \quad (\text{B.16})$$

$$\beta_3 = \frac{1}{a_r} \left(12x_0 \frac{\dot{x}_0}{n} - 6x_0 y_0 + 7\dot{x}_0 \frac{\dot{y}_0}{n^2} - 3y_0 \frac{\dot{y}_0}{n} + z_0 \frac{\dot{z}_0}{n} \right) \quad (\text{B.17})$$

$$\beta_4 = \frac{1}{a_r} \left(-\frac{3}{2}y_0^2 - 5\frac{\dot{y}_0^2}{n} - 15x_0^2 + 2\frac{\dot{x}_0^2}{n} - 18x_0\frac{\dot{y}_0}{n} - \frac{\dot{z}_0^2}{n} - \frac{z_0^2}{2} \right) \quad (\text{B.18})$$

$$\beta_5 = \frac{1}{a_r} \left(-2\frac{\dot{x}_0\dot{y}_0}{n} - 3x_0\frac{\dot{x}_0}{n} - z_0\frac{\dot{z}_0}{2n} \right) \quad (\text{B.19})$$

$$\beta_6 = \frac{1}{a_r} \left(\frac{9}{2}x_0^2 + \frac{2\dot{y}_0^2}{n^2} - \frac{\dot{x}_0^2}{2n^2} + \frac{\dot{z}_0^2}{4n^2} - \frac{z_0^2}{4} + 6x_0\frac{\dot{y}_0}{n} \right) \quad (\text{B.20})$$

$$\beta_7 = -\frac{3}{a_r} \left(-7x_0\frac{\dot{y}_0}{n} - 2\frac{\dot{y}_0^2}{n} - 6x_0^2 \right) \quad (\text{B.21})$$

$$\beta_8 = \frac{3}{a_r} \left(\frac{\dot{x}_0\dot{y}_0}{n} + 2x_0\frac{\dot{x}_0}{n} \right) \quad (\text{B.22})$$

Finally, the γ coefficients are obtained from

$$\gamma_0 = \frac{3}{2a_r} \left(-\frac{2\dot{y}_0}{n}z_0 - 3x_0z_0 + \frac{\dot{x}_0\dot{z}_0}{n} \right) \quad (\text{B.23})$$

$$\gamma_1 = \frac{1}{a_r} \left(\frac{\dot{y}_0\dot{z}_0}{n} + 3x_0\frac{\dot{z}_0}{n} + z_0\frac{\dot{x}_0}{n} \right) \quad (\text{B.24})$$

$$\gamma_2 = \frac{1}{a_r} \left(2z_0\frac{\dot{y}_0}{n} + 3x_0z_0 - 2\frac{\dot{x}_0\dot{z}_0}{n} \right) \quad (\text{B.25})$$

$$\gamma_3 = \frac{1}{a_r} \left(\frac{\dot{y}_0 \dot{z}_0}{n} + \frac{3}{2} x_0 \frac{\dot{z}_0}{n} - z_0 \frac{\dot{x}_0}{2n} \right) \quad (\text{B.26})$$

$$\gamma_4 = \frac{1}{a_r} \left(z_0 \frac{\dot{y}_0}{n} + \frac{3}{2} x_0 z_0 + \frac{\dot{x}_0 \dot{z}_0}{2n^2} \right) \quad (\text{B.27})$$

$$\gamma_5 = \frac{1}{a_r} \left(6x_0 z_0 + 3z_0 \frac{\dot{y}_0}{n} \right) \quad (\text{B.28})$$

$$\gamma_6 = \frac{1}{a_r} \left(-6x_0 \frac{\dot{z}_0}{n} - 3\dot{y}_0 \frac{\dot{z}_0}{n^2} \right) \quad (\text{B.29})$$

B.2.2 Coefficients for the First-Order Solution

The following coefficients are required for the first-order solution:

$$\delta = 2 \left\{ f_0 - e \left[1 + \sqrt{1 - e^2} \right] s_{f_0} \right\} \quad (\text{B.30})$$

$$\theta_c = \omega + f_0 - 2es_{\delta/2} \quad (\text{B.31})$$

$$h_0 = -ec_{\theta_c - \delta/2} \quad (\text{B.32})$$

$$h_1 = -s_{\theta_c} \quad (\text{B.33})$$

$$h_2 = c_{\theta_c} \quad (\text{B.34})$$

$$h_3 = -es_{\theta_c + \delta/2} \quad (\text{B.35})$$

$$h_4 = ec_{\theta_c + \delta/2} \quad (\text{B.36})$$

$$h_5 = 2es_{2\theta_c} - \delta/2 \quad (\text{B.37})$$

$$h_6 = -2ec_{2\theta_c} - \delta/2 \quad (\text{B.38})$$

$$h_7 = -s_{2\theta_c} \quad (\text{B.39})$$

$$h'_7 = -2es_{2\theta_c} + \delta/2 \quad (\text{B.40})$$

$$h_8 = c_{2\theta_c} \quad (\text{B.41})$$

$$h'_8 = 2ec_{2\theta_c} + \delta/2 \quad (\text{B.42})$$

$$g_0 = -es_{\theta_c} - \delta/2 \quad (\text{B.43})$$

$$g_1 = c_{\theta_c} \quad (\text{B.44})$$

$$g_2 = s_{\theta_c} \quad (\text{B.45})$$

$$g_3 = ec_{\theta_c} + \delta/2 \quad (\text{B.46})$$

$$g_4 = es_{\theta_c} + \delta/2 \quad (\text{B.47})$$

$$g_5 = -2ec_{2\theta_c} - \delta/2 \quad (\text{B.48})$$

$$g_6 = 2es_{2\theta_c} - \delta/2 \quad (\text{B.49})$$

$$g_7 = c_{2\theta_c} \quad (\text{B.50})$$

$$g'_7 = 2ec_{2\theta_c} + \delta/2 \quad (\text{B.51})$$

$$g_8 = s_{2\theta_c} \quad (\text{B.52})$$

$$g'_8 = 2es_{2\theta_c} + \delta/2 \quad (\text{B.53})$$

$$a_2 = c_{\omega} h_0 + s_{\omega} g_0 \quad (\text{B.54})$$

$$a_3 = c_{\omega} h_1 + s_{\omega} g_1 \quad (\text{B.55})$$

$$a_4 = c_\omega h_2 + s_\omega g_2 \quad (\text{B.56})$$

$$a_5 = c_\omega h_3 + s_\omega g_3 \quad (\text{B.57})$$

$$a_6 = c_\omega h_4 + s_\omega g_4 \quad (\text{B.58})$$

$$a_1 = \frac{-3n^2 J_2 r_e^2 s_i^2}{a(1-e^2)^4} \quad (\text{B.59})$$

$$a'_1 = \frac{-3n^2 J_2 r_e^2}{2a(1-e^2)^4} \quad (\text{B.60})$$

$$a''_1 = \frac{-3n^2 J_2 r_e^2 s_i c_i}{a(1-e^2)^4} \quad (\text{B.61})$$

The above coefficients are used to obtain the b , c , d , and K coefficients used directly in the solution to the first-order equations given in **Subsection 4.2.3**.

The b coefficients are obtained from

$$b_0 = ea_1(a_3g_5 + a_4g_6 + a_5g_7 + a_6g_8) \quad (\text{B.62})$$

$$b_1 = \frac{a_1g_5}{2} + a_1e(2a_2g_5 - a_6g_5 + a_5g_6 + a_4g_7 - a_3g_8 \\ + a_6g'_7 - a_5g'_8) \quad (\text{B.63})$$

$$b'_1 = \frac{a_1g_6}{2} + a_1e(a_5g_5 + 2a_2g_6 + a_6g_6 + a_3g_7 + a_4g_8 \\ + a_5g'_7 + a_6g'_8) \quad (\text{B.64})$$

$$b_2 = \frac{a_1 g_7}{2} + a_1 e(a_4 g_5 + a_3 g_6 + 2a_2 g_7 + a_4 g'_7 - a_3 g'_8) \quad (\text{B.65})$$

$$b'_2 = \frac{a_1 g_8}{2} + a_1 e(a_4 g_6 - a_3 g_5 + 2a_2 g_8 + a_3 g'_7 + a_4 g'_8) \quad (\text{B.66})$$

$$b_3 = \frac{a_1 g'_7}{2} + a_1 e(a_6 g_5 + a_5 g_6 + a_4 g_7 + a_3 g_8 + 2a_2 g'_7) \quad (\text{B.67})$$

$$b'_3 = \frac{a_1 g'_8}{2} + a_1 e(a_6 g_6 - a_5 g_5 - a_3 g_7 + a_4 g_8 + 2a_2 g'_8) \quad (\text{B.68})$$

$$b_4 = a_1 e(a_6 g_7 + a_5 g_8 + a_4 g'_7 + a_3 g'_8) \quad (\text{B.69})$$

$$b'_4 = a_1 e(a_6 g_8 - a_5 g_7 - a_3 g'_7 + a_4 g'_8) \quad (\text{B.70})$$

$$b_5 = a_1 e(a_6 g'_7 + a_5 g'_8) \quad (\text{B.71})$$

$$b'_5 = a_1 e(a_6 g'_8 - a_5 g'_7) \quad (\text{B.72})$$

The c coefficients are obtained from

$$c_0 = a'_1 \left[1 - \frac{3}{2} s_i^2 + 2a_2 e(2 - 3s_i^2) + 3es_i^2 (a_3 h_5 + a_4 h_6 + a_5 h_7 + a_6 h_8) \right] \quad (\text{B.73})$$

$$c_1 = a'_1 \left[\frac{3}{2} s_i^2 h_5 + 2a_3 e(2 - 3s_i^2) + 6es_i^2 a_2 h_5 + 3es_i^2 (a_5 h_6 - a_6 h_5 + a_4 h_7 - a_3 h_8 + a_6 h'_7 - a_5 h'_8) \right] \quad (\text{B.74})$$

$$c'_1 = a'_1 \left[\frac{3}{2} s_i^2 h_6 + 2a_4 e(2 - 3s_i^2) + 6es_i^2 a_2 h_6 \right. \\ \left. + 3es_i^2 (a_5 h_5 + a_6 h_6 + a_3 h_7 + a_4 h_8 + a_3 h'_7 \right. \\ \left. + a_6 h'_8) \right] \quad (\text{B.75})$$

$$c_2 = a'_1 \left[\frac{3}{2} s_i^2 h_7 + 2a_5 e(2 - 3s_i^2) + 6es_i^2 a_2 h_7 \right. \\ \left. + 3es_i^2 (a_4 h_5 + a_3 h_6 + a_4 h'_7 - a_3 h'_8) \right] \quad (\text{B.76})$$

$$c'_2 = a'_1 \left[\frac{3}{2} s_i^2 h_8 + 2a_6 e(2 - 3s_i^2) + 6es_i^2 a_2 h_8 \right. \\ \left. + 3es_i^2 (a_4 h_6 - a_3 h_5 + a_3 h'_7 + a_4 h'_8) \right] \quad (\text{B.77})$$

$$c_3 = \frac{3}{2} a'_1 s_i^2 h'_7 + 3a'_1 es_i^2 (a_6 h_5 + a_5 h_6 + a_4 h_7 + a_3 h_8 \\ + 2a_2 h'_7) \quad (\text{B.78})$$

$$c'_3 = \frac{3}{2} a'_1 s_i^2 h'_8 + 3a'_1 es_i^2 (a_6 h_6 - a_5 h_5 - a_3 h_7 + a_4 h_8 \\ + 2a_2 h'_8) \quad (\text{B.79})$$

$$c_4 = 3a'_1 es_i^2 (a_6 h_7 + a_5 h_8 + a_4 h'_7 + a_3 h'_8) \quad (\text{B.80})$$

$$c'_4 = 3a'_1 es_i^2 (a_6 h_8 - a_5 h_7 - a_3 h'_7 + a_4 h'_8) \quad (\text{B.81})$$

$$c_5 = 3a'_1 es_i^2 (a_6 h'_7 + a_5 h'_8) \quad (\text{B.82})$$

$$c'_5 = 3a'_1 es_i^2 (a_6 h'_8 - a_5 h'_7) \quad (\text{B.83})$$

The d coefficients are obtained from

$$d_0 = a''_1 g_0 + 2a''_1 e(2a_2 g_0 + a_3 g_1 + a_4 g_2 + a_5 g_3 + a_6 g_4) \quad (\text{B.84})$$

$$d_1 = a''_1 g_1 + 2a''_1 e(2a_2 g_1 + 2a_3 g_0 - a_3 g_4 + a_4 g_3 + a_5 g_2 - a_6 g_1) \quad (\text{B.85})$$

$$d'_1 = a''_1 g_2 + 2a''_1 e(2a_2 g_2 + a_3 g_3 + a_4 g_4 + 2a_4 g_0 + a_5 g_1 + a_6 g_2) \quad (\text{B.86})$$

$$d_2 = a''_1 g_3 + 2a''_1 e(2a_2 g_3 + a_3 g_2 + a_4 g_1 + 2a_5 g_0) \quad (\text{B.87})$$

$$d'_2 = a''_1 g_4 + 2a''_1 e(2a_2 g_4 - a_3 g_1 + a_4 g_2 + a_4 g_2 + 2a_6 g_0) \quad (\text{B.88})$$

$$d_3 = 2a''_1 e(a_3 g_4 + a_4 g_3 + a_5 g_2 + a_6 g_1) \quad (\text{B.89})$$

$$d'_3 = 2a''_1 e(a_4 g_4 - a_3 g_3 - a_5 g_1 + a_6 g_2) \quad (\text{B.90})$$

$$d_4 = 2a''_1 e(a_5 g_4 + a_6 g_3) \quad (\text{B.91})$$

$$d'_4 = 2a''_1 e(a_6 g_4 - a_5 g_3) \quad (\text{B.92})$$

Finally, the K constants are obtained from

$$K = \dot{y}_0 + 2nx_0 + \sum_{j=1}^5 \frac{b_j}{jn} \quad (\text{B.93})$$

$$K' = y_0 - 2\frac{\dot{x}_0}{n} + 4\frac{b_0}{n^2} - \sum_{j=2}^5 \frac{2}{jn^2} \left(2\frac{b'_j}{j} + c_j \right) + \sum_{j=1}^5 \frac{b'_j}{2jn^2} - \frac{2}{n^2} (2b'_1 + c_1) \quad (\text{B.94})$$

Once all the coefficients have been computed the second approximation, **Equations (4.28-33)**, and the first-order solution, **Equations (4.37-42)**, can be obtained as well as the final relative solution, or the sum of the two, **Equation (4.43)**. The inertial position and velocities are determined by the equations given in the following subsection. All these equations may be used to propagate an orbit by using the results of one time step propagation as the initial conditions, and repeating the process. The time variable, t , is increased by a time increment for each loop. For this study, the equations were computed once for each time step (1 second) and then re-initialized for the next time step by determining the orbital elements, and then following the procedure described in this appendix.

B.3 Conversion to Inertial Frame

Once the second-order approximations are added to the perturbed first-order solution to obtain the final relative positions and velocities given in **Equation (4.43)**, the inertial position components are obtained from

$$\begin{bmatrix} X \\ Y \\ Z \end{bmatrix} = a_r \begin{bmatrix} (R_{\Omega i \theta})_{11} \\ (R_{\Omega i \theta})_{21} \\ (R_{\Omega i \theta})_{31} \end{bmatrix} + \begin{bmatrix} \rho_{\hat{x}} \\ \rho_{\hat{y}} \\ \rho_{\hat{z}} \end{bmatrix} \quad (\text{B.95})$$

where

$$R_{\Omega i \theta} = \begin{bmatrix} c_{\Omega} c_{\theta} - s_{\Omega} c_i s_{\theta} & -c_{\Omega} s_{\theta} - s_{\Omega} c_i c_{\theta} & s_{\Omega} s_i \\ s_{\Omega} c_{\theta} + c_{\Omega} c_i s_{\theta} & -s_{\Omega} s_{\theta} + c_{\Omega} c_i c_{\theta} & -c_{\Omega} s_i \\ s_i s_{\theta} & s_i c_{\theta} & c_i \end{bmatrix}$$

$$\begin{bmatrix} \rho_{\hat{x}} \\ \rho_{\hat{y}} \\ \rho_{\hat{z}} \end{bmatrix} = R_{\Omega i \theta} \begin{bmatrix} x_f \\ y_f \\ z_f \end{bmatrix}$$

$$\theta = \theta_0 + nt$$

with

t = time measured from epoch

The inertial velocity components are obtained from

$$\begin{aligned} \dot{X} &= \frac{\mu}{h_{ref}} (R_{\Omega i \theta})_{12} + \dot{x}(I) \\ &\quad - \frac{h_{ref}}{2 a_r} (-(R_{\Omega i \theta})_{23} \rho_{\hat{z}} + (R_{\Omega i \theta})_{33} \rho_{\hat{y}}) \end{aligned} \quad (\text{B.96})$$

$$\begin{aligned} \dot{Y} &= \frac{\mu}{h_{ref}} (R_{\Omega i \theta})_{22} + \dot{y}(I) \\ &\quad - \frac{h_{ref}}{2 a_r} ((R_{\Omega i \theta})_{13} \rho_{\hat{z}} - (R_{\Omega i \theta})_{33} \rho_{\hat{x}}) \end{aligned} \quad (\text{B.97})$$

$$\dot{Z} = \frac{\mu}{h_{ref}} (R_{\Omega i \theta})_{32} + \dot{z}(I) \quad (\text{B.98})$$

$$+ \frac{h_{ref}}{a_r} ((R_{\Omega i \theta})_{13} \rho_{\hat{y}} - (R_{\Omega i \theta})_{23} \rho_{\hat{x}})$$

where

$$\begin{bmatrix} \dot{x}(I) \\ \dot{y}(I) \\ \dot{z}(I) \end{bmatrix} = R_{\Omega i \theta} \begin{bmatrix} \dot{x}_f \\ \dot{y}_f \\ \dot{z}_f \end{bmatrix}$$

Appendix C

Errata in References

Several errors were found in some of the references. These are delineated below.

C.1 Errors in Reference [2]

The errors in this reference are in Equation (9.7-6) on page 422 of the reference. The exponents on the first two $\left(\frac{r_e}{r}\right)$ terms are reversed. The first $\left(\frac{r_e}{r}\right)$ term should be raised to the second power instead of the third such that $\left(\frac{r_e}{r}\right)^2$. The second term should be $\left(\frac{r_e}{r}\right)^3$.

C.2 Errors in Reference [14]

There is a sign error in one of the coefficient equations for the second approximation. The last element in the equation for β_1 (p. 380) should be preceded with a positive sign instead of a negative sign. It should read:

$$\beta_1 = -\frac{3}{a_r} \left(-2x_0y_0 - y_0\frac{\dot{y}_0}{n} + 4x_0\frac{\dot{x}_0}{n} + 2\dot{x}_0\frac{\dot{y}_0}{n} \right) \quad (\text{C.1})$$

Another error exists in the equations that determine the initial, inertial velocity conditions on page 383. In the equation just below Equation (30) solving for $\dot{x}_0(I)$, the very last element in the second row should end with a cosine instead of a sine. That is,

$$\begin{aligned} \dot{x}_0(I) = & \frac{\mu}{h_{sc}} [-c_{\Omega}(s_{\theta_0} + es_{\omega}) - s_{\Omega}(c_{\theta_0} + ec_{\omega})c_i] & (C.2) \\ & - \frac{\mu}{h_{ref}} (-c_{\Omega}s_{\theta_0} - s_{\Omega}c_i c_{\theta_0}) \\ & + \frac{h_{ref}}{2a_r} (c_{\Omega}s_i \rho_{\hat{z}}^0 + c_i \rho_{\hat{y}}^0) \end{aligned}$$

References

- [1] Axelrad, P.A., *Near Earth Orbit Determination and Rendezvous Navigation Using GPS*, S.M. Thesis, Department of Aeronautics and Astronautics, MIT, February 1985, pp. 20-31.
- [2] Bate, R.R., et al, *Fundamentals of Astrodynamics*, Dover Publications, Inc., New York, 1971, pp. 419-425.
- [3] Battin, R.H., *An Introduction to the Mathematics and Methods of Astrodynamics*, AIAA, Inc., New York, 1987, pp. 464-467.
- [4] Battin, R.H., *Astrodynamics Class Notes (16.346-16.347)*, Department of Aeronautics and Astronautics, MIT, 1997-1998.
- [5] Braasch, M.S., et al, "Improved Modeling of GPS Selective Availability," *Proceedings of the National Technical Meeting of the Institute of Navigation*, San Francisco, CA, January 20-22, 1993, pp. 121-130.
- [6] Brown, R.G. and P.Y.C. Hwang, *Introduction to Random Signals and Applied Kalman Filtering*, John Wiley & Sons, New York, 1997, pp. 214-220.
- [7] Clark, F.D. & A. Christofferson, "Applicability of Relative GPS to Automated Rendezvous Between the Space Shuttle and Space Station," Lockheed Engineering and Sciences Company, Houston, TX, November 1991.
- [8] Clohessy, W.H. & R.S. Wiltshire, "Terminal Guidance System for Satellite Rendezvous" *Journal of Aerospace Sciences*, Vol. 27, No. 9, 1960, pp. 653-658.
- [9] Frezet, M., et al, "Relative GPS Navigation for ATV Rendezvous," *Proceedings of ION GPS-95: 8th International Technical Meeting of the Satellite Division of the Institute of Navigation*, Alexandria, VA, September 12-15, 1995, pp. 269-278.
- [10] Galdos, J.I., et al, "A GPS Relative Navigation Filter for Automatic Rendezvous and Capture", *Proceedings of the Institute of Navigation 1993 Technical Meeting*, January 1993, pp. 83-94.

- [11] Hofmann-Wellenhof, B., et al, *Global Positioning System: Theory and Practice, Second Edition*, Springer-Verlag Wien, New York, 1993, pp. 5-17.
- [12] Hollister, W.H., *Satellite Engineering Class Notes (16.851)*, Department of Aeronautics and Astronautics, MIT, 1998.
- [13] Kaplan, E.D., *Understanding GPS Principles and Applications*, Artech House Publishers, Boston, 1996, pp. 2-38.
- [14] Kechichian, J.A., "Techniques of Accurate Analytic Terminal Rendezvous In Near-Circular Orbit," *Acta Astronautica*, Vol. 26, No. 6, 1992, pp. 377-394.
- [15] Kawano, I., et al, "In-orbit Demonstration of an Unmanned Automatic Rendezvous and Docking System by the Japanese Engineering Test Satellite ETS-VII," *Proceedings of the AIAA Guidance and Control Conference*, Scottsdale, August 1994. Report No. AIAA-94-3648-CP, pp. 950-960.
- [16] Kawano, I., et al, "Relative GPS Navigation for Automated Rendezvous Docking Test Satellite ETS-VII," *Proceedings of ION GPS-97: 10th International Technical Meeting of the Satellite Division of the Institute of Navigation*, Kansas City, MO, September. 1997, pp. 707-716.
- [17] Lawrence, P.J., Jr., "GPS Selective Availability and Kalman Filter Simulation Task Using MATLAB V5.1," Charles Stark Draper Laboratory Memorandum, Memo No. E42-98-031, Cambridge, MA, April 1, 1998.
- [18] Legido, J.M., et al, "Differential and Relative Navigation Results with a GPS Receiver for Space Applications," *Proceedings of the 2nd ESA Symposium on Spacecraft Guidance, Navigation & Control Systems*, ESTEC, Noordwijk, Netherlands, April 12-15, 1994, pp. 189-196.
- [19] Lemke, N., et al, "Relative GPS Experiments During MIT '96 and ATV Rendezvous Predevelopment Flight Demonstration Missions," *47th International Astronautical Congress*, Beijing, China, October 7-11, 1996, pp. 1-10.
- [20] Levy, L.J., "The Kalman Filter: Navigation's Integration Workhorse", *GPS World*, September 1997, pp. 65-71.

- [21] Marcille, H., et al, "Relative GPS Navigation Design and Validation for ATV Rendezvous", *Proceedings of the 3rd ESA Symposium on Spacecraft Guidance, Navigation & Control Systems*, ESTEC, Noordwijk, Netherlands, November 25-28, 1996, pp. 77-82.
- [22] Martin, E.H., "GPS User Equipment Error Models," *Global Position System: Volume 1*, Institute of Navigation, 1980, pp. 109-118.
- [23] Matchett, G., "Navigation Accuracy Issues for Near-Earth Orbital Users of GPS," *AAS & AIAA, Annual Meeting on Space Enhancing Technological Leadership*, AAS, 1980.
- [24] Maybeck, P.S., *Stochastic Models, Estimation, and Control, Volume 1*, Academic Press, Inc., Orlando, Florida, 1979.
- [25] NATO-Team, U.S. Air Force Space Systems Division, Navstar-GPS Joint Program Office, *Navstar GPS User Equipment Introduction*, U.S. Government Printing Office, February 1991.
- [26] Navtech Seminars, Inc., *Course 355: Navstar GPS for Test and Evaluation*, Eglin Air Force Base, Florida, August 1-5, 1994.
- [27] Park, Y.W., et al, "Flight Test Results from Real-Time Relative Global Positioning System Flight Experiment on STS-69," National Aeronautics and Space Administration, Technical Memorandum 104824, Houston, TX, November 1996.
- [28] Parkinson, B.W., et al, *Global Positioning System: Theory and Applications, Volume I*, AIAA, Inc., Washington, DC, 1996.
- [29] Phillips, R.E. and G.T. Schmidt, "Relative and Differential GPS," Charles Stark Draper Laboratory, System Implications and Innovative Applications of Satellite Navigation, NATO / AGARD Lecture Series No. 207, Paris, France, July 1-2, 1996.
- [30] Shepperd, S.W., "Constant Covariance in Local Vertical Coordinates for Near-Circular Orbits", *Journal of Guidance, Controls, and Dynamics, Vol. 14, No. 6, Engineering Notes*, November-December 1991, pp. 1318-1322.

- [31] Shepperd, S.W., "Universal Keplerian State Transition Matrix," *Celestial Mechanics, Vol. 35*, Reidel Publishing Company, 1985, pp. 129-144.
- [32] Soltz, J.A., "Fast Near-Optimum GPS Satellite Selection Algorithm," Charles Stark Draper Laboratory Interlab Memorandum, Memo No. ESD-94-213, Cambridge, MA, April 20, 1994.
- [33] Stoll, J.C., *Performance Analysis of a GPS Interferometric Attitude Determination System for a Gravity Gradient Stabilized Spacecraft*, S.M. Thesis, Department of Aeronautics and Astronautics, MIT, May 1995, p. 42.
- [34] Strang, G., *Introduction to Applied Mathematics*, Wellesley-Cambridge Press, Wellesley, MA, 1986, p. 569.
- [35] U.S. Coast Guard Web-site: <http://www.navcen.uscg.mil/gps/almanacs/>, November 21, 1998.
- [36] Zyla, L.V. & M.N. Montez, "Use of Two GPS Receivers in Order to Perform Space Vehicle Orbital Rendezvous," *Proceedings of the ION GPS-93, The Institute of Navigation*, Salt Lake City, UT, September 1993, pp. 301-312.